

Progress Report 2017

Laboratory for Waste Management :: Nuclear Energy and Safety Department

Cover

Conceptualization of ion transport in Opalinus Clay using Poisson-Boltzmann (PB), Anion Exclusion (AE) and Donnan (D) equilibrium models. Ions and water are transported in a complex network of pores confined between surfaces of clay minerals. Due to the permanent charge of clay particles, near surface regions are enriched and depleted by cations (red points) and anions (yellow points), respectively. The PB model uses a mean field electrostatic potential to describe the ion concentrations. The AE model excludes anions from the near surface region. The thermodynamic Donnan concept considers different, but uniform anion and cation concentrations in pores affected by surface charges. The anion and cation concentrations in each model are shown by yellow and red lines, respectively.

PAUL SCHERRER INSTITUT



Progress Report 2017

**Laboratory for Waste Management
Nuclear Energy and Safety Department**



See also our web-page
<http://www.psi.ch/les/>

Preface

The mission of the Laboratory for Waste Management (LES) is to carry out a comprehensive research and development (R&D) programme in support of Swiss radioactive waste disposal options. In particular, the aim is to be one of the world-leading laboratories in the fields of geochemistry of disposal systems and transport mechanisms of radionuclides, including geochemical retardation and immobilisation.

The laboratory serves an important national role by supporting the Swiss Federal Government and Nagra in their tasks to safely dispose of radioactive wastes from medical, industrial and research applications as well as from nuclear power plants. The research activities cover fundamental aspects of repository geochemistry, chemistry and physics of radionuclides at geological interfaces, and radionuclide transport and retardation in geological and technical barriers. The work performed is a balanced combination of experimental activities in dedicated laboratories for handling radioactive isotopes, field experiments and modelling. The work is directed towards repository implementation and the results find their application in comprehensive performance assessments carried out by Nagra. In particular, a major priority for LES for the next decade will be to contribute to the advance of the Swiss Sectoral Plan for Geological Waste Disposal (Sachplan geologische Tiefenlagerung, SGT).

This report summarizes the research activities and results achieved in 2017. It gives a detailed overview of research projects, personnel management, national and international collaboration, and individual contributions on the work progress achieved by scientists in the four research groups.

We gratefully acknowledge the support of our work by the PSI management and Nagra.

Table of Contents

1	OVERVIEW	1
1.1	Introduction.....	1
1.2	General.....	1
1.3	Sectoral plan for deep geological disposal.....	4
1.4	Repository near field.....	4
1.4.1	Repository chemistry.....	4
1.4.2	Clay systems.....	5
1.4.3	Cement systems.....	6
1.4.4	Interfacial processes.....	7
1.5	Repository far field.....	8
1.6	Model development and code benchmarking.....	9
2	GEOCHEMICAL EVOLUTION OF REPOSITORY NEAR FIELD.....	13
2.1	Introduction.....	13
2.2	Modelling of the Mont Terri Cement Interaction (CI) experiment.....	14
2.3	Cement-clay interaction, technical barrier evolution, modelling and experiments.....	15
2.3.1	Cement-clay interfaces: evolution of transport properties, porosity and mineralogy.....	15
2.3.2	Electrochemical transport across reactive interfaces.....	16
2.3.3	Porosity evolution at clay – cement interfaces using neutron radiography: Accelerated carbonation at clay/cement interfaces.....	17
2.3.4	Resolving carbonation mechanisms of cement-based materials through multi-scale microstructural simulations.....	17
2.3.5	Multiscale modelling of ion transfer mechanisms in clay and cement materials.....	18
2.4	Fundamental understanding of transport and sorption mechanisms.....	18
2.4.1	Transport simulations including the Donnan approach.....	18
2.5	Multiscale modelling of reactive transport mechanisms and upscaling.....	20
2.5.1	Pore scale control of mineral precipitation: from atomistic model to macroscopic modelling and experimental observations.....	20
2.5.2	Pore-level Lattice Boltzmann modelling of precipitation processes.....	21
2.5.3	Extraction of porosity permeability relationships from pore-level analysis.....	22
2.6	Benchmarking, validation and application of coupled codes.....	22
2.6.1	Pore-level dissolution benchmarking.....	23
2.7	Thermodynamic modelling framework and thermodynamic databases.....	23
2.7.1	On-demand machine-learning (ODML) approach for ultra-fast reactive transport simulations and parameter optimization.....	23
2.7.2	GEMS training events.....	25
2.8	References.....	25
3	DEVELOPMENT OF MECHANISTIC SORPTION MODELS AND EXPERIMENTAL VALIDATION.....	27
3.1	Introduction.....	27
3.2	Mechanistic sorption studies and experimental validation.....	27
3.2.1	Competition: experimental and modelling.....	27
3.2.2	Sorption of U ^{VI} on Illite du Puy: influence of accessory minerals.....	30
3.2.3	Influence of structural Fe ^{II} in montmorillonite on the retention of Np ^V	31

3.2.4	Cs, Rb and Tl sorption on illite	32
3.2.5	Immobilisation of selenium and iodine in cementitious systems	33
3.2.6	Mechanism of Fe incorporation in montmorillonite	34
3.2.7	Microscale distribution and speciation of thallium in contaminated soils	35
3.3	References	36
4	¹⁴C SPECIATION AND TRANSPORT IN REPOSITORY	37
4.1	Introduction	37
4.2	Release and speciation of ¹⁴ C-bearing compounds	37
4.3	Chemical stability of organic compounds in repository relevant conditions	41
4.4	Retardation and migration studies	42
4.5	References	44
5	RADIONUCLIDES TRANSPORT AND RETENTION IN COMPACTED SYSTEMS AT FULL AND PARTIAL SATURATION	47
5.1	Introduction	47
5.2	Desktop study: status report on "transferability"	47
5.3	Sorption/diffusion studies on compacted illite	47
5.4	Sorption/diffusion studies on intact Opalinus Clay	49
5.5	Modelling the effect of surface diffusion on Cs transport in Opalinus Clay	50
5.6	Inter valent sorption competition between Eu(III) and Ni(II) during diffusion through bentonite	50
5.7	Anion accessible porosity in low porosity argillaceous rocks (ANPOR)	51
5.8	Ions transport in compacted clays at partially saturated conditions	52
5.9	References	52
6	THERMODYNAMIC MODELS AND DATABASES	55
6.1	Introduction	55
6.2	Update of the Thermodynamic Data Base (TDB)	55
6.2.1	The solubility of FeS (mackinawite)	57
6.3	Prediction of temperature trends of standard thermodynamic properties by isocoulombic reactions generated within the ThermoMatch code	58
6.3.1	Systematic study of isocoulombic reactions for Ln(III)-fluoride complexation	59
6.4	G-values for gas production (H ₂) during irradiation of organic and inorganic materials present in a repository for low- and intermediate-level radioactive waste	61
6.5	References	61
7	CEMENT-WASTE INTERACTION AND UPSCALING TO THE FIELD SCALE	63
7.1	Introduction	63
7.2	Geochemical modelling of the temporal evolution of waste packages	63
7.3	Multi-phase mass transport in waste-packages using a look-up table approach for description of cement degradation	65
7.4	Interaction of iron corrosion products with cement	66
7.5	Alkali-silica reaction in concrete	68
7.6	References	68
8	DISSOLUTION OF SPENT FUEL AND VITRIFIED WASTE	69
8.1	Overview	69
8.2	Spent fuel dissolution	69
8.2.1	DisCo project	69

8.2.2	Comparative analysis of Instant Release Fraction (IRF) data from Swiss spent fuel obtained in the framework of the GAP and FIRST-Nuclides projects	69
8.3	References	73
9	PUBLICATIONS	75
9.1	Peer reviewed journals	75
9.2	PSI and Nagra reports	76
9.3	Conference Proceedings	76
9.4	Conferences/workshops/presentations	76
9.5	Invited talks	80
9.6	Teaching	80
9.7	PhD thesis defences	80
9.8	Other	80

1 OVERVIEW

S.V. Churakov

1.1 Introduction

Overall progress made in the Laboratory for Waste Management (LES) over the period from January 1st, 2017 to December 31th, 2017 is summarized in the first part of the report. The report is organised thematically according to seven projects. These projects are multidisciplinary in nature and contain contributions from the different groups.

1.2 General

The site selection process for geological disposal of radioactive waste in Switzerland, the so called Sectoral Plan for Deep Geological Disposal (SGT), is ongoing. According to the current planning, the formal completion of Stage 2 and the official launch of Stage 3 are anticipated by the end of 2018. The goal of Stage 3 is to select one disposal site for each repository type and to submit a General Licence Application (RBG) for the selected site(s) later on. Several disposal sites for Spent fuel/High Level Waste (SF/HLW) and Low/Intermediate Level Waste (L/ILW) have been proposed by Nagra for further investigations. All these sites are located in the Opalinus Clay (OPA) formation. The technical documentation for Stage 2 was reviewed by ENSI (Federal Nuclear Safety Inspectorate) in 2016-2017. ENSI supports further investigation of the sites selected by Nagra but also suggests considering "Nördlich Lägern" for a detailed study in Stage 3 of the SGT.

A critical evaluation of the research needs and a general planning of technical documentation for Stage 3 of the SGT have been conducted in 2017 in a series of bilateral meetings between Nagra and LES. A catalogue of safety relevant Features, Events and Processes (FEPs) for the multi-barrier repository system has been revised. Remaining critical knowledge gaps and the needs for the long-term knowledge transfer have been identified.

Present and future research activities focuses on the behaviour of modern spent fuel at repository conditions, the chemical evolution of the repository near field, performance of the Engineered Gas Transport System (EGTS), the behaviour of redox-sensitive elements, the role of mineral surface induced redox reactions, the transfer of sorption models and data from dispersed to compacted systems. These studies help in filling the remaining knowledge gaps and provide scientific justifications for model assumptions made in safety assessment studies.

Reactive transport simulations and complementary experiments are essential for understanding the long-term evolution of *in situ* repository conditions and the interaction between repository barriers causing an alteration of their retention and transport properties. Special attention is paid to understand the role of heterogeneities in a cementitious repository taking into account spatial and temporal variation of waste reactivity and degradation rates. These aspects have important implications for minimisation of detrimental effects of organics degradation and metal corrosion on repository safety. In this context LES has developed a state-of-the-art expertise in pore scale reactive transport simulations which takes rigorously into account the dissolution and precipitation phenomena and their feedback on transport. LES' long-term goal is to maintain existing datasets for safety analysis, including sorption, diffusion and thermodynamics and to develop beyond state-of-the-art expertise in the quantitative description of the long-term repository evolution.

In the year 2017 LES has continued successful acquisition of competitive funding for PhD projects and postdoc fellowships from the EU-HORIZON 2020 programme, the Swiss National Science Foundation (SNSF) and other non-Nagra funding agencies. These projects broaden LES' competences, bring fresh research ideas and help to stay competitive with other research groups and, last but not least, contribute to the education of young researchers in the field of geological waste disposal. Recruitment of competent PhD and postdoctoral students is a challenging process, which needs a careful evaluation of candidates. Four new postdoc projects were approved in 2017 with the total duration adding up to 10 personnel years. Further, a 4Y-SNSF PhD project on pore scale simulations has been approved by the Swiss National Science Foundation. Four postdoc positions were successfully filled. One new PhD student will start in February 2018.

A 4 years EURATOM project (DisCo, Modern spent fuel dissolution and chemistry in failed container conditions, (H2020 <http://www.disco.eu/>)) has been approved by the European Commission in April 2017. The DisCo project focusses on the dissolution of Cr/Al doped and MOX spent fuels under repository conditions. A subproject hosted at LES will focus on the thermodynamic modelling aspects.

Furthermore LES provided an in-kind contribution to the development of the programme document of the

Euratom Horizon 2020 Joint Programme on Radioactive Waste Disposal (JOPRAD, <http://www.joprad.eu>). In particular LES hosted a first European Joint Programme (EJP) meeting of the work package on radionuclide transport and co-coordinates further project development.

A collaborative SNSF-Sinergia project "COTHERM-II" (Combined hydrological, geochemical and geophysical modelling of geothermal systems), with ETHZ as the leading house has been successfully finalised in May 2017. In a postdoc subproject hosted at LES, a novel reactive transport simulation approach for two-phase fluid transport with volatiles partitioning has been developed for the simulation of boiling geothermal systems. The main outcome of the project was the validation of the modelling concepts and thermodynamic data used in simulations for geological disposal against other natural systems. This model could also be applied for future simulations of two-phase fluid transport in a geological repository.

The first phase of a collaborative project funded by the German Ministry of Education and Finances (BMBF) "Thermodynamik und Speziation von Actiniden bei höheren Temperaturen" (ThermAc) was completed in 2017. The second phase of the project has been approved and the funding for further development of a database for actinides at higher temperatures will be conducted.

Two PSI-FELLOW-II-3i projects focused on the development of reactive transport pore scale simulation methods, taking into account dissolution and precipitation processes and their feedback on transport, have been approved. These developments will allow a better prediction of the long-term evolution of chemically heterogeneous repository systems and provide macroscopic parameters for large-scale simulations.

A multi-institutional three year SNSF-project "Effect of aluminum on C-S-H structure, stability and solubility" has been approved (EMPA(Lead)-PSI-EPFL). The postdoc fellow to be hosted by PSI will start in 2018. The goal of the PSI hosted subproject will be to further improve the in-house solid-solution model for calcium silicate hydrates. Within a new SNSF-Sinergia project: "Alkali-silica reaction in concrete" (EMPA(Lead)-EPFL-PSI) a postdoc fellow hosted at LES will work on the development of synchrotron based characterization techniques for phases produced by the alkali-silica reaction. Such techniques are also indispensable for the characterisation of mineral phases formed at cement-clay interfaces in repository relevant conditions.

In the framework of a cross-department initiative supported by the PSI directorate (CROSS-PSI) a

postdoc project "Cryo-microspectroscopy at the microXAS beamline for the investigation of redox- and radiation-sensitive samples" (R. Dähn, D. Grolimund, A. Vögelin) will develop a cryo-stabilisation approach for spectroscopic characterisation of redox-sensitive elements.

The development and testing of an experimental set-up for compound-specific analysis of ^{14}C released during the corrosion of irradiated steel, has been accomplished. The project has been funded by Swiss nuclear since 2013. First measurements with the active materials have been started in 2016. A complementary study within the collaborative EU FP7 project CAST "Carbon-14 Source Term" is ongoing, and will be finalised in 2018. LES actively maintains collaboration with national and international research institutes in the field of waste management and environmental research. The main multi- and bilateral co-operations with external institutions and universities are summarized in Table 1.1.

Table 1.1: National and international co-operations.

Co-operations
Nagra Major financial contribution Various technical working groups
Multinational 7 th EU FP (CAST) EURATOM HORIZON2020 (SITEX-II) EURATOM HORIZON2020 (CEBAMA) EU (DisCo) Mont Terri Projects (diffusion retardation, clay-cement interaction)
Universities Bern*, Switzerland (mineralogy, petrography, water chemistry, C-14 AMS) EPFL, Switzerland (cement systems) Dijon, France (molecular modelling) ETH*, Zürich, Switzerland (GEMS) Hiroshima University, Japan (clay-cement interaction) Tokyo Institute of Technology, Japan (clay systems) Xi'an Jiaotong University, China (clay systems)
Research Centres CEA*, France (near- and far-field) EMPA*, Switzerland (cement) IFR, HZDR*, Germany (XAS, TRLFS) INE, KIT*, Germany (near- and far field; TRLFS) FZJ, Germany (sorption/diffusion of Ra) SCK/CEN, Belgium (clay and cement systems) UFZ*, Germany (reactive transport, clay systems) *formal co-operation agreements

Ongoing PhD and postdoc projects hosted at LES are listed below:

L. Hax Damiani (PhD Student): "Modelling transport across reactive interfaces with the Nernst-Planck approach" Start date: January 2016. (Funding: EU).

A. Keri (PhD Student): "Shedding light on metal adsorption processes on clay minerals inferred from atomistic simulations and X-ray absorption spectroscopy." Start date: January 2015. (Funding: SNSF).

P. Luraschi (PhD Student): "Evolution of transport properties, mineralogy, and porosity of cement-clay interfaces." Start date: April 2017. (Funding: Nagra/PSI).

Ph. Krejci (PhD Student): "Multispecies cation transport in compacted clays." Start date: December 2016 (Funding: SNSF).

A. Mancini (PhD Student): "Thermodynamic and spectroscopic investigations of the Fe and S speciation in anoxic cementitious systems". Start date: April 2016 (Funding: SNSF).

A. Nedyakova (PhD Student): "A structural and thermodynamic study of the intercalation of selenium(IV), selenium(-II), sulfur(-II) and I(-I) in AFm-phases." Start date: February 2016. (Funding: EU).

R. Schliemann (PhD Student): "Dissolution, growth and ion uptake at phyllosilicate surfaces: Coupling atomistic interactions at the mineral-water interface with Kinetic Monte Carlo model." Start date: July 2016. (Funding: SNSF).

S. Wick (PhD Student): "Sorption of thallium on illite and birnessite and its impact on thallium solubility in soils". Start date: April 2016 (Funding: SNSF).

Dr. B. Cvetković (postdoc): "Development of C-14 AMS-based analytical methods for the identification and quantification of C-14 labelled dissolved and volatile organic compounds." (Funding: Swiss-nuclear).

Dr. G. Geng (PSI-FELLOW-II-3i postdoc): "Alkali-silica reaction in concrete." Start date: July 2017 (Funding: SNSF, EU Horizon 2020 Marie Skłodowska-Curie grant).

Dr. F. Marafatto (postdoc): "Cryo-microspectroscopy at the microXAS beamline for the investigation of redox- and radiation-sensitive samples." Start date: June 2017 (Funding: PSI/EAWAG).

Dr. D. Miron (postdoc): "Thermodynamik und Speziation von Actiniden bei höheren Temperaturen." Start date: April 2016 (Funding: BMBF, Germany).

Dr. R. Patel (PSI-FELLOW-II-3i postdoc): "Resolving carbonation mechanisms of cement-based

materials through multi-scale microstructural simulations." Start date: August 2017. (Funding: EU Horizon 2020 Marie Skłodowska-Curie grant).

Dr. G. Yang (PSI-FELLOW-II-3i postdoc): "Pore scale control of mineral precipitation: from atomistic model to macroscopic modelling and experimental observations." Start date: July 2017. (Funding: EU Horizon 2020 Marie Skłodowska-Curie grant).

Dr. A. Yapparova (postdoc): "COTHERM2 – combined hydrological, geochemical and geophysical modelling of geo-thermal systems II". Start date: April 2016 finalised May 2017 (Funding: SNSF).

Dr. Y. Chen has successfully defended her PhD thesis "Retardation of low-molecular weight organic compounds in clays" at the University of Bern (Defence date: 1st June 2017).

Dr. C. Wigger has successfully defended her PhD thesis "Anion Accessibility in Low Porosity Argillaceous rocks (ANPOR)" at the University of Bern (Defence date: 19th December 2017).

LES comprises four research groups located at PSI (organisation chart, Fig. 1.1). A fifth research group located at the "Institute for Geological Sciences" strengthens the collaboration with the University of Bern in the field of mineral dissolution kinetics, structural studies of high porous materials and X-ray diffraction based structure refinement. This expertise complements the LES traditional modelling and experimental capabilities. The research group in Bern is also included in the organisation chart.

In contrast to the previous LES annual reports, the current issue is organised in seven thematic research projects addressing specific aspects of repository geochemistry and radionuclide transport:

Chapter 2: Geochemical evolution of repository near field

Chapter 3: Development of mechanistic sorption models and experimental validation

Chapter 4: ¹⁴C speciation and transport in repository

Chapter 5: Radionuclides transport and retention in compacted systems at full and partial saturation

Chapter 6: Thermodynamic models and databases

Chapter 7: Cement-waste interaction and upscaling to the field scale

Chapter 8: Dissolution of spent fuel and vitrified waste.

The following section provides an overview of activities related to the Sectoral Plan for Deep Geological Disposal, repository near- and far field, reactivity of barrier systems and code benchmarking activities.

1.3 Sectoral plan for deep geological disposal

The potential radiological impact of a repository is one of the safety relevant criteria employed in the site selection process. Sorption and diffusion databases are the basis for such calculations. The sorption databases are derived based on thermodynamic calculations. Therefore, a "frozen" Thermodynamic Data Base (TDB) must be available before the development of the sorption databases and the modelling of the in situ repository conditions can start. A high quality core TDB is currently in place. This database needs to be kept state-of-the-art by periodic updates and filling remaining safety relevant data gaps. The thermodynamic data for Fe, Cu, Hg, Pb and Po have been reviewed in 2017. Other elements C (organic/inorganic), Si (silicate complexes), Nb, Mo, Pd, Sn, Eu, Ti, Cu, Ag, Sm, Ho, Ac, Pa and Cf will be reviewed in the following years. The data mainly stem from the NEA-reviews, which are known to be very thorough, and contain selected high quality data. However, a "blind" import of recommended NEA data without a scrutinising review of the remaining data can lead to erroneous results in thermodynamic calculations. For example, the use of the only NEA recommended data for iron lead to a wrong estimation of the Fe concentration in pore water, because of missing solubility controlling species in the database. (see section 6.2).

The release and retention of radionuclides in a repository will take place at 40-60 degree Celsius. Most of the available experimental data are limited to room temperature, however. Theoretically justified extrapolation methods for the evaluation of radionuclide's complexation constants at elevated temperatures can help to deal with the lack of experimental data. In the framework of the joint project ThermAc, financed by the German Federal Ministry of Education and Research (BMBF), a method of so called iso-coulombic reactions have been applied to evaluate thermodynamic properties of actinides at elevated temperatures using the standard thermodynamic properties (e.g. $\Delta_r G^0$) and some known thermodynamic relationships for similar (e.g. isocoulombic) reactions. To facilitate the data analysis, an additional module named "isocoulombic reaction generator" has been implemented in the GEMs package. This module generates all possible reactions having the same number of species with the same species charge for both products and reactants (see section 6.3). Further activities in this project include the development of an advanced user-friendly interface for managing thermodynamic data sets in the ThermoHub database, which was developed as a replacement of our former PMATCHC code.

Two reports summarizing sorption data and models for montmorillonite (NTB-17-13) and illite (NTB-17-14), respectively, were finalised in 2017. These reports form the basis for the development of sorption databases (SDBs) to be applied in the safety analysis of SGT-E3 for bentonite and Opalinus Clay (see section 3.1).

Irradiation of organic and inorganic waste forms results in the release of volatile molecules. The gas release during the irradiation of materials is characterised by the so called G-values, representing the number of gas molecules per 100 eV absorbed energy. These G-values are used to estimate the amount of gases produced by radiolysis in a repository for low- and intermediate-level waste. The currently used values are based on a database established back in 1992. This database was reviewed and updated based on the new data published in the period 1992-2017 (see section 6.4).

1.4 Repository near field

1.4.1 Repository chemistry

Dissolution of spent fuel and vitrified nuclear waste defines the radionuclide's release after breaching of the disposal casks in the repository for high-level radioactive waste. This source term has been therefore intensively studied for decades. The manufacturing recipe of nuclear fuels is evolving to improve the reactors performance. Thus, modern fuel types are doped with Cr or Al to increase the grain-size of the UO₂ particles. The use of such a nuclear fuel allows increasing the linear power rating of the fuels, thereby increasing the release of volatile nuclides as well as achievable burn-ups and modifying microstructural features of spent fuel. The effects of these changes on the release of radionuclides under repository conditions need to be understood and quantified. A four years EURATOM project DisCo addressing this issues has been approved by the European Commission in April 2017. The DisCo project has officially started on June 1st, 2017. The subproject hosted at LES focuses on thermodynamic modelling of chemical equilibrium in water saturated Cr/Al doped and MOX spent fuels under repository relevant conditions (see section 8.2).

The L/ILW repository contains a variety of materials embedded in a cement matrix. The barrier function of the cementitious near field is expected to change over time due to the interaction of hydrated cement with CO₂ produced by chemical degradation of organic waste forms, the corrosion of activated metallic waste and the interaction of highly alkaline cement pore water with silica aggregates present in concrete or by groundwater ingress from the host rock. The

modelling studies on the temporal evolution of waste packages launched in the year 2016 have been continued in 2017. These simulations aim at predicting the chemical conditions within selected waste packages over the time span of 100'000 years. The focus of the modelling in 2017 was on operational and decommissioning waste sorts. The operational waste sorts contain large amounts of organic materials, such as spent ion exchange resins or cellulose, whereas the decommissioning waste sorts are predominantly metals. Scenarios with both limited and unlimited water availability were taken into account. The first scenario is based on the assumption that the waste packages remain intact over a long time period ("closed system") while the second scenario implies that small openings (e.g. cracks, holes caused by pit corrosion, etc.) exist in the walls of the waste packages already at the start of waste emplacement in the deep geological repository ("semi-open system"). The two scenarios were modelled, either allowing for the formation of thermodynamically stable zeolites or assuming that zeolite formation is inhibited (see section 7.2).

1.4.2 Clay systems

The most successful and widely used mechanistic sorption model for clay systems (2SPNE SC/CE model) describes the retention of cations assuming a fixed density of surface sites and cation specific surface complexation constants. Experimental observations confirm that chemically similar cations (similar valence and hydrolysis constants) occupy the same sorption sites and thus are competitive. Recent analysis of experimental data further suggests that elements in different valence state can also be competitive and that the sequence of the elements addition may influence the retention. A series of experimental studies testing mutual effects of different elements are ongoing. Following general rules could be formulated based on the currently available experimental observations:

- Divalent metals (e.g. Ni, Co, Fe) are mutually competitive if introduced simultaneously. Partial competition has been observed, if the trace element is first allowed to react with the clay before the blocking element is added. However, even in this case ~ 90 % of the trace element is competitive.
- Trivalent metals (e.g. Am and Eu) are mutually competitive.
- Divalent and trivalent metals are essentially competitive if the trivalent element is the blocking radionuclide, and non-competitive, if the divalent metal is the blocking element.

The effect of sorption competition has far-reaching consequences for the development of sorption

databases for performance assessment. So far K_d values for performance assessment have been derived for trace concentrations of radionuclides neglecting the possible presence of other potentially competing ions. Appropriate consideration of sorption competition leads to a reduction of K_d values by 1 to 2 orders of magnitude. A general strategy for the development of a sorption database taking into account competition effects has been summarized in NTB-17-11. This report evaluates the effect of competition on the sorption values of the SDBs used in SGT-E2, and provides a scientific basis for the development of SDBs for the SGT-E3 (see section 3.2).

Several studies of uranyl (U^{VI}) uptake on purified illite show an unexpected sorption enhancement which could not be described by the 2SPNE SC/CE model. An EXAFS study conducted in collaboration with ROBL/HZDR demonstrated that this anomalous behaviour could be attributed to U uptake by an apatite-like mineral which is present at a level below the detection limit of common analytical methods such as XRD or TEM. These results demonstrate that accessory phases might substantially contribute to the sorption in poly-mineral rocks. Therefore, the development of reliable sorption models requires experimental data covering large ranges of geochemical conditions and also a mechanistic understanding of the retention processes (see section 3.2.2).

Ferrous iron (Fe^{II}) in clay minerals may reduce redox sensitive radionuclides such as Np^V (NpO_2^+) at their surface, thereby considerably increasing the retardation factor. The influence of Fe^{II} on the uptake of Np^V by montmorillonite (SWy) was studied on natural and chemically reduced SWy. Combined wet chemical and X-ray absorption spectroscopy studies (ROBL/HZDR) showed that Np^V was the sorbing species on native SWy whereas much stronger sorbing Np^{IV} was the dominant surface species on the reduced SWy. The sorption of Np^V on the reduced SWy was found to be up to four log units higher compared to the sorption on the natural (oxidized) SWy. Principal analysis of all reduced SWy spectra suggests the formation of only one distinct Np species (see section 3.2.3).

In the past, the 2SPNE SC/CE sorption model has been successfully tested for different types of elements, clay minerals and poly-mineral rocks. Further validation of the model continued within a SNSF-funded collaborative project between LES and Eawag (A. Voegelin): "Sorption of thallium to illite and birnessite and its impact on thallium solubility in soils". In this project $NH_4^+Tl(I)$ sorption was measured on homoionic Na-, K-, and Ca-illites. The data could

be successfully modelled using three different sorption sites on Na-, K-, NH₄- and Ca-illites (see section 3.2.4).

Molecular mechanism of Fe uptake by clay minerals is investigated in the framework of a SNSF funded PhD project: "Detailed understanding of metal adsorption on clay minerals obtained by combining atomistic simulations and X-ray absorption spectroscopy". Ab initio molecular dynamics simulations were applied to investigate the mechanism of iron incorporation into bulk montmorillonite. Using a linear combination fit resulted in a consistent interpretation of calculated and measured Fe-EXAFS and Fe-XANES spectra of iron incorporated into Milos-montmorillonite. Simulations of Fe adsorbed on the edge sites of montmorillonite are still ongoing (see section 3.2.6).

Current performance assessment studies consider ¹⁴C-bearing molecules as non-retarding. In a PhD project partially supported by Nagra, it has been demonstrated that aliphatic or hydroxylated carboxylic acids and alcohols are retarded by pure clay minerals and their mixtures to an extent that would actually lead to a considerable reduction of the predicted radiation dose. The analysis of the relationship between the observed retardation and structural properties of the test compounds suggested that ligand exchange at aluminol sites are most probably involved in the binding of hydroxylated carboxylic acids and dipole interactions in the uptake of alcohols. The results observed in single-clay systems (kaolinite or illite, respectively) could be successfully used to predict the behaviour of the test compounds in kaolinite/illite mixtures. The transferability of the results from single-clay mineral systems to compacted clay rocks by means of the component additivity approach was found to be challenging. It was not possible to confirm a generic positive sorption distribution value for different organic ¹⁴C-bearing compounds in an intact Opalinus Clay samples (see section 4.4).

Dissolved CO₂ reacts with water to form carbonate and bicarbonate ions. Through-diffusion experiments in Opalinus clay samples from the Mont Terri rock laboratory were set up to evaluate the retention of ¹⁴C transported in an inorganic form as carbonate ions. A rapid exponential decay of ¹⁴C concentration in the source reservoir has been observed. However, ¹⁴C could not be detected in the downstream reservoir so far. Such behaviour could indicate a strong retention of HCO₃⁻/CO₃²⁻ ions by re-crystallization of carbonate minerals. In a similar experiment performed in a compacted illite with admixture of carbonates, a ¹⁴C breakthrough could be observed after 5 days and a steady state was reached after 15 days. In the same experiment, no significant effect of calcite addition

could be observed. Modelling of the data is currently ongoing (see section 4.4).

1.4.3 Cement systems

Carbon-14 has been identified as a major contributor to the long-term release of radioactivity from a cement-based repository into the host rock. Corrosion of activated steel is the main source of ¹⁴C in the Swiss waste disposal system. The mobility of the ¹⁴C depends on its speciation. While the overall ¹⁴C inventory in the radioactive waste is well known, the chemical form of ¹⁴C-bearing compounds is poorly understood. The speciation of the ¹⁴C-bearing molecules is investigated in the framework of the project: "Investigation of the chemical speciation of ¹⁴C released from activated steel" (partial financial support by Swissnuclear and the EU FP7 collaborative project "CAST" (CARbon Source Term)). The development of a corrosion reactor and the testing of a sampling system have been completed. The first corrosion experiment with activated steel was started in May 2016 with the aim to identify and quantify the ¹⁴C-bearing compounds present in the gas and liquid phase using compound-specific ¹⁴C accelerator mass spectrometry (¹⁴C AMS, co-operation with PD Dr. S. Szidat and Dr. G. Salazar (Department of Chemistry & Biochemistry at the University of Bern, Switzerland)). Since the beginning of the corrosion experiment with the activated steel, samples have been taken after 1, 15, 29, 93, 286 and 412 days reaction time. An extensive analytical protocol was applied to determine several parameters that are related to the identification and quantification of organic compounds, e.g. individual ¹²C and ¹⁴C compounds in the liquid phase by ion chromatography (IC) and in the gas phase by gas chromatography (GC), both with mass spectrometry detection (MS), total organic carbon (TOC) of the liquid phase, and the total content of ¹⁴C-bearing organic compounds (TO¹⁴C). Furthermore, the total ¹⁴C and ⁶⁰Co activity were quantified by liquid scintillation counting and by gamma counting, respectively.

Analysis of the first series of samples between 1 and 93 days showed that the concentration of the individual organic compounds in the liquid and gas phase is below or close to the detection limit of IC-MS and GC-MS, respectively. Only methane was identified as carbon species in the gas phase after 93 days reaction time. In the liquid phase formate and lactate were clearly identified at concentrations significantly above the detection limit. Oxalate and glycolate were identified at concentrations close to the detection limit. At present, the concentration of the ¹⁴C-bearing gaseous compounds in the corrosion experiment cannot be determined using standard GC-MS as their concentrations are below the detection

limit of the analytical technique. The methodology for compound-specific ^{14}C AMS detection in the gaseous phase is currently under development. The installation of a fraction sampling system for the gas phase has been completed (collaboration with Brechbühler AG, Schlieren, Switzerland). The recovery tests and final optimization of the entire sampling system is planned for 2018 (see section 4.2).

^{14}C -containing low molecular weight (LMW) organic molecules released during the corrosion of activated steel may be thermodynamically unstable under the hyper-alkaline, reducing conditions prevailing in a cement-based L/ILW repository and could eventually be transformed into CH_4 or CO_2 and its bases). The kinetics of these transformation reactions is very slow and thus complete thermodynamic equilibrium is rarely achieved in the C-H-O system at repository relevant temperatures. The chemical stabilities of formate and acetate in hyper-alkaline, anoxic and reducing conditions are currently being studied with the aim to obtain a better insight in the degradation kinetics of LMW organic molecules under cementitious near-field conditions. Degradation of formate and acetate could not be detected in pure water at anoxic conditions (stainless steel surface as a catalyst, temperatures up to 150°C and N_2 atmosphere) over time period of up to 8 months. A new series of experiments was carried out in 2017 under reducing conditions and at elevated temperature (up to 200°C), either in the presence of Fe powder as a reducing agent or under 2 atm gas pressure maintained by a mix of N_2 (95%) and H_2 (5%). A steady decrease of the formate concentration in the reactor could be observed over a period of 60 days both in Milli-Q water and in artificial cement water (ACW). Subsequent experiments with different alkali content in the liquid phase and pH has shown that formate is more readily decomposed at alkali conditions, especially in the presence of Ca ions. This finding contradicts literature data, which suggest that formate degradation is slower at high pH than at near-neutral pH. The reason for these inconsistencies is presently unknown. In the next step of this project, the analytical procedure for the gas phase will be improved with the aim to analyse not only the hydrocarbons in the gas phase but also the oxidized species CO and CO_2 (see section 4.3).

The immobilization of selenium and iodine in AFm phases is investigated in the framework of a joined PhD study with Empa (B. Lothenbach) funded by the Horizon 2020 EC project "Cebama". In this project pure AFm phases with various intercalating anions (OH^- , CO_3^{2-} , SO_4^{2-} , SO_3^{2-} , $\text{S}_2\text{O}_3^{2-}$, SeO_4^{2-} , SeO_3^{2-} , I^-) were successfully synthesized. These phases were characterized with the help of different techniques

(XRD, TG, IR, aqueous phase analysis) and their solubility were determined. Experiments in binary systems showed that solid solutions were formed in $\text{SeO}_3\text{-SO}_4$, $\text{SO}_3\text{-SO}_4$, I-CO_3 , I-OH-CO_3 , systems. (see 3.2.5).

Large quantities of metallic waste in a L/ILW repository will form corrosion products that interact with cement minerals. Current thermodynamic databases used to describe the interaction of iron corrosion products with cement pastes under reducing conditions are very limited. Magnetite (Fe_3O_4) and pyrite (FeS_2) are the only products currently considered in conjunction with iron corrosion in anoxic alkaline conditions. A PhD project financed by the SNFS grant No 200021_162342) was started in 2016 with the aim to critically assess Fe(II) interaction with cement phases. Preliminary studies indicate that Fe(II) is chemically very unstable in alkaline solutions and readily oxidizes to Fe(III). As a consequence, the experimental set-up for sorption studies with Fe(II) has been modified and an electrochemical cell is used to control the redox stability of Fe(II). Furthermore, the spectroscopic characterisation of Fe(II) doped calcium silicate hydrate (C-S-H) samples has to be conducted under cryogenic conditions to prevent beam-induced redox reactions (see section 7.4).

1.4.4 Interfacial processes

A multi-barrier concept is applied to ensure safe disposal of radioactive waste. Each barrier is optimised to fulfil a certain retention function. However, barrier materials are not in thermodynamic equilibrium with each other and will undergo slow chemical transformations. These chemical reactions result in changes of transport properties of materials and interfaces. The overall chemical evolution of a repository and the performance of multi-barrier systems are evaluated based on numerical simulations, and by dedicated experiments.

Fully coupled thermo-hydraulic-chemical (THC) simulations of two-phase mass transport with a complex chemistry in heterogeneous 2D and 3D systems are currently not feasible. We therefore developed a simplified "look-up table" based approach, which replaces numerically expensive calculations of complex chemical equilibria in reactive transport calculations, and in the same time allows an efficient description of the degradation processes in heterogeneous cementitious systems. In cooperation with the Helmholtz Centre for Environmental Research – UFZ, Leipzig, Germany (Dr. Y. Huang and Dr. H. Shao), the look-up table approach was implemented in a new multi-component multi-phase solver platform OpenGeoSys-6. Degradation processes considered in the model are the

Alkali-Silica-Reaction (ASR) and carbonation due to ingress of CO₂. The look-up table defines source and sink terms for gases, specifically H₂, CH₄ and CO₂ (gas consumption/production due to (bio)-chemical reactions), changes in porosity (due to mineral precipitation/dissolution reactions), and source and sink terms for water (water consumption/production due to (bio)-chemical reactions). These source and sink terms provide a feedback mechanism for a reactive multi-phase multi-component transport model. The state of concrete degradation can be estimated based on the amount of CO₂ that is consumed in a specific concrete volume and the amount of SiO₂-containing aggregate reacted within the same volume over time. The approach has been successfully validated against a fully coupled one dimensional set-up (see section 7.3).

The ASR is the interaction of the alkaline pore solution of concrete with silica rich aggregates. The ASR products can accumulate water and swell, consequently generating stress and cracks. These reactions may occur in certain types of conditioned waste in the cementitious repository. The structure of the ASR products and the structural transformations during the ASR is investigated by state-of-the-art synchrotron spectroscopic techniques within a SNSF funded Sinergia project conducted by a consortium of research teams from EMPA, EPFL and PSI (see section 7.5).

Chemical and mineralogical data from cement clay interfaces reacted for 2, 5 and 8 years (CI experiment at the Mont Terry test site) were modelled with OpenGeoSys-GEM using the most advanced thermodynamic model for cement systems. The project focused on comparing modelling results with the experimental findings and on a sensitivity study with respect to the thermodynamic databases and the transport parameters assigned to the interface. Particularly challenging turned out to be the modelling of the experimentally observed magnesium profiles that were found to form a high concentration anomaly near the Opalinus Clay/ ordinary Portland cement (OPC) interface after a period of 5 years. The magnesium anomaly could be modelled but its predicted location was slightly different from the experimental observations. The modelling suggests that the anomaly is related to the precipitation of magnesium silicate hydrate (M-S-H) phases. The main driving force for Mg accumulation is the alkali diffusion from the OPC into the Opalinus Clay, which changes the cation exchange occupancy and releases magnesium into the porewater. Because the magnesium concentration in the Opalinus Clay porewater is higher than in the OPC, magnesium diffuses towards the OPC. The evolution Mg

concentration profile is linked to the pH front progressing from the cement side, as the increased pH causes the subsequent precipitation of Mg-bearing phases like hydrotalcite, M-S-H or brucite. The rate of the front propagation depends on several factors such as cation exchange reactions, mineral surface charge and kinetics of mineral reactions. Therefore, it is expected that more detailed experimental information on the nature of the phases that cause the magnesium anomaly could further improve and constrain the modelling and improve the model predictions (see section 2.2).

Mineralogical and porosity changes at the cement-clay interface and their subsequent effect on transport parameters are further investigated at a micrometer scale in the framework of the Nagra supported PhD project: "Evolution of transport properties, mineralogy, and porosity of cement-clay interfaces" (P. Luraschi). Goal of the project is to investigate the interaction between various cement and clay materials by means of neutron imaging and diffusion experiments. One set of montmorillonite-OPC samples originates from a former PhD project on cement-clay interfaces. In addition, new samples are prepared using different clays (e.g., crushed and re-compacted Opalinus Clay, intact Opalinus Clay, bentonite) and different cements (e.g., OPC, ESDRED, both hardened and fresh). Furthermore, samples from the 3rd and 4th sampling campaigns of the CI experiment have been obtained. Through-diffusion experiments with HTO performed on several >4 years old Na-montmorillonite-OPC interfaces showed a further decrease of the flux with reaction time. This observation suggests that the precipitation-dissolution processes at the interface were ongoing for more than 4 years. To achieve more precise and detailed information regarding porosity changes, the samples were analysed by neutron radiography at PSI. Radiography data and D₂O diffusion experiments are currently under evaluation (see section 2.2.1).

1.5 Repository far field

Experimental sorption studies conducted on dispersed systems are the basis for the development of sorption models. Argillaceous rocks and compacted clays are very dense and are characterised by a high solid-to-liquid ratio. It is still questionable whether the data and models derived for dispersed systems are directly applicable to highly compacted natural rocks. Because of the complexity of pore microstructure in clay minerals and clay rocks, answers to this question have to be given on a case-by-case basis. A set of sorption experiments with different nuclides performed on compacted systems is ongoing.

In-diffusion experiments with Eu(III) on compacted homo-ionic Na-illite were performed at a broad range of experimental conditions including variations of pH, ionic strength, stable Eu(III) concentration, and the use of selected ligands. A good agreement between the R_d values measured in dispersed suspensions of Na-IdP-B and the results of in-diffusion experiments as a function of pH at a constant background electrolyte concentration of 0.1 M could be obtained using a modified 2SPNE SC/CE model. The modified model replaces the cation exchange by an electrical double layer (EDL). The EDL species included in the Stern-layer are considered as immobile, and those in the diffuse layer are considered as mobile. Analysis of the experimental data indicates that the D_e and R_d values for Eu(III) are not linearly correlated. This is in clear contrast to the observations made for the diffusion and sorption of cations preferentially adsorbed by cation exchange mechanism. Therefore, the use of apparent diffusion coefficients, which are directly proportional to the ratio of D_e/R_d for strongly sorbing species, determined for a particular set of boundary conditions (pH, ionic strength, etc.) may not be valid for other chemical environments. A careful analysis of the dependence of apparent diffusion coefficients on the chemical conditions in the liquid phase may therefore be required for the application of data to the performance assessment studies. A consistent description of the tracer depletion in the reservoir solution and the tracer profiles in the clay could only be obtained taking the mobility of sorption species into account. Neglecting the surface mobility leads to strong underestimation of diffusion profiles. It can therefore be concluded that the use of effective diffusion coefficients derived from proportionalities of bulk-water diffusion coefficients will not lead to conservative predictions of dose rates in performance assessment for surface complexing cations (see section 5.3).

The effect of sorption competition on the radionuclide mobility has been further investigated by generic calculations of radionuclide breakthrough at the bentonite/OPA interface using the 2SPNE SC/CE sorption model. The consequences of sorption competition between tri- and di-valent cations were evaluated in detail. The model set-up sums up all trivalent cations in solution at the "canister-bentonite-interface" and assumes an instantaneous radionuclide release after 10'000 years. The calculations suggest that sorption competition can lead to up to one order of magnitude earlier breakthrough compared to the scenario neglecting sorption competition (see section 5.6).

Anion accessible porosity is an important parameter in performance assessment studies controlling the

prediction of anion mobility in compacted bentonite and clay rocks. The nature and transport properties of pores in Swiss and Canadian host rocks have been investigated in the framework of a PhD project funded by NWMO (Canada). Three kinds of pores could be identified based on the diffusive behaviour of ^{36}Cl and HTO. In the Opalinus Clay ~23% of pore space is permanently accessible for anions, independent of the pore water composition (ionic strength). Approximately 40% of pores are inaccessible at any pore water compositions. These pores were understood as interlayer equivalent pores and bottleneck pores. The rest of the pore space represents a Donnan space, in which anion accessibility depends on the overlap of diffuse double layer controlled by the background electrolyte (see section 5.7).

1.6 Model development and code benchmarking

The benchmarking and verification of reactive transport coupled codes is an ongoing activity which is necessary to demonstrate the credibility of numerical simulations, and improve the description of complex geochemical interactions and/or radionuclide transport in a nuclear waste repository. Mineral reactions generally lead to changes in total porosity and pore-space connectivity. The most common approach used in reactive transport simulations is to correlate the changes in total porosity to permeability and diffusivity using the Kozeny-Carman and Archie-like relationships, accordingly. Such correlations are theoretically justified only for most simple systems of spherical particles. Real porous media are much more complex. Various experimental observations including reacting interfaces indicate that localized precipitation may reduce diffusivity and permeability by orders of magnitude, while total porosity remains essentially unchanged. Direct pore scale simulations of porosity evolution and consequent evaluation of the diffusivity and permeability relationships are a promising alternative to the use of empirical equations. To this end, a pore-scale reactive transport model has been developed which takes into account the homogeneous and heterogeneous nucleation of minerals and ion transport based on a Lattice-Boltzmann simulation technique (see section 2.5).

LES further participates in an on-going SeS Benchmark initiative: "A benchmark for mineral dissolution at the pore scale", proposed by S. Molins (LBNL, USA), C. Soulaine (Stanford, USA) and D. Trebotich (LBNL, USA). The aim of this initiative is to test the performance of different reactive transport codes with a well-defined dissolution experiment. The experimental set-up describes the acids inflow dissolving a spherical calcite grain in a cylindrical channel. The reaction results in changes in flow field, shape of the solid and evolution of the pH profile.

LES applies an in-house developed reactive transport Lattice Boltzmann simulator. Remarkably, a grid convergence of the LES code could be demonstrated for a core grid with 128x64 elements. This illustrates that our model can be efficiently applied to very complex geometries at low computational costs (see section 2.6.1).

Clay rocks are composed by aggregates of clay particles with a complex geometry of interconnected pore space. The negatively charged clay mineral surfaces result in accumulation of cations close to the mineral fluid interface and repel anions, thus reducing the pore space available for the negatively charged ions. Explicit consideration of the inhomogeneous ions distribution in pore space is essential for the correct description of cations and anions fluxes in clays. In a Ph.D. project "Modelling transport across reactive interfaces" a reactive transport toolbox that couples electrochemical transport in porous media at the level of the Nernst-Planck equation with state-of-the-art geochemical solvers has been developed. The code was successfully validated against simplified chemical systems and is currently applied to simulate ion transport in two dimensional systems (see section 2.3.2).

A model of Donnan equilibria has been tested on experimental data from Mont Terri and on laboratory

diffusion experiments. The new model implemented in the FLOWTRAN code allows to investigate the role of ion mobility in the Donnan space. The simulations demonstrate that a set-up with full mobility of ions in the Donnan space substantially overestimate the fluxes. In contrast the fluxes are underestimated if ions in the Donnan space are considered as immobile. The best results were obtained assigning partial (reduced) mobility to the ions in the Donnan space (see section 2.4.1).

In reactive transport simulations, chemical equilibrium calculations are performed in every mesh cell at each time step. These calculations usually take 10–100 times more computational resources than that of the transport model. Hence, any effort in developing fast-converging numerical solvers for chemical equilibrium will substantially speed up reactive transport simulations. To this end, an unconventional On-Demand Machine Learning (ODML) approach has been developed and tested for a model reactive transport set-up involving a 1-D reactive transport experiment (Collaboration with Dr. A. Leal, ETHZ). Using such an algorithm speeds up the simulation time up to two orders of magnitude. Application of this approach thus opens up the opportunity for fully coupled simulations in 2D or 3D (see section 2.7.1).

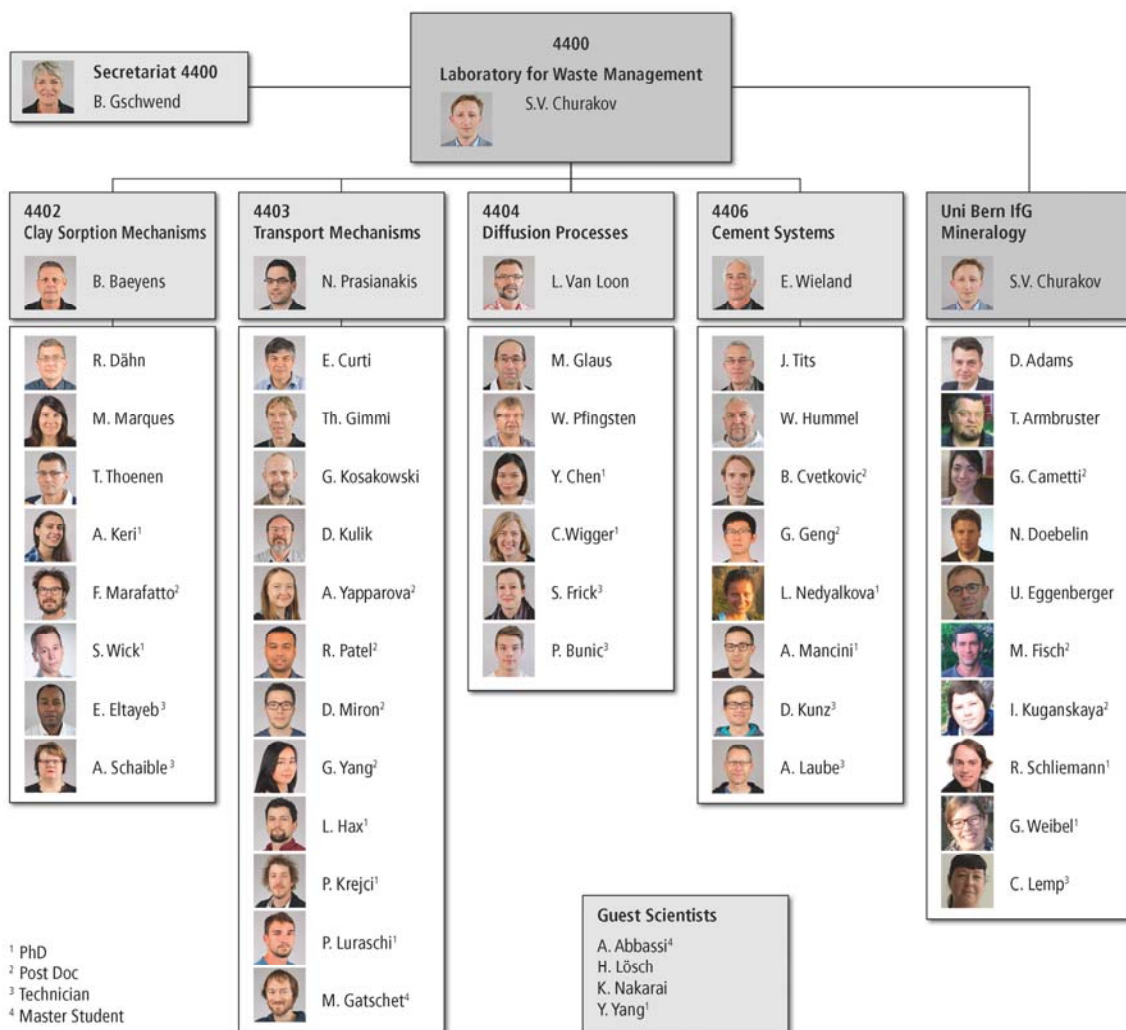


Fig. 1.1: Organisation chart of LES.

2 GEOCHEMICAL EVOLUTION OF REPOSITORY NEAR FIELD

N.I. Prasianakis, S.V. Churakov, L.R. Van Loon, E. Curti, Th. Gimmi, A. Jakob, G. Kosakowski, D. Kulik, P. Bunic, S. Frick, K. Nakarai (guest Professor), D. Miron (postdoc), G. Yang (Postdoc), R. Patel (Postdoc), L.H. Damiani, (PhD), Ph. Krejci (PhD), P. Luraschi (PhD), Y. Yang (exchange PhD student), A. Abbasi (master student), M. Gatschet (master student)

2.1 Introduction

This project aims at providing model based descriptions for the long-term evolution of the repository near field with different conceptual design of the multibarrier system. This expertise is essential for the site selection process in the Sectoral Plan for Deep Geological Disposal (SGT) Stage 3 and the following general license application. The project is focusing on three main topics: 1) Numerical modelling of the evolution of the technical barriers and their respective interfaces e.g. cement evolution and cement-clay interaction; 2) Interpretation of completed, running and preparation of future experiments at Underground Rock Laboratory (URL) at the MontTerri testsite 3) Multiscale modelling and upscaling of parameters relevant for reactive transport phenomena. The benchmarking and application of state-of-the-art coupled codes as well as the development and coupling of thermodynamic modelling and database tools are an integral part of these activities. Overarching thematic contributions and modelling support is provided in the area of radionuclides retention in host rock, heterogeneities, uncertainties and diffusion in disperse/compacted systems.

To test the models at the field scale, group members participate in the experimental and modelling projects conducted at the URL Mont Terri which explores the interaction between Opalinus Clay and three different types of concrete. The experiment has been modelled using the OpenGeoSys-GEM coupled code and advanced quantitative comparison of mineralogical profiles produced by the reactive transport models has been completed.

Mineralogical and porosity changes at interfaces of technical barriers (e.g. cement-clay) have an impact on the diffusion processes and on the overall geochemical evolution of the waste repository. Within the Nagra supported PhD project: "Evolution of transport properties, mineralogy, and porosity of cement-clay interfaces" (P. Luraschi), the interaction between various cement and clay materials is investigated by means of neutron imaging and diffusion experiments. LES participates in the HORIZON 2020 Collaborative Project "Cement-based materials, properties, evolution, barrier functions" (CEBAMA) with 2 PhD projects. In 2017, the PhD project "Modelling transport across reactive

interfaces" (L. Hax Damiani) continued with the development of a reactive transport solver that combines Nernst-Planck electrochemical transport in porous media with state-of-the-art geochemical solvers. The ability of reactive transport codes to predict clogging processes can be enhanced and verified via specifically designed laboratory experiments. Prof. Kenichiro Nakarai from Hiroshima University spent his sabbatical at PSI to investigate the effect of admixtures on porosity reduction in clay. In his project, he conducted both HTO diffusion experiments and neutron radiography measurements.

The understanding of the degradation mechanisms of cementitious materials plays an important role in predicting the service life of concrete structures. The PSI-FELLOW-II-3i project "Resolving carbonation mechanisms of cement-based materials through multiscale microstructural simulations" (R. Patel) was initiated in 2017. This project aims at developing a multiscale microstructure model describing the carbonation process of cement-based materials under saturated and unsaturated conditions. Complementary, the project "Ion transfer mechanisms in clay and cement materials" (guest PhD student Y. Yang) is a collaborative project between LES, PSI and Tsinghua University, Beijing, China (Prof. M. Wang group, Department of Engineering Mechanics) which focuses this year on the description of ion transport in gel pores of cementitious materials.

The further improvement of the predictive capabilities of reactive transport codes can be achieved through multiscale modelling of the transport mechanisms and a subsequent upscaling. The PSI-FELLOW-II-3i project "Pore scale control of mineral precipitation: from atomistic model to macroscopic modelling and experimental observations" (G. Yang) was initiated in 2017. This activity aims at applying reactive transport multiscale modelling for the study of dissolution and growth in porous media after gaining insight into the mechanical processes that govern cations retardation, such as cations diffusion, kinetic sorption, and anion exclusion. Fluid-density functional theory (DFT) calculations and molecular dynamics results will be upscaled to the pore-level reactive transport codes. Pore-level Lattice Boltzmann modelling was able to reproduce the evolution of a reactive transport experiment which involved simultaneous dissolution and precipitation processes under the presence of

strong chemical gradients (PRASIANAKIS et al. 2017). At the same time, pore-level methods offer the ideal modelling framework to extract more accurate porosity-permeability correlations for upscaling purposes, once the microstructural geometry is sufficiently represented.

The benchmarking and verification of reactive transport coupled codes is an ongoing activity in LES. Among other benchmarks, LES participates in the ongoing Subsurface Environmental Simulation Benchmarking (SeS Benchmark) initiative: "A benchmark for mineral dissolution at the pore scale".

In reactive transport modelling, calculations of partial chemical equilibria in every mesh cell at each time step usually takes 10–100 times more time than that of the transport model, especially when complex chemistry is necessary. In collaboration with Dr. A. Leal and Prof. Dr. Martin Saar (GEG IG ETHZ). LEAL et al. presented an unconventional On-Demand Machine Learning (ODML) approach, in which most equilibrium states are quickly and accurately predicted from the results of previously performed GEM equilibrium speciation calculations. This much promising method is shown in specific cases to bring down the cost of chemical calculations to a level comparable to that of the transport itself thus significantly reducing the overall computational cost. GEM Software (GEMS, lead scientist D.A. Kulik) development has been continued and a number of training courses took place in Switzerland and abroad.

2.2 Modelling of the Mont Terri Cement Interaction (CI) experiment

The still ongoing Cement Interaction (CI) experiment is part of the Mont Terri Project, the underground research laboratory in Switzerland which is dedicated to investigating the Opalinus Clay formation. This geological formation is investigated as the host rock for deep geological disposal of radioactive waste. The CI experiment is dedicated to investigations of mineral reaction and porosity changes at the interface

of Opalinus Clay with different cements and concretes. Two boreholes in the Opalinus Clay formation were filled with sections of three different types of concrete and bentonite. Characteristic samples were extracted after 2.2, 5 and 8 years of interaction. The latest experimental results from the CI experiment are described in MÄDER et al. (2017) and JENNI et al. (2017).

The modelling of the evolution of cement/clay interfaces from the CI experiment using the OpenGeoSys-GEM code reached the final phase in 2017. The efforts were focused on comparing the new experimental results along with a sensitivity study to investigate the experimentally observed magnesium anomaly which was found near the Opalinus Clay/ordinary Portland cement (OPC) interface after a period of 5 years. The position of the anomaly with respect to the interface is verified by experimental findings (4-6 mm in the clay side, according to MÄDER et al. 2017), but the constitutive phases are not yet identified.

The presence of magnesium anomalies can be predicted from our models, but typically the location of the magnesium silicate hydrate (M-S-H) precipitation occurs first at the interface with a secondary anomaly appearing in the side of Opalinus Clay 10-15 mm deep, as shown in Fig. 2.1. Similar to the model of JENNI et al. (2017) the anomaly further away from the interface is caused by the precipitation of hydrotalcite, by the Fe rich end-member of the hydrotalcite solid solution (pyroaurite). The model of JENNI et al. (2017) uses slightly different thermodynamic data and different kinetic control on M-S-H and brucite. Therefore, in that model brucite precipitation was observed instead of the M-S-H precipitation at the interface. Interestingly, both models, ours and the one from JENNI et al. (2017), predict precipitation of magnesium hydrates or magnesium hydro-silicates at the interface which has not been experimentally observed in the case of OPC.

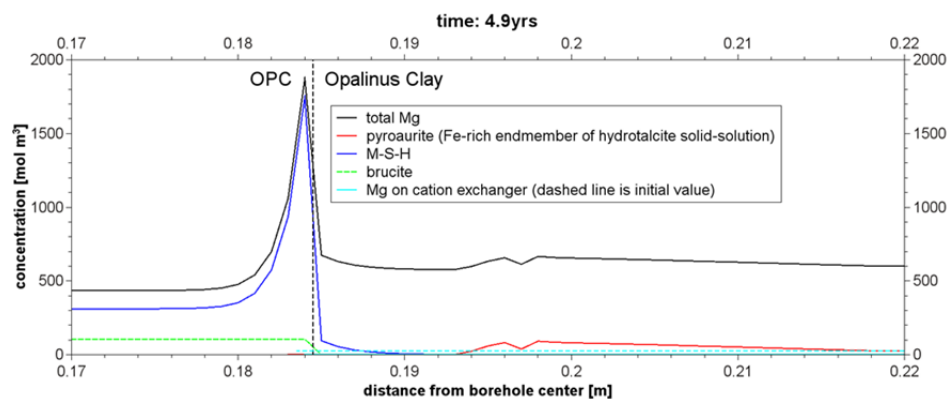


Fig. 2.1: Profiles across the OPC/Opalinus Clay interface. Profiles of total Mg, Mg in pyroaurite, Mg in M-S-H, Mg in brucite and Mg in the cation exchanger.

This Mg anomaly in the model seems to be caused by a combination of several coupled processes. The main driving process is the alkali diffusion from the OPC into the Opalinus Clay, which changes the cation exchanger occupancy and releases magnesium into the porewater. Since the magnesium concentration in the Opalinus Clay porewater is higher compared to the one in the OPC, the magnesium is generally diffusing towards the OPC.

In addition, a pH front originates from the OPC and triggers the dissolution of minerals. The occurrence of the anomaly is linked to the pH front, as the increased pH causes the subsequent precipitation of magnesium bearing phases like hydrotalcite, M-S-H or brucite. The movement of the alkali- and the pH front are also linked with the flux across the interface.

The propagation might be different, as fronts are affected by different processes: pH is buffered by mineral reactions and the alkali front is retarded by cation exchange reactions. Several parameters can be chosen during the model set-up: a) the precipitation and dissolution of minerals and pH, b) the diffusion coefficients, c) existence of mineral surface charge affecting the d) kinetic control of mineral reactions, e) the selectivity coefficients for the cation exchanger, and f) the mineral phases. Therefore, it is expected that more detailed experimental information on the nature of the phases that cause the magnesium anomaly could further support the modelling activities in order to improve the predictions.

The reactive transport code OpenGeoSys-GEM is an active development in co-operation with the Department Environmental Informatics (Prof. O. Kolditz) at the Helmholtz Centre for Environmental Research (UFZ, Leipzig, Germany). In 2017 development on OpenGeoSys-GEM concentrated mostly on benchmarking and bug fixing.

2.3 Cement-clay interaction, technical barrier evolution, modelling and experiments

2.3.1 Cement-clay interfaces: evolution of transport properties, porosity and mineralogy

Mineralogical and porosity changes at the cement-clay interface and their subsequent effect on transport parameters are further investigated at a micrometer scale in the framework of the Nagra supported PhD project "Evolution of transport properties, mineralogy, and porosity of cement-clay interfaces" (P. Luraschi). Goal of the project is to investigate the interaction between various cement and clay materials by means of neutron imaging and diffusion experiments. In addition, the composition of fresh and aged interfaces will be characterized analytically to correlate the measured changes in transport properties and porosity with chemical and mineralogical changes. In the last part of the project the obtained data and observed features will be integrated in reactive transport simulations to model the complex interaction of the cement-clay system. In this project investigations of the montmorillonite-OPC samples will be continued and at the same time new types of interfaces will be produced and analyzed.

The new samples will be prepared from different clays (e.g., crushed and re-compacted Opalinus Clay, intact Opalinus Clay, bentonite) and different cements (e.g., OPC, ESDRED, both hardened and fresh). Furthermore, samples from the 3rd and 4th sampling campaigns of the CI experiment have been obtained. Through-diffusion experiments with HTO were performed on several >4 years old Na montmorillonite-OPC interfaces.

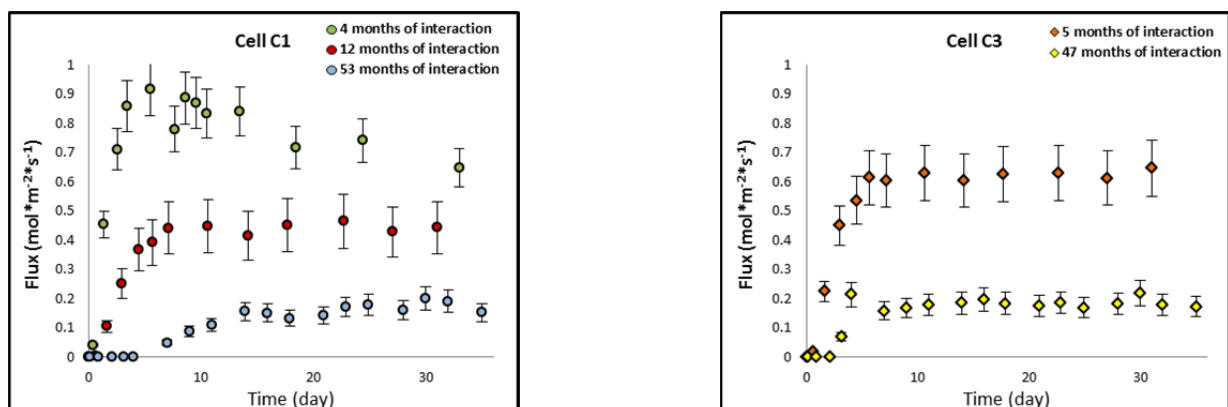


Fig. 2.2: Results of HTO diffusion experiments for two cells (C1 and C3) at different times. A decrease of the flux with increasing reaction time of the interface is observable; after 4 years of interaction the flux is significantly reduced in both cases. The reason for the later breakthrough of HTO in cell C1 after 53 months of interaction is not yet clear.

Results are plotted in Fig. 2.2 and show a further decrease of the flux with time. This fact suggests that the precipitation-dissolution processes at the interface were ongoing for more than 4 years. To achieve more precise and detailed information regarding porosity changes, the samples were analysed at the source for cold neutrons at PSI (ICON). Radiographies and D₂O diffusion experiments were performed on new and old interface samples; the data are currently under evaluation. Moreover, during the measuring campaign neutron tomographies have been obtained for the first time for two samples. This technique is expected to give complementary information regarding porosity distribution in three dimensions.

In order to characterize the mineralogical and chemical changes at the interface several samples have been prepared in collaboration with the University of Bern for scanning electron microscopy SEM analysis and are currently under examination. Finally, new experiments with HTO combined with an anion tracer to further investigate the porosity evolution at the interface are planned to be performed.

2.3.2 Electrochemical transport across reactive interfaces

In the Ph.D. project "Modelling transport across reactive interfaces" L. Hax Damiani developed a reactive transport solver that combines electrochemical transport in porous media with state-of-the-art geochemical solvers. The software will be used to model electrochemical transport across reactive interfaces. This project is part of a HORIZON 2020 Collaborative Project CEBAMA.

The newly developed NPS code is a Nernst-Planck reactive transport solver based on the finite element framework FEniCS (ALNÆS et al. 2015) and on the chemical equilibrium solver Reaktoro (LEAL et al. 2016). NPS was successfully validated using several benchmarks (HAX DAMIANI et al. 2017). The transport code (without reactions) was used to model the diffusion of ions in a constricted pore. At the bottleneck, the pore surfaces are charged as shown in Fig. 2.3. Such a geometrical set-up is typical for interlayers and outer surface contacts of certain cement and clay minerals (see WIGGER et al. 2017). Very often the constriction surfaces have a fixed negative potential, whereas the other pore surfaces are uncharged. The surface charge is compensated by an abundance of cations and a lower concentration of anions near the surfaces.

The accessible porosity of anions in such media is influenced directly by the ionic strength of the solution and the minimum pore diameter which is related to the degree of compaction for clay materials

(VAN LOON et al. 2007). The spatial extension of the electric potential does not only depend on the surface charge, but it is also influenced by the ionic strength of the solution. Therefore, the pore volume which is accessible for anions directly depends on the ionic strength of the solution and on the distance between charged surfaces, which can be for example manipulated by compaction of clays (VAN LOON et al. 2007).

With a steady state 2D model, the diffusion of NaCl in the presence of a constriction with charged surfaces was investigated. The NaCl concentration was fixed at 5 mol/m³ on the left boundary, and at 1 mol/m³ on the right boundary. The electric potential was set to -0.03 V at the charged mineral surfaces and to 0V on the right and left boundaries to ensure electro-neutrality of the ion fluxes across boundaries. Results of the calculation are shown in Fig. 2.4 with respect to the electric potential (upper part), the anion (Cl⁻) and the cation (Na⁺) concentrations.

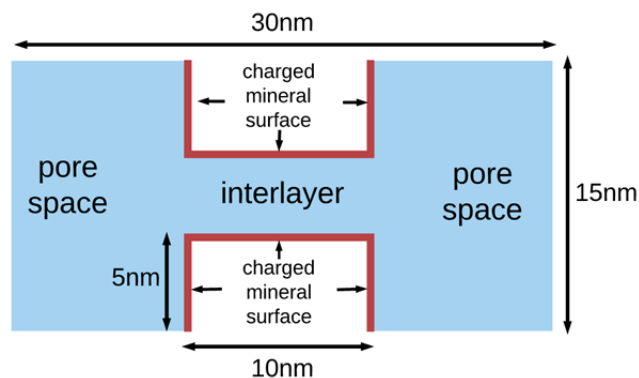


Fig.2.3: Schematic set-up of the 2D model of a pore and charged mineral surface.

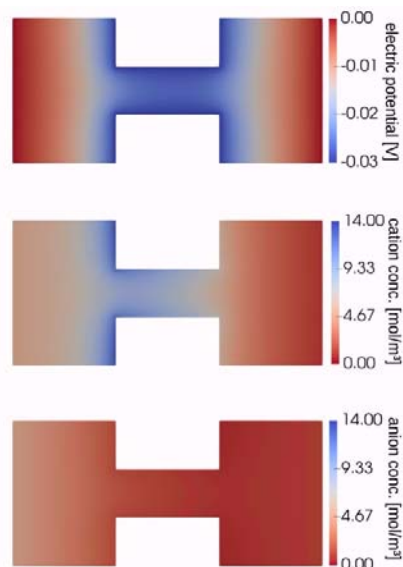


Fig. 2.4: Steady state electric potential (top), cation (middle) and anion concentrations (bottom) throughout the domain.

Cation concentrations are indeed higher near the charged surfaces, whereas anions are expelled towards regions of lower potential. For the same concentration, gradient fluxes across the constriction are smaller in the presence of charged surfaces. The approach implemented within the NPS code allowed addressing specific problems related to reactive transport in the presence of charged mineral surfaces in a flexible and fast-reconfigurable result-oriented way.

2.3.3 Porosity evolution at clay – cement interfaces using neutron radiography: Accelerated carbonation at clay/cement interfaces

Prof. Kenichiro Nakarai from Hiroshima University re-visited PSI for a period of two months in fall 2017, thanks to a mobility grant from the JSPS (Japan Society for the Promotion of Science) on international scientific cooperation in the field of waste management research. His research project is aimed at experimental and modelling studies of clay/cement interaction. In order to speed up the chemical transformation at the interfaces, which typically occur over long time scales due to slow mass transport and kinetics, admixtures are added to the clay resulting in fast clogging. In 2017, HTO diffusion experiments across reacted samples were completed. In addition it was possible to conduct radiography measurements and diffusion experiments with deuterium at the ICON beamline at the neutron spallation source (SINQ). The results of this very fruitful collaboration provide a basis for several publications which are currently being in preparation. Moreover, the data obtained in this project will serve as experimental benchmark for reactive transport simulations in repository near conditions.

2.3.4 Resolving carbonation mechanisms of cement-based materials through multi-scale microstructural simulations

The PSI-FELLOW-II-3i project "Resolving carbonation mechanisms of cement-based materials through multi-scale microstructural simulations" (R. Patel) was initiated in 2017. The project receives partial funding from the European Union's Horizon 2020 research and innovation programme under the Marie Skłodowska-Curie grant agreement No 701647. The core activity aims at developing a multiscale microstructure model to simulate the carbonation process of cement-based materials under saturated and unsaturated conditions. Understanding carbonation of cementitious materials is an important issue for

varieties of application such as predicting service life of concrete structures, to assess whether a clay-cement system will clog in case of deep nuclear waste disposal facilities or to improve the process of developing durable cast concrete blocks by controlled carbonation. Modelling and simulation at cement paste microstructural level will be carried out using both in-house lattice Boltzmann models (LBM) and the LBM based simulation tool Yantra stemming from the PhD thesis of R. Patel (PATEL 2016). Yantra is an open-source validated numerical tool that has the capability to carry out pore-scale reactive transport simulations and has been already coupled with the geochemical reaction code PHREEQC. This allows accounting for a wide range of chemical reactions through the use of several thermodynamic databases. The current implementation of reactive transport algorithm will also allow coupling Yantra with state-of-the-art geochemical reaction tools developed at LES, such as GEMS, and its newest xLMA accelerated routines (REAKTORO) (LEAL et al. 2016).

The relevant inputs for the simulation of carbonation through cement paste microstructures are the thermodynamic parameters and rate constants relevant to the chemical reaction of carbonation calcium silicate hydrate (C-S-H) and portlandite dissolution, calcite nucleation and transport parameters of the porous C-S-H phase. The microstructure of cement paste will be obtained using microstructure simulation tools (THOMAS et al. 2011) and existing datasets at PSI from cSAXS beamline (TRTIK et al. 2013).

At the scale of cement paste microstructure, the so called "gel pores" (2-30 nm) in C-S-H phase cannot be resolved but they constitute a considerable fraction of the cement paste porosity. The transport parameters in a single C-S-H pore is obtained via molecular dynamics were parameters such as thickness of double layers, surface potential and changes in structure/water film thickness at different Ca/Si ratios can be considered. The microstructure of C-S-H gels needed for the pore-scale simulations are generated using off-lattice Monte Carlo schemes (TYAGI et al. 2013). The thermodynamic parameters relevant to chemical reactions related to carbonation process are obtained from the geochemical database CEMDATA developed at EMPA. The overall methodology is depicted in Fig. 2.5. The result of this project will allow to assess the underlying mechanisms and an upscaling procedure will improve the continuum scale models.

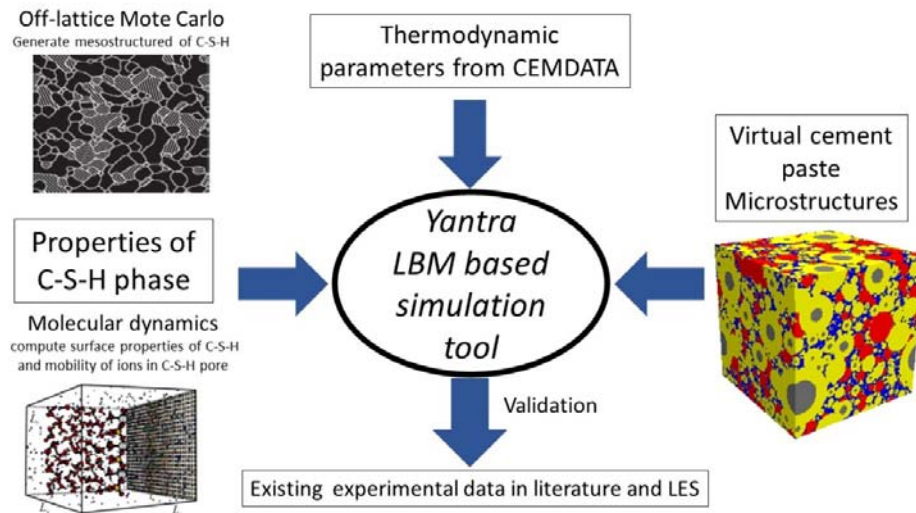


Fig. 2.5: Schematic approach of the multiscale project "Resolving carbonation mechanisms of cement-based materials through multi-scale microstructural simulations".

2.3.5 Multiscale modelling of ion transfer mechanisms in clay and cement materials

The understanding of ion transport processes near the clay-cement interface is of prime importance for deep geological waste disposal. The project "Ion transfer mechanisms in clay and cement materials" (Y. Yang) is a collaborative project between LES and Tsinghua University, Beijing, China (Prof. M. Wang group, Department of Engineering Mechanics) funded by a prestigious Chinese government grant (China Scholarship Council). During his 6 month stay at PSI Y. Yang focuses on developing and testing Lattice Boltzmann Method (LBM) based pore scale models in order to bridge the scales between continuum and molecular models. More specific, the electro-kinetic effects in charged porous media due to diffusion in the Stern and the diffuse double layer will be investigated. In the first part of his work, Y. Yang applied the jointly developed models in the description of ion transport in gel pores of cementitious materials. In the second part, which will be completed in 2018, he will extend this approach to clay systems which typically show higher surface charges.

2.4 Fundamental understanding of transport and sorption mechanisms

2.4.1 Transport simulations including the Donnan approach

Diffusion of charged ions through clays is affected by the clay's charged solid surfaces. For instance, measured fluxes of anions in steady-state diffusion experiments are lower than those of water tracers, and the fluxes of cations are higher, as also evidenced in the DR-A Mont Terri field experiment. The first effect is commonly attributed to anion exclusion. The latter

can be related to diffusion of cations in a diffuse layer or in interlayers, or generally to diffusion of cations which are considered as sorbed in typical batch experiments. The Donnan approach (see Fig. 2.6) can be used to represent such features depending on the ionic strength of the solution. Often, however, required parameters such as the relevant surface charge, or the fraction of pore water belonging to the Donnan pore space, have to be adjusted in order to match experimental data. A new method was introduced to simulate Donnan equilibria based on the Nernst-Planck equation (GIMMI & ALT-EPPING 2017) and was tested for various cases. Two examples are presented. First, anion accessibilities derived for Opalinus Clay directly from Mont Terri field experiments fall in a range of ~0.5 to 0.65. Attributing the whole cation exchange capacity and all pore water to the Donnan space, the simulated anion accessibility would be clearly lower ('full Donnan' curve in Fig. 2.7, assuming pore water being dominated by Na^+ and Cl^-). The simulated anion accessibility increases if some surface charges are neutralized by ion exchange reactions ('partial Donnan' depending on the parameter K_{NaX}). An approximate match with the range of field data can be obtained by $K_{\text{NaX}}=10$. However, other parameter combinations, as for instance consideration of some 'free' pore water unaffected by surface charges beside Donnan pore water, can also lead to an approximate match. As second example, Fig. 2.8 shows the simulation results for experimental data of GLAUS et al. (2013). In this experiment, a steady concentration gradient of NaClO_4 was maintained across a Na montmorillonite sample (0.5 M on one side, 0.1 M on the other side), and then ^{22}Na was added at both sides at equal trace concentrations. Initially, no ^{22}Na concentration gradient existed across the sample. Nevertheless, the

^{22}Na concentration increased with time in the reservoir with the 0.5 M NaClO_4 solution and decreased in the other reservoir. This behaviour can be simulated with a partial Donnan approach (Fig. 2.8a). The observations cannot be reproduced assuming only ion exchange reactions with sorbed ions being immobile. An initial increase of ^{22}Na in the high salinity reservoir occurs only when cations compensating the negative surface charges are partly mobile. Assuming

a full Donnan situation, where all cations are fully mobile, leads to an overestimation of the ^{22}Na increase. To match equally the profile data, the CEC value had to be slightly increased compared to a literature value (Fig. 2.8b).

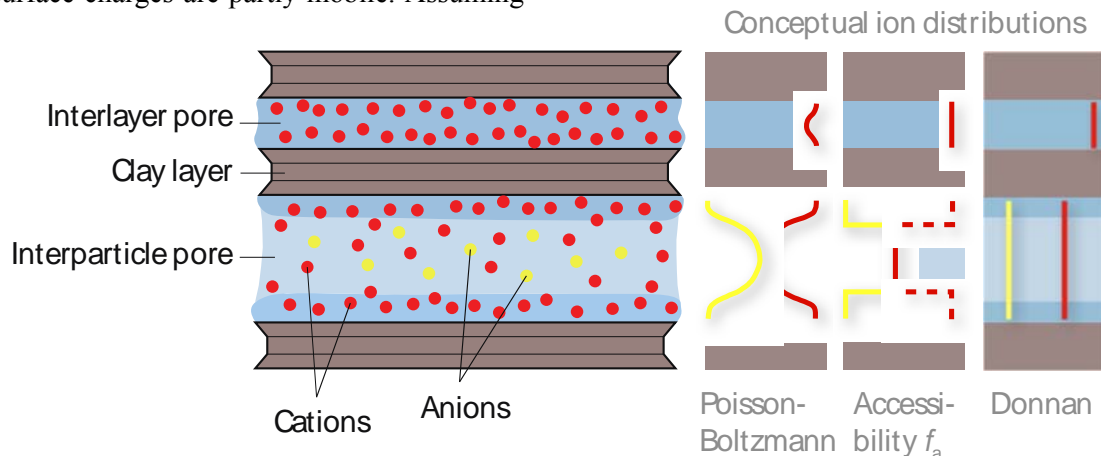


Fig. 2.6: Schematic representation of anion and cation distributions near negatively charged clay surfaces (left) and of concepts to model such distributions (right). The Donnan concept considers different, but uniform anion and cation concentrations in pores affected by surface charges. Blue areas represent pore water.

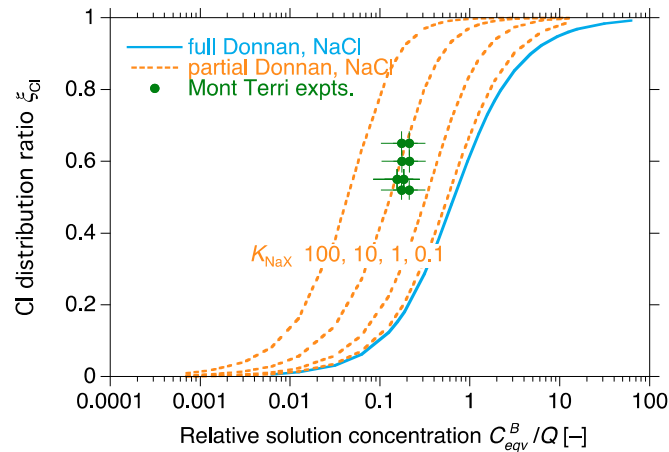


Fig. 2.7: Simulated Cl accessibility as a function of the relative solution concentration (equilibrium bulk concentration divided by surface charge concentration) for full Donnan case (blue solid line) or partial Donnan, partial ion exchange cases (dashed lines, lower Donnan charge for larger K_{Na}). GIMMI & ALT-EPPING 2017). For comparison, some results from Mont Terri field experiments are also shown.

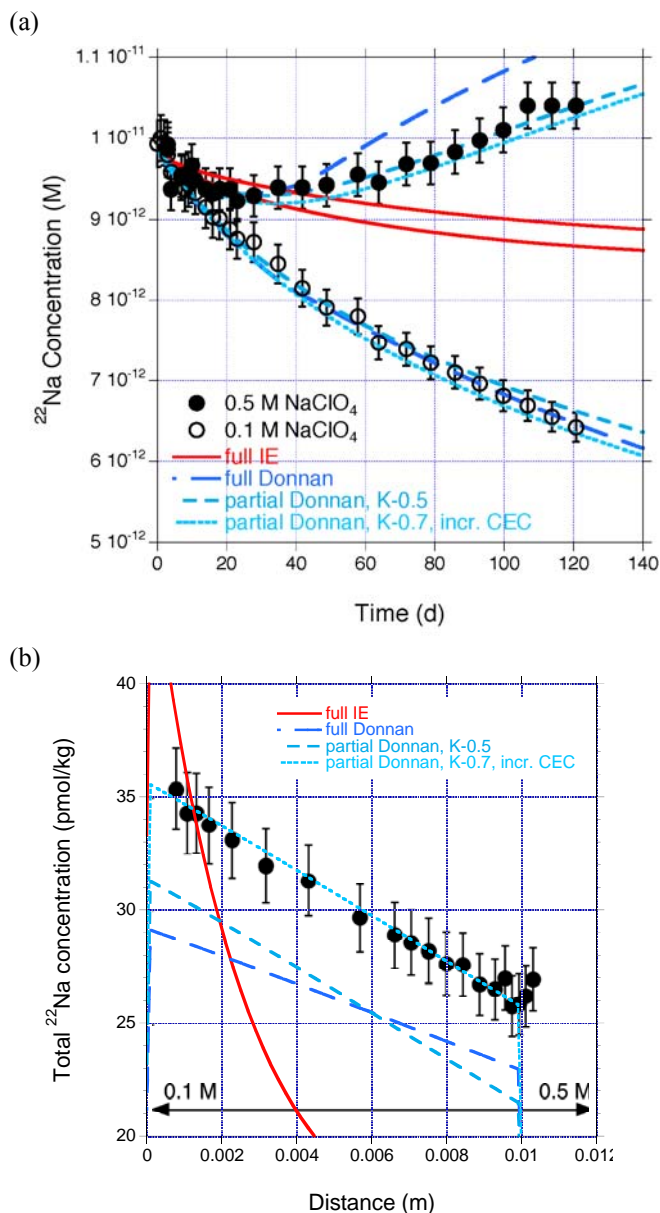


Fig. 2.8: Simulation of one of the ^{22}Na tracer diffusion experiments of Glaus et al. (2013) with an ion exchange approach (full IE), a full Donnan approach, or a partial Donnan approach with two different parameter sets. (a) Reservoir concentrations, (b) profile at the end of the experiment.

2.5 Multiscale modelling of reactive transport mechanisms and upscaling

2.5.1 Pore scale control of mineral precipitation: from atomistic model to macroscopic modelling and experimental observations

The PSI-FELLOW-II-3i project "Pore scale control of mineral precipitation: from atomistic model to macroscopic modelling and experimental observations" (G. Yang) was initiated in 2017. The project receives partial funding from the European Union's Horizon 2020 research and innovation programme under the Marie Skłodowska-Curie grant agreement No 701647.

Dissolution and growth of minerals in natural environment is largely controlled by delicate equilibrium at solid fluid interfaces. Mineral surfaces often carry structural charges, which lead to heterogeneous distribution of ions in the pore space. These compositional heterogeneities are neglected in macroscopic reactive transport simulations. This activity aims in reactive transport multiscale modelling for the study of dissolution and growth in porous media after gaining insight into the mechanical processes that govern cations retardation, such as cations diffusion, kinetic sorption, and anion exclusion. Toward that end, fluid density functional theory (f-DFT) using the open source package Tramonto (Sandia National Laboratories, <https://software.sandia.gov/DFTfluids/>) is introduced for descriptions of ion distributions and ion transport in nanopores for complex 2D/3D clay systems and will be validated by molecular simulations (Fig. 2.9 (top left) and (top right) (YANG et al. 2017)). The f-DFT method is free from various constraints, thus not limited to system sizes, simulation times or one-dimensional problems.

Therefore, it can be used as a connection between atomistic and macroscopic models. Moreover, f-DFT provides a computationally inexpensive way to describe structure and thermodynamic properties of clay mineral/fluid interface. Solvent effects can be investigated by employing molecular modelling via effective atom radius. F-DFT calculations accounting for water molecules and Lenard-Jones attractions have been compared with molecular dynamics simulations. Figure 2.9 (bottom) shows the first results proving that ion distributions from f-DFT quantitatively agree well with molecular simulations. Within this project, the coupling with the Lattice Boltzmann (LB) codes will allow detailed pore-scale modelling of ion transport and reactive flow in complex (charged) porous media. Validation will be conducted using in-house diffusion experiments.

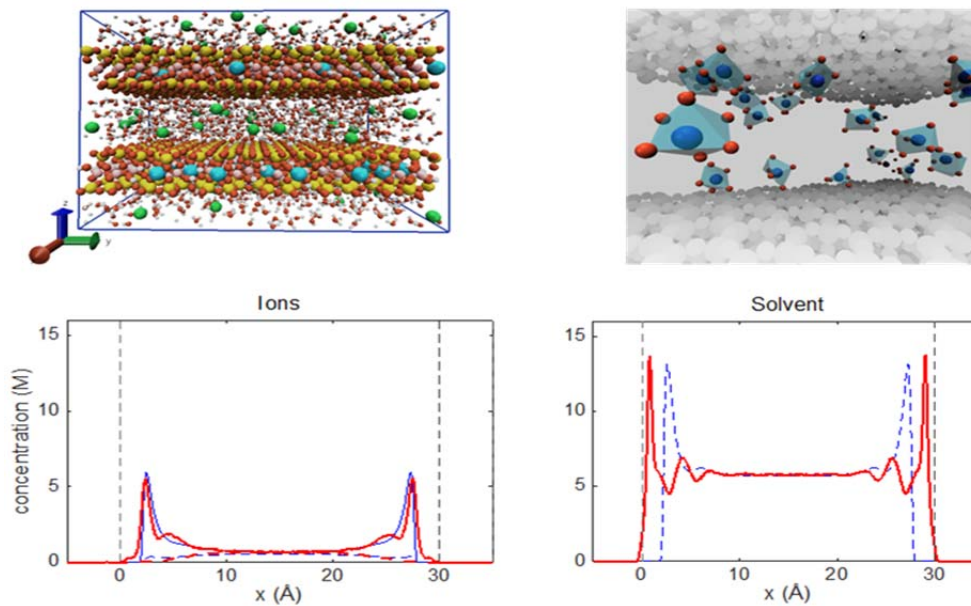


Fig. 2.9: (top left) Molecular dynamics can predict the cation exchange mechanisms, (top right) Polyhedral structure of hydration complex at mineral-fluid interfaces, (bottom) Density profiles of ions and water molecules from f-DFT are compared with molecular simulations. Solid lines represent molecular simulation, dashed lines represent f-DFT results.

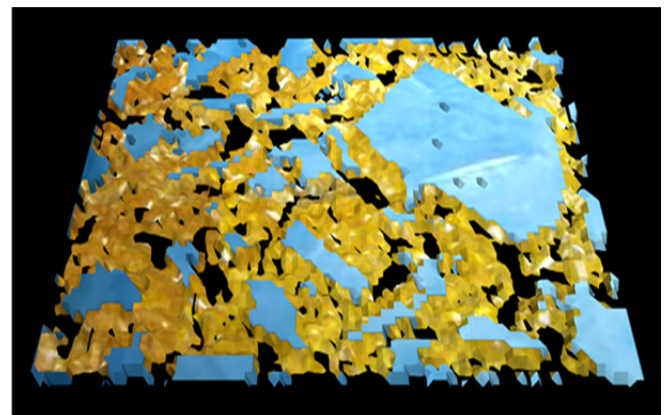
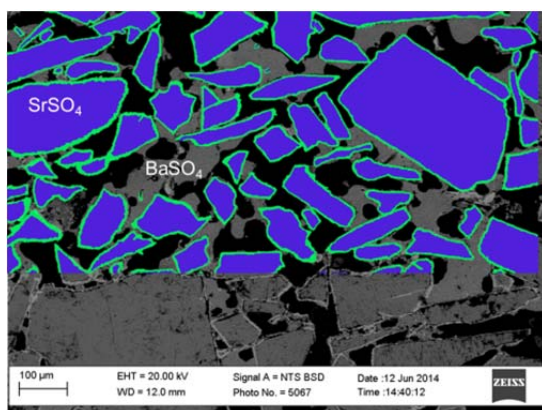


Fig. 2.10: (left): Scanning electron microscopic picture of a sample from the experiment of POONOOSAMY et al. (2015) where celestine crystals (blue) dissolve and baryte precipitates as a rim (green) or as a nanocrystalline phase (grey-in between the crystals) (right): Modelling prediction where all baryte phases are rendered yellow and celestine crystals blue (PRASIANAKIS et al. 2017).

2.5.2 Pore-level Lattice Boltzmann modelling of precipitation processes

The porosity and mineralogical evolution of the technical barriers and their respective interfaces, plays a key role in the performance assessment of the radioactive waste repository. The porosity alterations, due to geochemical reactions, directly affect important processes such as re-saturation times, corrosion rates, or the gas pressure build up within the barriers. At the same time, local transport properties at mineralogical interfaces can be altered, which in turn can affect the intermediate and longer time evolution of the entire barriers. The cross-scale concept developed at LES

(PRASIANAKIS et al. 2017) enhanced the reactive transport modelling capabilities since it allows to differentiate between heterogeneous and homogeneous nucleation precipitation mechanisms within the pore-level Lattice Boltzmann framework (see Fig. 2.10). Incorporation of the classical nucleation theory allowed modelling the sub-micrometer scales and the critical nuclei's formation rate in the bulk solution. Qualitative and quantitative prediction of the evolution of the in-house baryte-celestine reactive transport experiment (POONOOSAMY et al. 2015, 2016) sets the basis to expand this description and application to more complex reactive systems.

2.5.3 Extraction of porosity permeability relationships from pore-level analysis

The dissolution-precipitation of minerals from aqueous solutions alters the pore space and its connectivity in a way that has a complex feedback to the ion transport in aqueous phase itself. When a mineral precipitates/dissolves in the pore space, the overall porosity decreases/increases leading to a subsequent decrease/increase in permeability and effective diffusivity. At the same time the connectivity of the pores can also change in a way to block or to facilitate the mass diffusion processes. Macroscopic solvers usually work at the level of homogenized representative element volumes and porosity-permeability correlation is expressed via Kozeny-Carman type of equations. Within the master thesis of A. Abbasi (completed) and of M. Gatschet (ongoing) a microstructural analysis of the evolution of representative element volumes under reactive environments is conducted. For that, computer generated pore spaces with target porosity are created. Reactive transport simulations were conducted for different chemical conditions as shown in Fig. 2.11. During their dissolution due to reaction, the evolution

of permeability is correlated to the respective change of the porosity thus resulting in a more realistic porosity-permeability correlation. The fitting of the simulation data can provide the means to upscale the microscopic results for use with the macroscopic codes.

2.6 Benchmarking, validation and application of coupled codes

The benchmarking and verification of reactive transport coupled codes is an ongoing activity in the Transport Mechanisms Group. This activity is important to support the credibility of numerical simulations and is essential for advancing the modelling and description of complex geochemical interactions and/or radionuclide migration in the vicinity of a nuclear waste repository or in laboratory experiments. Comparison of output results among different codes in LES, as well as the participation in international benchmarks ensures correctness, guarantees the quality of results and keeps the pace with the international scientific community.

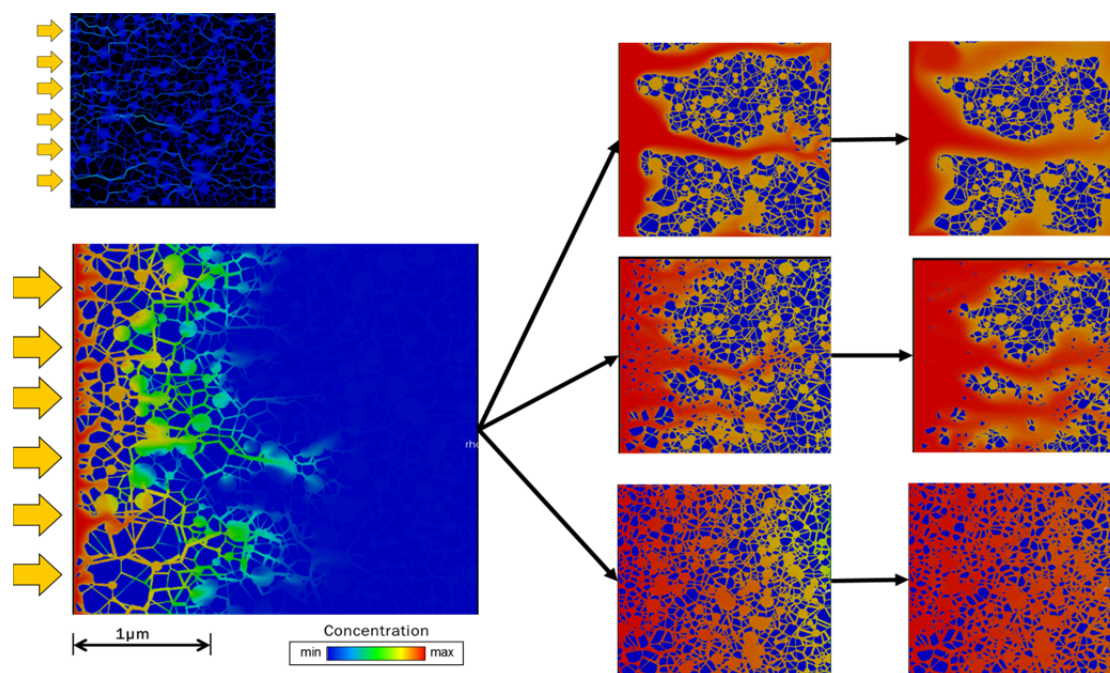


Fig. 2.11: (left): Reactive transport simulations describing dissolution of porous medium. On top the preferential flow paths are plotted. Below, the concentration of the dissolving chemical element is plotted at the initial stage. (right): Under different chemical conditions (reactivity) the evolution of porosity (and respective permeability) follows a different path. From top to bottom the cases with decreasing reactivity are plotted at two instances.

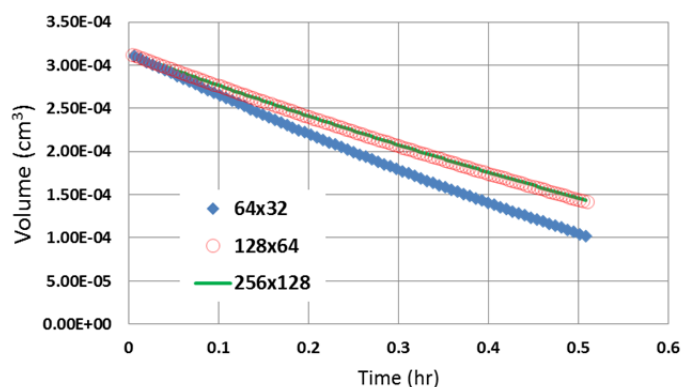
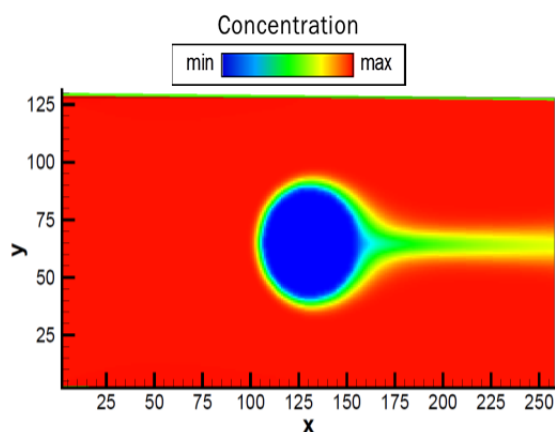


Fig. 2.12: (left): Dissolving particle due to acid flow (left to right). Contours of concentration of acid are plotted for the 256×128 case. (right): Grid convergence study showing the evolution of the dissolving particle volume with respect to time.

2.6.1 Pore-level dissolution benchmarking

In the area of code benchmarking LES participates in the ongoing Subsurface Environmental Simulation Benchmarking (SeS Benchmark) initiative: "A benchmark for mineral dissolution at the pore scale", proposed by S. Molins (LBNL, USA), C. Soulaine (Stanford, USA) and D. Trebotich (LBNL, USA). The scope of this initiative is to compare the results of several codes and to create a validation case for testing new models and methods. Within the master thesis of A. Abbasi several test cases were simulated. For such a case, the set-up describes the acid flow (left to right) around a dissolving calcite cylinder as shown in Fig. 2.12 (left). In Fig. 2.12 (right), the time evolution of the volume of the reacting and dissolving particle object is shown for different grid resolutions. For a coarse grid of 64×32 grid points the qualitative behavior is correctly predicted but the simulation is under-resolved resulting in a deviation from the converged solution. For a grid finer than 128×64 the simulation is grid convergent, which is an important quality of pore-level codes.

2.7 Thermodynamic modelling framework and thermodynamic databases

2.7.1 On-demand machine-learning (ODML) approach for ultra-fast reactive transport simulations and parameter optimization (in collaboration with Dr. Allan Leal and Prof. Martin Saar, GEG IG ETHZ)

In reactive transport modelling, calculations of partial chemical equilibria in every mesh cell at each time step usually takes 10–100 times more time than that of the transport model. This is because solving for chemical equilibrium speciation occurs in several iterations of non-linear Gibbs energy minimization

(GEM) (LEAL et al. 2017a). Even one such iteration is much more computationally expensive than the transport model integration per mesh cell; hence, any effort in developing fast-converging numerical GEM and LMA algorithms cannot make them significantly faster. Based on these considerations, LEAL et al. presented an unconventional On-Demand Machine Learning (ODML) approach, in which most equilibrium states are quickly and accurately predicted from the results of previously performed GEM equilibrium speciation calculations.

As a proof of concept, this approach was used in a reactive transport modelling example (Fig. 2.13) showing that 99.7% of total 60000 equilibrium speciation calculations were quickly predicted, and only 0.3% (mainly at the beginning of the simulation run) had to be obtained from full GEM calculations, which brings in total a speed-up factor of 63 to 125. These test runs showed (Fig. 2.14) that after a few first time steps, the ODML-accelerated chemical solver was "trained" enough to rapidly perform all subsequent equilibrium speciation predictions, so that its cumulative cost rapidly becomes the same or less than that of the transport algorithm (Fig. 2.15). In contrast with traditional machine learning algorithms (WITTEN et al. 2011), the ODML approach does not require a training phase collecting a lot of statistics before the actual simulations start. Therefore, the use of ODML algorithms, now implemented in the Reaktoro framework for modelling chemically reactive systems (<http://reaktoro.org>), is expected to be very beneficial in reactive transport simulators such as OpenGeoSys-GEM or in parameter optimization codes such as GEMSFITS, where millions of equilibrium speciation calculations must be performed within one simulation task.

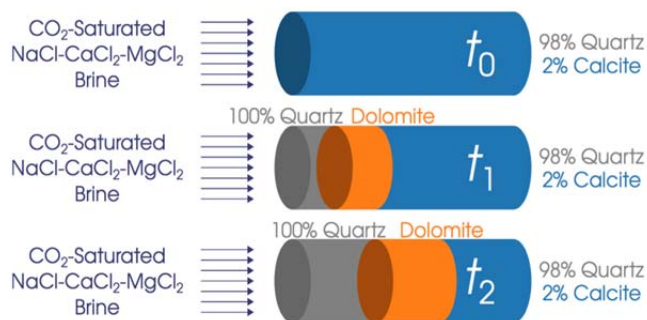


Fig. 2.13: Schematics of the 1-D reactive transport column model at three arbitrary time steps t_0 , t_1 and t_2 . Injection fluid composition: 0.9 m NaCl, 0.05 m MgCl₂, 0.01 m CaCl₂, 0.75 m CO₂. Initial rock composition (vol. %): 98% quartz, 2% calcite. Initial porosity 10%, advection velocity 1 m/day, diffusivity 10⁻⁹ m²/s. Temperature 60 °C, overall pressure 100 bar, local equilibrium is assumed in all 100 nodes of the column of 1 m length at time step of 10 min. From A. Leal (personal communication).

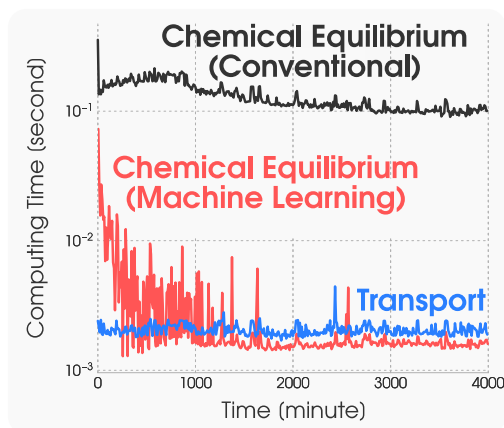


Fig. 2.14: Computational costs of ODML calculations of chemical speciation (orange curve) with that of conventional GEM calculations in all nodes at all time steps (blue) and that of the transport model calculations (green). The cost per time step is the sum of individual costs for all cells. The cost of transport calculations per time step is the cost of solving discretized algebraic transport equations for all cells. In this specific example, the overall ODML speedup factor (relative to the case of GEM calculations for all cells at all time steps) is between 63 and 125. From A. Leal (personal communication).

The ODML approach to chemical speciation calculations is especially promising for the reactive transport modelling in 2D or 3D meshes. When the algorithm eventually achieves a knowledgeable state, (almost) all equilibrium speciations will be rapidly and accurately predicted using the previously learned states.

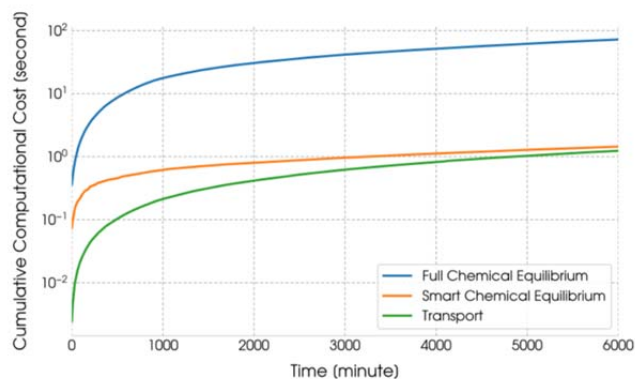


Fig. 2.15: Logarithmic costs (CPU time in seconds) of conventional equilibrium (GEM, blue), and ODML-based (orange) calculations and of transport integration (green) over the simulated time. The cost per time step is the sum of individual costs for all cells. The cost of transport calculations per time step is the cost of solving discretized algebraic transport equations for all cells. From A. Leal (personal communication).

Traditional machine learning methods (e.g. WITTEN et al., 2011) first require a data-rich and/or time-consuming training phase, similar to "attending the school" to learn things most of which will never be used again. There are no clear criteria to decide whether the training phase is completed (i.e. when it is time to "leave the school"). Contrary to that, the ODML algorithm is more akin to constantly "learning by doing" in the practical simulation process, and can start from scratch, without any prior "experience".

It is hypothesized that ODML shall probe only small regions of the overall "chemical space" that are limited by characteristic ranges of bulk compositions, temperature, pressure, and kinetic rates typical for the simulated medium of interest. Chemical and phase changes usually occur in subsurface along some heterogeneities such as contacts of rock beds, fault zones, or redox barriers, which display some similarities even when moving in space and time. At the learning stage, all those regions get "learned" by saving at least one fully calculated equilibrium state per region, so further chemical evolution can be fast-predicted in 99.99% cases.

As a next step stemming from the ongoing collaboration with A. Leal and M. Saar, it is foreseen to couple Reaktoro ODML GEM solvers with LES Lattice Boltzmann pore-scale transport simulators and implement them into the next releases of GEMS codes (<http://gems.web.psi.ch>), thus adding value to GEMS and the already existing coupled codes that use it.

2.7.2 GEMS training events

There is a growing demand for introductory and advanced training in GEM-Selektor and GEMS/FITS software. In 2017 D.A. Kulik performed two invited training events at the Hebrew University of Jerusalem in Israel (23-26 February 2017) and at the University of Melbourne in Australia (24-28 April 2017), and supported a GEM-Selektor training on modelling cement systems organized by B. Lothenbach and F. Winnefeld at Empa, Dübendorf, Switzerland. In addition, Prof. A. Gysi (Colorado School of Mines, Golden, CO, USA) has performed GEMS workshops and tutorials on modelling hydrothermal water-rock interaction systems using his MINES'16 thermodynamic database.

The training in Jerusalem, entitled "GEM-Selektor v.3.3: Thermodynamic Modelling of Element Uptake in Complex SSAS Systems", was mainly devoted to low-temperature SSAS systems and natural analogs of cement. The GEM-Selektor Training Workshop on chemical thermodynamic modelling in Melbourne was targeted at students in hydrogeology, environmental geochemistry, hydrothermal geochemistry, economic geology and petrology. Addressed worked examples ranged from aqueous speciation and mineral solubility calculations to forward modelling of SSAS equilibria, fluid-mineral reactions at hydrothermal conditions, and to kinetics of mineral dissolution and precipitation.

2.8 References

- ALNÆS M., BLECHTA J., HAKE J., JOHANSSON A., KEHLET B., LOGG A., RICHARDSON C., RING J., ROGNES M.E., WELLS G.N. (2015)
The FEniCS project version 1.5. Arch. Numer. Softw. 3. doi:10.11588/ANS.2015.100.20553
- BRADBURY M.H., BAEYENS B. (2000)
A generalised sorption model for the concentration dependent uptake of caesium by argillaceous rocks. J. Contam. Hydrol. 42, 141-163.
- GIMMI T., KOSAKOWSKI G. (2011)
How mobile are sorbed cations in clays and clay Rocks? Environ. Sci Technol. 45, 1443-1449.
- HAX DAMIANI L., GLAUS M.A., CHURAKOV S.V., KOSAKOWSKI G. (2017)
Rapid development of a reactive transport code with FeniCS and Reaktor, Proceedings of the Second Annual Workshop of the HORIZON 2020 CEBAMA Project, KIT Scientific Report, in print.
- JENNI A., GIMMI T., ALT-EPPING P., MÄDER U., CLOET V. (2017)
Interaction of ordinary Portland cement and Opalinus Clay: Dual porosity modelling compared to experimental data. Phys. Chem. Earth A/B/C. 99, 22–37.
- KULIK D.A., KOSAKOWSKI G., CURTI E., THOENEN T., LOTHENBACH B., WIELAND E., MARQUES FERNANDES M., BAEYENS B., MIRON G.D., PRASIANAKIS N.I. (2017)
The Gibbs Energy Minimization Software for Thermodynamic Modelling (GEMS TM) project: Codes, databases and relevant applications. Nagra Arbeitsbericht NAB 17-43, 123 pp.
- LEAL A.M.M., KULIK D.A., SAAR M.O. (2017b)
Ultra-fast reactive transport simulations when chemical reactions meet machine learning: Chemical equilibrium. E-print at <https://arxiv.org/abs/1708.04825>.
- LEAL A.M.M., KULIK D.A., KOSAKOWSKI G. (2016)
Computational methods for reactive transport modelling: A Gibbs energy minimization approach for multiphase equilibrium calculations. Adv. Water Res. 88, 231–240.
- LEAL A.M.M., KULIK D.A., KOSAKOWSKI G., SAAR M.O. (2016)
Computational methods for reactive transport modelling: An extended law of mass-action, xLMA, method for multiphase equilibrium calculations. Adv. Water Resour. 96, 405–422.
- LEAL A. M.M., KULIK D. A., SMITH W.R., SAAR M.O. (2017a)
An overview of computational methods for chemical equilibrium and kinetic calculations for geochemical and reactive transport modelling. Pure Appl. Chem. 89, 597–643.
- LICHTNER P. (2007)
FLOTRAN User's Manual: Two-phase nonisothermal coupled thermo-hydraulic-chemical (THC) reactive flow and transport code. Version 2. Los Alamos National Laboratory, Los Alamos, New Mexico.
- MÄDER U., JENNI A., LEROUGE C., GABOREAU S., MIYOSHI S., KIMURA Y., CLOET V., FUKAYA M., CLARET F., OTAKE T., SHIBATA M., LOTHENBACH B. (2017).
5-year chemico-physical evolution of concrete-claystone interfaces, Mont Terri rock laboratory (Switzerland). Swiss J. Geosci. 110, 307–327.
- PATEL R. (2016)
Lattice Boltzmann Method Based Framework for Simulating Physico-Chemical Processes in Heterogeneous Porous Media and Its Application to Cement Paste. PhD thesis, Ghent University.

- POONOOSAMY J., KOSAKOWSKI G., VAN LOON L.R., MÄDER U. (2015)
Dissolution-precipitation processes in tank experiments for testing numerical models for reactive transport calculations: experiments and modelling. *J. Contam. Hydrol.* 177–178, 1–17.
- POONOOSAMY J., CURTI E., KOSAKOWSKI G., GROLIMUND D., VAN LOON L.R., MÄDER U. (2016)
Barite precipitation following celestite dissolution in a porous medium: A SEM/BSE and μ -XRD/XRF study. *Geochim. Cosmochim. Acta* 182, 131–144.
- PRASIANAKIS N.I., CURTI E., KOSAKOWSKI G., POONOOSAMY J., CHURAKOV S.V. (2017)
Deciphering pore-level precipitation mechanisms. *Scientific Reports*, 13765.
- THOENEN T., HUMMEL V., BERNER U., CURTI E. (2014)
The PSI/Nagra Chemical Thermodynamic Data Base 12/07, PSI report 14-04, Villigen PSI, Switzerland.
- THOMAS J., BIERNACKI J., BULLARD J. (2011)
Modelling and simulation of cement hydration kinetics and microstructure development. *Cem. Concr. Res.* 41(12), 1257–1278.
- TRTIK P., DIAZ A., GUIZAR-SICAIROS M., MENZEL A., BUNK O. (2013)
Density mapping of hardened cement paste using ptychographic X-ray computed tomography. *Cem. Concr. Composites* 36, 71–77.
- TYAGI M., GIMMI T., CHURAKOV S.V. (2013)
Multi-scale micro-structure generation strategy for up-scaling transport in clays. *Adv. Water Res.* 59, 181–195.
- VAN LOON L.R., GLAUS M.A., MÜLLER W. (2007)
Anion exclusion effects in compacted bentonites: Towards a better understanding of anion diffusion. *Appl. Geochem.* 22, 2536–2552.
- VAN LOON L.R., MÜLLER W. (2014)
A modified version of the combined in-diffusion/abrasive peeling technique for measuring diffusion of strongly sorbing radionuclides in argillaceous rocks: A test study on the diffusion of caesium in Opalinus Clay. *Appl. Radiat. Isotopes* 90, 197–202.
- WIGGER C., VAN LOON L.R. (2017)
Importance of interlayer equivalent pores for anion diffusion in clay-rich sedimentary rocks. <https://doi.org/10.1021/acs.est.6b03781>
- WITTEN I., FRANK E., HALL M. (2011)
Data Mining: Practical machine learning tools and techniques, 3rd Edition. Morgan Kaufmann, San Mateo, CA.
- YANG G., NERETNIEKS I., HOLMBOE M. (2017)
Atomistic simulations of cation hydration in sodium and calcium montmorillonite nanopores. *J. Chem. Phys.* 147, 084705.
- FENICS MODELLING PLATFORM
<http://fenicsproject.org/>
- GEOCHEMICAL MODELLING SOFTWARE GEMS
<http://gems.web.psi.ch>
- REAKTORO FRAMEWORK: <http://www.reaktoro.org>
- YANTRA FRAMEWORK:
<https://bitbucket.org/yantralbm/yantra>

3 DEVELOPMENT OF MECHANISTIC SORPTION MODELS AND EXPERIMENTAL VALIDATION

B. Baeyens, R. Dähn, M. Marques Fernandes, J. Tits, S.V. Churakov, A. Schaible, E. Eltayeb, F. Marafatto, A. Kéri (PhD), S. Wick (PhD), L. Nedyalkova (PhD)

3.1 Introduction

The aim of this project is to improve the mechanistic understanding of radionuclide (RN) uptake processes in particular on 2:1 type clay minerals which are key minerals present in the near field (montmorillonite/bentonite) and the far field (illite/Opalinus Clay) of potential sites for the deep disposal of high-level radioactive waste (HLW) in geological formations. A thorough understanding of the retention behaviour of relevant radionuclides is crucial for a reliable safety analysis. The focus in 2017 was put on the following research activities:

In preparation for the safety assessment planned for the 3rd phase in the Sectoral Plan (SGT-E3) two important reports were finalized. For the near- and far-fields of a HLW repository a thermodynamic sorption database was compiled for montmorillonite (BAEYENS & BRADBURY 2017) and illite (BRADBURY & BAEYENS 2017), respectively. These reports form the basis for the development of sorption databases (SDBs) to be applied in the safety analysis of SGT-E3 for bentonite and Opalinus Clay.

Competitive sorption is an important issue for the quantification of RN retention on clays and clay rocks. A report has been finalized evaluating the influence of competitive sorption on the values of the SDBs used in SGT-E2 (BRADBURY et al. 2017). Currently, experimental studies on 2:1 type clay minerals are ongoing, evaluating the groups of radionuclides which are mutually competitive and which are non-competitive. The application of the 2SPNE SC/CE sorption model to reproduce the experimental data allows a quantitative description of sorption taking into account competitive, partial competitive or non-competitive sorption.

The uptake of uranyl (U^{VI}) on purified illite has shown under certain experimental conditions an unexpected enhancement which could not be modelled with the 2SPNE SC/CE sorption model. An EXAFS study in collaboration with ROBL/HZDR demonstrated that the anomalous behaviour could be ascribed to an accessory apatite-like mineral phase which was present at a level below the detection limit of common analytical methods such as e.g. XRD or TEM.

The influence of ferrous iron (Fe^{II}) on the uptake of Np^V on montmorillonite (SWy) was studied on natural and chemically reduced SWy. Combined wet

chemical and surface analysis studies showed that on native SWy the sorbing species was Np^V whereas on the reduced SWy the much stronger sorbing Np^{IV} was the dominant surface species.

The sorption studies of thallium on illite (SNSF founded PhD project) have been finalized and a paper on this topic is published (WICK et al. 2018). The generalized Cs sorption model (BRADBURY & BAEYENS 2000) could be successfully applied to describe the uptake of Tl on three different sorption sites on Na-, K-, NH_4 - and Ca-illites.

The immobilization of selenium and iodine in AFm phases is investigated in the framework of a joined PhD study of L. Nedyalkova with Empa (B. Lothenbach) and financed by the Horizon 2020 EC project "Cebama".

Structural position and oxidation state of Fe incorporated in Milos montmorillonite (SNSF founded PhD project) were studied by molecular dynamics simulations. The data analysis allowed a consistent description of the measured EXAFS and XANES spectra. The results were published in KÉRI et al. (2017).

In the framework of the joined CROSS-PSI-Eawag project the new postdoc Francesco Marafatto has started working on the 1st of June 2017. The purchase of a He/N-cryostat has been ordered and the delivery at the microXAS beamline is expected in beginning of 2018, allowing first measurements on redox and radiation sensitive samples.

3.2 Mechanistic sorption studies and experimental validation

3.2.1 Competition: experimental and modelling

In a deep geological repository for HLW, stable elements originating from many different sources such as porewaters, tunnel back fill materials and host rock formations, corrosion of the carbon steel canister, and finally dissolution of the spent fuel and vitrified HLW are ubiquitous. These stable elements and the released radionuclides can compete with one another for the sorption sites on the backfill material and the host rock, and thus reduce their uptake on them. Such competitive effects may have consequences for the selection of sorption values for sorption databases

used in the safety assessment of radioactive waste repositories.

The competitive or non-competitive sorption behaviour of relevant radionuclides, comprising inter and intra valences, on montmorillonite and illite which are major components of bentonite and argillaceous rocks, respectively have been investigated. The experimental results have been modelled with the 2 site protolysis non electrostatic surface complexation and cation exchange (2SPNE SC/CE) model developed for montmorillonite and illite (BRADBURY & BAEYENS 1997; BRADBURY & BAEYENS 2009).

To quantify the degree of competition on strong sites between relevant nuclides, sorption isotherms for a given sorbate (blocking element) were measured in the presence of a second element at trace concentration (**trace element**). If these two elements compete, it is expected that the sorption of the

blocking element will progressively fill up the strong site types and thereby reduce the sorption of the trace element.

The sorption of pairs of radionuclides on homoionic Na forms of illite du Puy (IdP) and montmorillonite (SWy) which are mutually competitive, partially competitive or non-competitive are shown in Figs. 3.1 and 3.2. The divalent transition metals Ni and Co are competitive when the trace element (Ni) is added simultaneously with the blocking element (Co) (Fig. 3.1a,b). If Ni is equilibrated for 3 days with the clay before Co is added only part of the sorbed Ni is competitive. Using the 2SPNE SC/CE model together with the surface complexation constants for both elements the fraction of Ni that is non-competitive can be calculated. The modelling indicated that at the highest Co concentration $\sim 13\%$ of the adsorbed Ni is non-competitive (Fig. 3.1d).

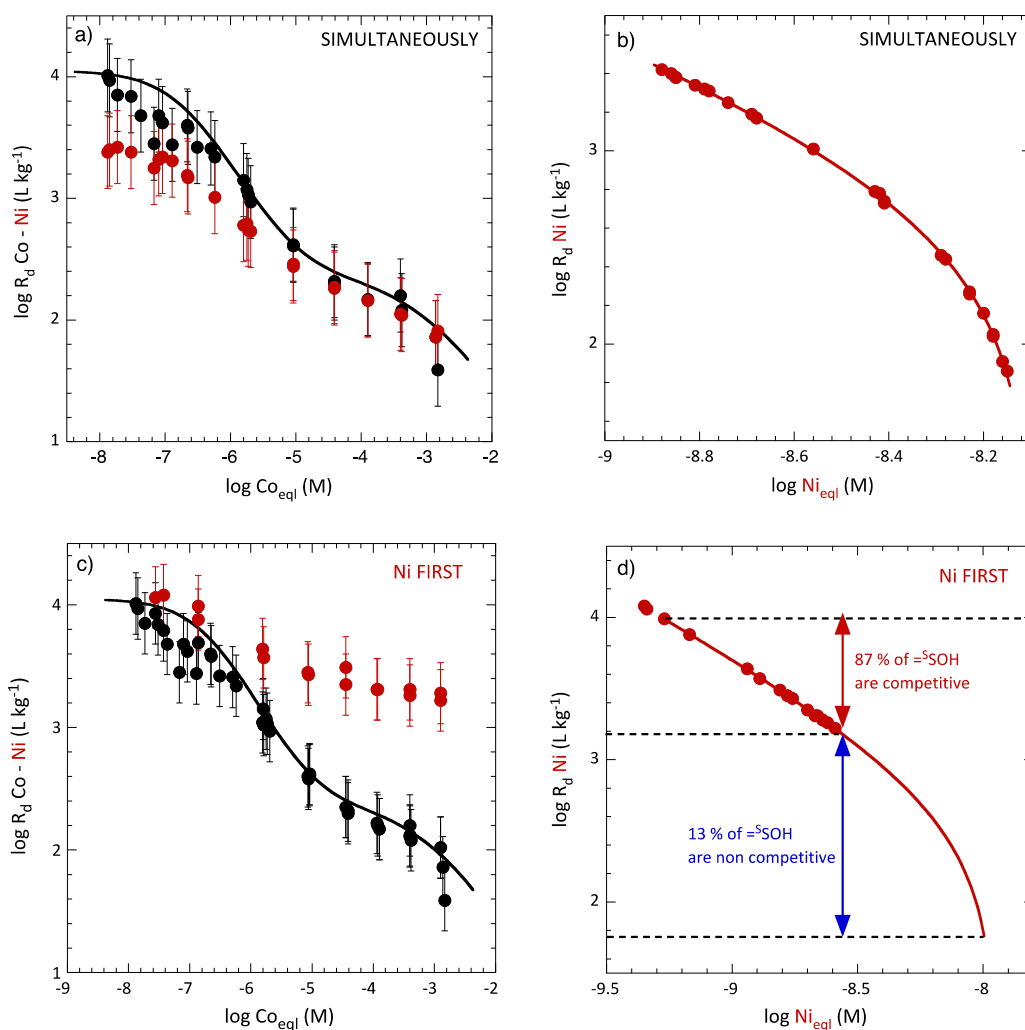


Fig. 3.1: Competitive sorption of Ni^{II} - Co^{II} on SWy-1 in 0.1 M $NaClO_4$ at $pH\ 7.1 \pm 0.2$. (a) Ni and Co are added simultaneously to the clay. (c) Ni is reacted for 3 days with SWy before Co is added to the clay suspension. The black curves in (a) and (c) are the calculated sorption for the blocking element and the curves in (b) and (d) represent the sorption of the trace element (Ni) under the assumption that Ni and Co are competitive using the 2SPNE SC/CE sorption model.

In the presence of high Ni^{II} concentrations Eu^{III} is non-competitive as shown in Fig. 3.2a. The $\log R_d$ values for Eu remain constant at 5.3 ± 0.3 L/kg and are not affected by Ni concentrations up to $\sim 10^{-3}$ M. However, if trace Ni is sorbed in the presence of Eu as blocking element sorption is partially competitive (Fig. 3.2c). In the presence of the highest Eu concentration ($3 \cdot 10^{-5}$ M) 94 % of Ni on the strong sites is competitive and only 6 % of sorbed Ni is non-competitive (Fig. 3.2d).

The preliminary conclusion from these experiments is that in general, metals with the same valence and similar hydrolysis behaviour compete, whereas metals with different valences do not compete. For performance assessment competitive sorption should be considered in the near field (montmorillonite/bentonite) and the far field (illite/argillaceous rocks) for the following systems:

- Divalent metals (*e.g.* Ni / Co / Fe) are generally competitive. If the elements are reacted simultaneously with the clay they are mutually competitive. Partial competition has been observed if the trace element is allowed to react with the clay before the blocking element is added. However, ~ 90 % of the trace element remained competitive.
- Trivalent metals (*e.g.* Am - Eu) are mutually competitive.
- Divalent - trivalent metals are essentially competitive if the trivalent element is the blocking radionuclide whereas if the divalent metal is the blocking element these elements are non-competitive.

Finally, sorption competition can be quantified by modelling and hence, can be taken into the sorption databases used in the safety analysis of radioactive waste repositories.

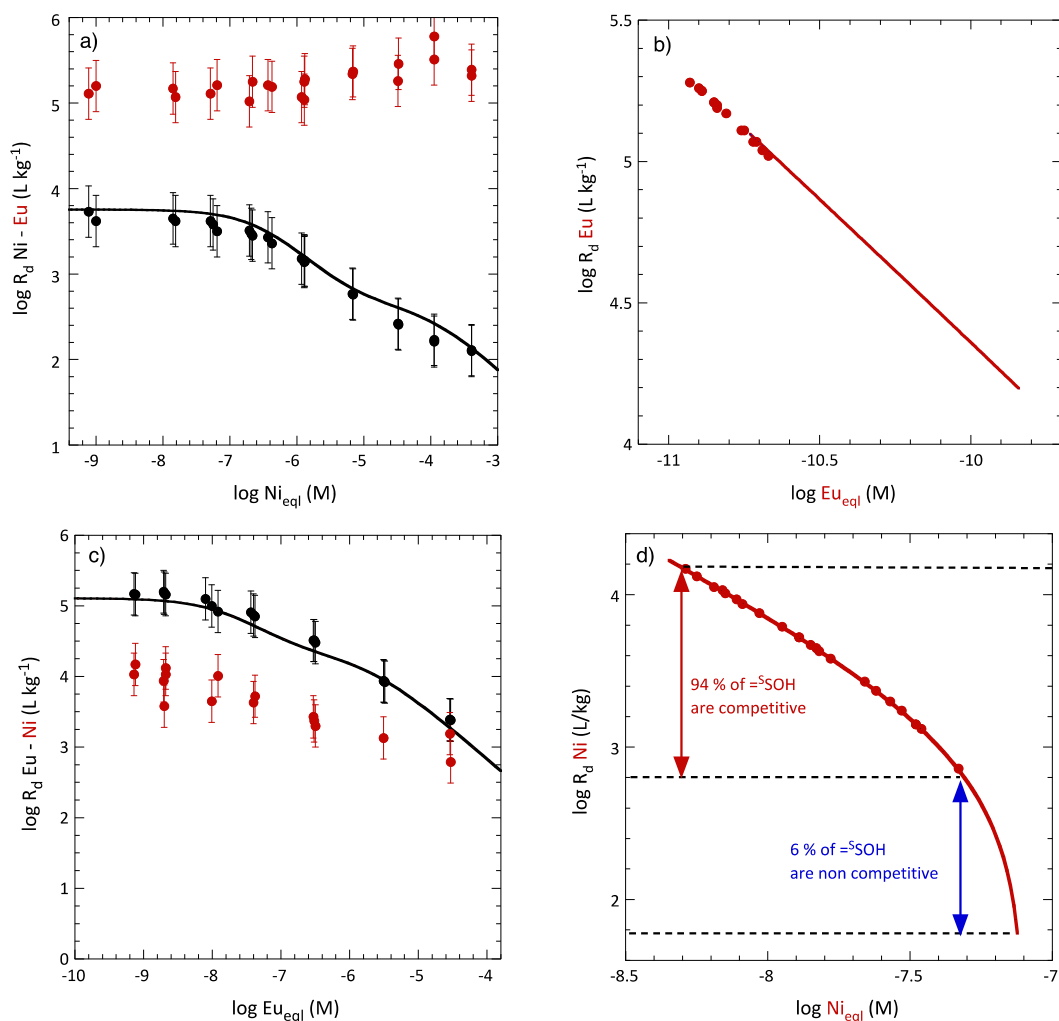


Fig. 3.2: Competitive sorption of Ni^{II} - Eu^{III} on IdP in 0.1 M NaClO_4 at $\text{pH } 7.1 \pm 0.2$. (a) Trace Eu^{III} in the presence of blocking Ni^{II} . (c) Trace Ni^{II} in the presence of blocking Eu^{III} . The black curves in (a) and (c) are the calculated sorption for the blocking element and the red curves in (b) and (d) represent the sorption of the trace element under the assumption that Ni and Eu are competitive using the 2SPNE SC/CE sorption model.

3.2.2 Sorption of U^{VI} on Illite du Puy: influence of accessory minerals

The interaction of radio(-contaminants) at water-mineral interfaces present in natural environments is a key process in retarding their migration. Therefore, elucidation of the processes involved, and the development of sorption models predicting these processes, is crucial for a reliable risk assessment. This task can realistically only be tackled if for a given multi-mineral rock the most relevant minerals can be identified. Only for these, the sorption processes need to be determined and modelled, and the sorption by the rock entity is then reasonably predictable by summing up the models for these few minerals according to their fraction in the rock. This procedure can already be impeded at the level of a presumably pure clay mineral.

U^{VI} sorption experiments conducted with purified IdP show an unexpected enhancement of the U^{VI} retention under certain conditions (pH and U^{VI} concentration). This anomalous sorption behaviour is illustrated by the U^{VI} sorption isotherm on purified IdP at pH 4.9 (Fig. 3.3a). In the U^{VI} equilibrium concentration range 10^{-7} M to 10^{-5} M, the U sorption increases considerably and deviates from the expected isotherm shape. A similar isotherm shape was observed at pH 5.8 (results not shown here). Only after a severe acid treatment (repeated cycles of acid washings) of the illite the degree of sorption approaches that expected for pure illite (BRADBURY & BAEYENS 2005).

In order to identify the U species formed at the IdP surface, extended X-ray absorption fine structure (EXAFS) measurements at the U-L_{III} edge were carried out at the Rossendorf Beamline (ROBL) at the ESRF (Grenoble, France). EXAFS spectra of U samples prepared along the sorption isotherm on purified IdP (*i.e.* IdP_1 to IdP_4) and on untreated IdP (IdP_raw) (Fig. 3.3a, black dots) were recorded and investigated using the iterative target-transformation factor analysis (ITFA) (ROSSBERG et al. 2003), to derive the number of chemically different U^{VI} species on illite based on their short range structure. The Malinowski indicator as well as the good reconstruction of the experimental EXAFS spectra with 2 principal components (blue lines in Fig. 3.3b and c) suggest that two structurally different U^{VI} species are present on illite, which were subsequently identified as (1) a U-illite inner sphere sorption complex predominant in sample IdP_4 and (2) a autunite-like $(Ca(UO_2)_2(PO_4)_2 \cdot xH_2O)$ species predominant in sample IdP_raw, *i.e.* without any acid treatment. For the purified samples, the fraction of autunite is highest in IdP_1, *i.e.* the sample with the largest deviation from the expected sorption isotherm, and lowest in IdP_4, *i.e.* the sample within the isotherm. The formation of autunite-like species

coincides with a release of Ca and P during the acid treatment and points to the presence of an accessory, apatite-like mineral phase, which explains the enhanced anomalous sorption behaviour of U. These results demonstrate that accessory phases might substantially contribute to the sorption of a bulk mineral phase. Therefore, the development of reliable sorption models requires experimental data covering large ranges of geochemical conditions and also the spectroscopic verification of the retention processes.

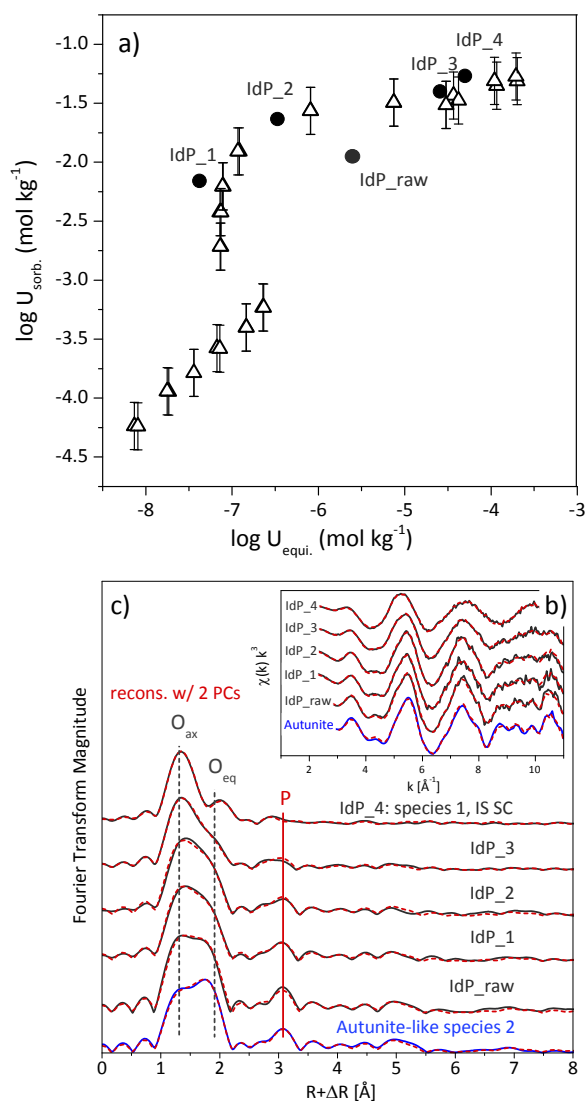


Fig. 3.3 a) Sorption isotherm of U^{VI} on Na-IdP at pH 4.9 in 0.1 NaClO₄. U-L_{III} edge XAFS spectra of autunite and of U^{VI} sorbed on treated/untreated IdP. (black dots: EXAFS samples) (b) k^3 -weighted EXAFS spectra, and (c) corresponding Fourier Transform Magnitudes (FTMs). (Black/blue lines: experimental data; dashed red lines: reconstruction of the spectra with two principal components).

3.2.3 Influence of structural Fe^{II} in montmorillonite on the retention of Np^V

Ferrous iron (Fe^{II}) in clay minerals may reduce weakly sorbing redox sensitive radionuclides such as Np^V (NpO₂⁺) at their surface, thereby considerably increasing their sorption. To quantify the influence of structural Fe^{II} in terms of mediated reduction on the retention of Np^V, sorption experiments were performed on natural Wyoming montmorillonite (SWy) (2.9 weight (wt.%) Fe^{III} in the lattice) and on dithionite–citrate–bicarbonate (DCB) reduced SWy (*i.e.* structural Fe^{III} fully reduced to Fe^{II}) in 0.1 M NaClO₄. Fig. 3.4a shows the pH dependent sorption of Np^V on Na-SWy (2.9 wt.% Fe^{III} in the lattice corresponding to ~400 mmol kg⁻¹) and on the DCB reduced natural SWy (*i.e.* structural Fe^{III} fully reduced to Fe^{II}). The sorption of Np^V on the reduced SWy is substantially increased (up 4 log units) compared to the sorption on the natural (oxidized) SWy, suggesting the formation of Np^{IV} surface complexes.

The oxidation state and the structure of the Np surface complexes were further investigated by X-ray absorption spectroscopy. L_{III} EXAFS spectra were collected at ROBL in fluorescence mode under cryogenic conditions at 15 K using a closed-cycle He-cryostat to avoid oxidation of the samples. Montmorillonite samples prepared at different pH and with different Np loadings: native SWy at pH 8 (with 2.5 mmol kg⁻¹) and on CBD treated SWy at pH 5, 4.9, 8.5 and 9.4 with ~3, 16, 13 and 16 mmol kg⁻¹ Np, respectively, were analysed (Fig. 3.4b). Principal analysis of all reduced SWy spectra necessitated one spectral component for satisfactory sample reconstruction, suggesting formation of only one distinct Np species. Structural parameters of the Np complex were determined by shell fitting. The results of the data analysis are summarized in Table 3.1. The parameters derived for the four reduced SWy samples are identical confirming the ITFA. Coordination number and bond distances of the first oxygen shell are consistent with Np^{IV} complexes, confirming the

complete reduction of Np^V. Two Fe shells could be fitted at ~ 3.40 Å and 4.11 Å suggesting the close association of Np with Fe. No NpO₂ formed despite the rather high initial Np^V concentrations ~ 10⁻⁴ M.

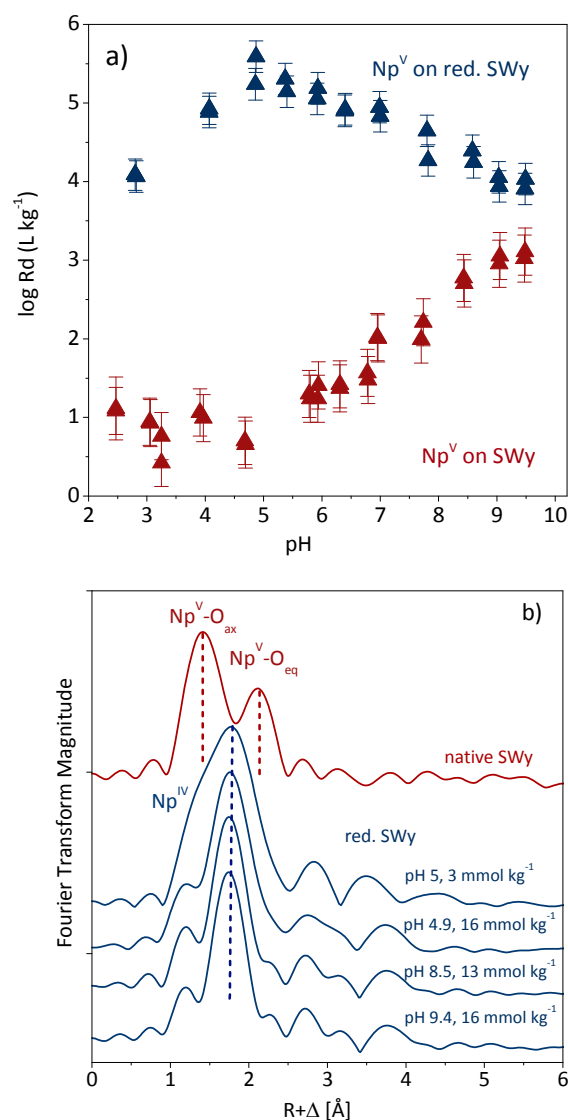


Fig. 3.4: Np^V on native (red) and reduced Na-SWy (blue) (a) pH dependent sorption of trace Np^V and (b) FTMs of the Np-L_{III} edge EXAFS data.

Table 3.1: Np-L_{III} EXAFS fit results of Np^V reacted with reduced SWy ($S_0^2 = 0.9$, fit range 2.0 - 9.5 Å⁻¹).

Sample	CN 1 st shell ^f	R(Å)	σ ² (Å ²)	CN 2 nd shell	R(Å)	σ ² (Å ²) ^c
pH 8.5, 13 mmol/kg	3.0 O	2.18	0.0085	2.3 Fe	3.40	0.0100
	6.0 O	2.35	0.0074	2.5 Fe	4.11	0.0100
pH 9.4, 16 mmol/kg	3.0 O	2.20	0.0100	2.0 Fe	3.40	0.0100
	6.0 O	2.35	0.0100	2.1 Fe	4.10	0.0100
pH 4.9, 16 mmol/kg	3.0 O	2.18	0.0047	2.1 Fe	3.44	0.0100
	6.0 O	2.37	0.0060	2.9 Fe	4.15	0.0100
pH 5, 5 mmol/kg	3.0 O	2.17	0.0046	0.9 Fe	3.38	0.0037
	6.0 O	2.37	0.0069	1.3 Fe	4.05	0.0037

f: fixed; c: correlated

3.2.4 Cs, Rb and Tl sorption on illite (PhD project of S. Wick)

BRADBURY & BAEYENS (2000) have developed a generalized Cs sorption model which was successfully applied in past performance assessments for potential Swiss repository sites for deriving sorption values (K_d) for Cs in argillaceous rocks (BRADBURY & BAEYENS 2003; BAEYENS et al. 2012).

Recently, the Cs sorption model developed for illite has been applied to Tl sorption studies carried out in the framework of a SNSF funded PhD study on "Sorption of thallium to illite and birnessite and its impact on thallium solubility in soils" in cooperation with Eawag (A. Voegelin). The uptake behaviour of Tl^+ on illite resembles the sorption behaviour of the alkali metals Cs^+ and Rb^+ on illite (BROUWER et al. 1983). The sorption model describes the uptake behaviour of these elements by a three site cation exchange model consisting of frayed edge sites (FES), type 2 sites (T2S) and planar sites (PS). A reference cation exchange capacity (CEC) of 200 mequiv/kg for illite and site capacities of 0.25 % for FES, 20 % for T2S and 80 % for PS of the CEC are non-adjustable parameters in the sorption model.

The experimental and modelled data of Tl exchange on homoionic Na-, K- and Ca-illites obtained within the PhD project (WICK et al. 2018) are compared with the original Cs and Rb data from BROUWER et al. (1983) in Fig. 3.5 and the best fitted parameters are summarized in Table 3.2. The sorption of Cs, Tl and Rb at trace concentration ($< 10^{-6}$ M) is mainly governed by the FES and Tl fits perfectly between Cs and Rb on this site on Na-, K- and Ca-illite. The driving force for the adsorption on the high affinity FES can be ascribed to the difference in free energies of hydration between e.g. Cs and Na or Ca (BROUWER et al., 1983). This is also applicable for Tl who has similar dehydration energy and ionic radius as Cs and Rb. At higher concentration, Tl is behaving similar to Cs and Rb on the Na- and K-illites whereas Tl appears to be more selective on the less energetic adsorption sites (T2S and PS) on Ca-illite.

This study nicely illustrates that sorption models developed within the framework of safety assessment of HLW repositories can also be very useful for characterising the speciation and solubility of toxic trace metals in soils and sediments.

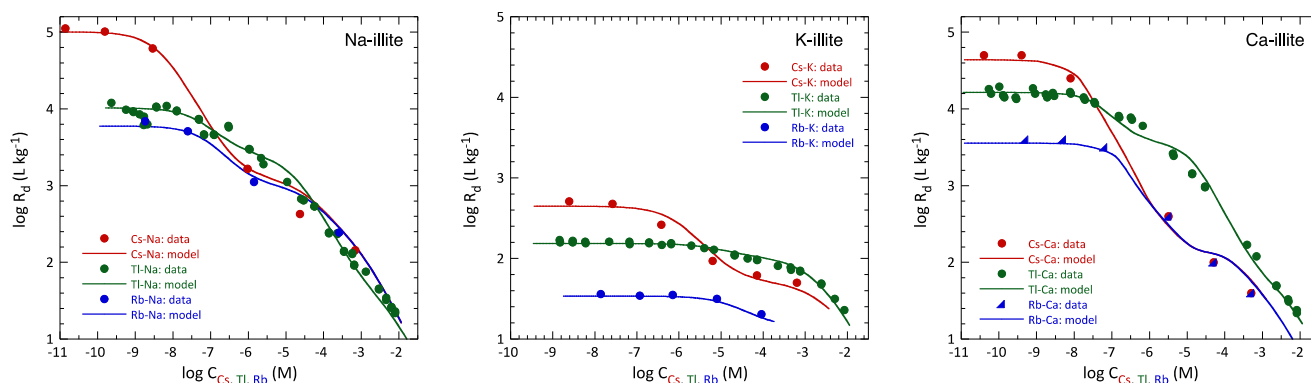


Fig. 3.5: Data and modelling of Cs^+ , Tl^+ and Rb^+ on Na-, K- and Ca-illites (data from BROUWER et al. (1983) and WICK et al. (2018)).

Table 3.2: $\ln K_c$ values for the exchanges (25 °C) on frayed edge sites (FES), type II sites (T2S) and planar sites (PS) of illite for Cs^+ , Tl^+ and Rb^+ on Na^+ -, K^+ - and Ca^{2+} -illites.

Site type	FES	T2S	PS
Site capacity (meq/kg)	5×10^{-4}	4×10^{-2}	1.6×10^{-1}
Exchange equilibrium	$\ln K_c$		
$Cs^+ + Na^+ \text{-illite} \Leftrightarrow Cs^+ \text{-illite} + Na^+$	15.2	6.2	3.2
$Tl^+ + Na^+ \text{-illite} \Leftrightarrow Tl^+ \text{-illite} + Na^+$	14.5	9.0	3.2
$Rb^+ + Na^+ \text{-illite} \Leftrightarrow Rb^+ \text{-illite} + Na^+$	12.2	6.0	3.2
$Cs^+ + K^+ \text{-illite} \Leftrightarrow Cs^+ \text{-illite} + K^+$	9.7	2.5	1.2
$Tl^+ + K^+ \text{-illite} \Leftrightarrow Tl^+ \text{-illite} + K^+$	6.9	2.3	1.4
$Rb^+ + K^+ \text{-illite} \Leftrightarrow Rb^+ \text{-illite} + K^+$	6.7	1.2	0.0
$2 Cs^+ + Ca^{2+} \text{-illite} \Leftrightarrow 2 Cs^+ \text{-illite} + Ca^{2+}$	32.2	11.7	1.2
$2 Tl^+ + Ca^{2+} \text{-illite} \Leftrightarrow 2 Tl^+ \text{-illite} + Ca^{2+}$	28.6	17.3	5.3
$2 Rb^+ + Ca^{2+} \text{-illite} \Leftrightarrow 2 Rb^+ \text{-illite} + Ca^{2+}$	27.2	11.8	1.2

3.2.5 Immobilisation of selenium and iodine in cementitious systems (PhD project of L. Nedyalkova)

During the first year of the PhD project, pure AFm phases with various intercalating anions (OH^- , CO_3^{2-} , SO_4^{2-} , SO_3^{2-} , $\text{S}_2\text{O}_3^{2-}$, SeO_4^{2-} , SeO_3^{2-} , I^-) were synthesized. These pure phases were characterized with the help of different techniques (XRD, TG, IR, aqueous phase analysis) and their solubilities were determined. In a next step several types of solid solutions with AFm phases containing various ratios of SeO_3^{2-} to X^{n-} and I^- to X^{n-} ($\text{X}^{n-} = \text{SO}_4^{2-}$, CO_3^{2-} , OH^- , $\text{OH}^- \text{CO}_3^{2-}$, $\text{S}_2\text{O}_3^{2-}$) were synthesized and characterized. Solid solutions series with OH-AFm and OH- CO_3 -AFm were synthesized in the presence of 0.1 M NaOH; for the synthesis of the remaining solids appropriate $\text{Na}_2\text{-X}$ salts were used. In both cases the resulting pH was ~ 13 . Based on x-ray diffraction (XRD) observations, solid solution formation was observed between the following pairs: SeO_3 - SO_4 , SO_3 - SO_4 , I- CO_3 , I-OH- CO_3 , and I-OH.

On a XRD diagram, a solid solution is characterized by a gradual peak shift from one end member to the other. A continuous solid solution was found between the end members SeO_3 -AFm and SO_4 -AFm. In this case, the larger ionic radius of the SO_4^{2-} anion (2.58 Å) compared to the SeO_3^{2-} anion (2.39 Å) (JENKINS & THAKUR 1979) results in a continuous peak shift towards higher basal spacing (d-values) with increasing amount of SO_4^{2-} (Fig. 3.6a).

For other pairs only limited solid solutions with miscibility gaps were observed. Such is the case with the I₂-AFm and CO_3 -AFm, where small amounts of CO_3^{2-} ($0.3 \leq \text{CO}_3/(2\text{I}+\text{CO}_3)$) are well incorporated in the I₂-AFm structure and form a mixed I₂- CO_3 -AFm phase as seen by the initial peak shift (Fig. 3.6b). At compositions $0.5 \leq \text{CO}_3/(2\text{I}+\text{CO}_3)$ a miscibility gap was observed indicated by the presence of two coexisting phases – an I₂- CO_3 -AFm mixed phase and pure CO_3 -AFm. The obtained data together with bulk chemical analysis of the liquid phases and pH measurements will be used for the construction of thermodynamic models describing the above-mentioned solid solutions using GEMS.

In addition, it was attempted to synthesize pure AFm phases with S^{2-} and Se^{2-} as intercalating anions. S(-II)-AFm was synthesized successfully by mixing stoichiometric amounts of C_3A , CaO and $\text{Na}_2\text{S} \cdot 9\text{H}_2\text{O}$ in 0.1 M NaOH and ageing for 1 month under N_2 atmosphere (O_2 partial pressure < 0.1 ppm). XRD revealed the formation of an AFm phase with d-spacing = 8.46 Å.

Se(-II)-AFm phases were synthesized by mixing stoichiometric amounts of C_3A , CaO and $\text{Na}_2\text{Se} \cdot 9\text{H}_2\text{O}$ in 0.1 M NaOH. The $\text{Na}_2\text{Se} \cdot 9\text{H}_2\text{O}$ salt was obtained by electrochemical reduction of Na_2SeO_3 in 4 M NaOH in a home-made three electrode electrochemical cell (LES PROGRESS REPORT 2013).

Analysis of the aqueous phase with ion chromatography and a sulphide specific electrode confirmed the absence of sulfide oxidation during the AFm synthesis.

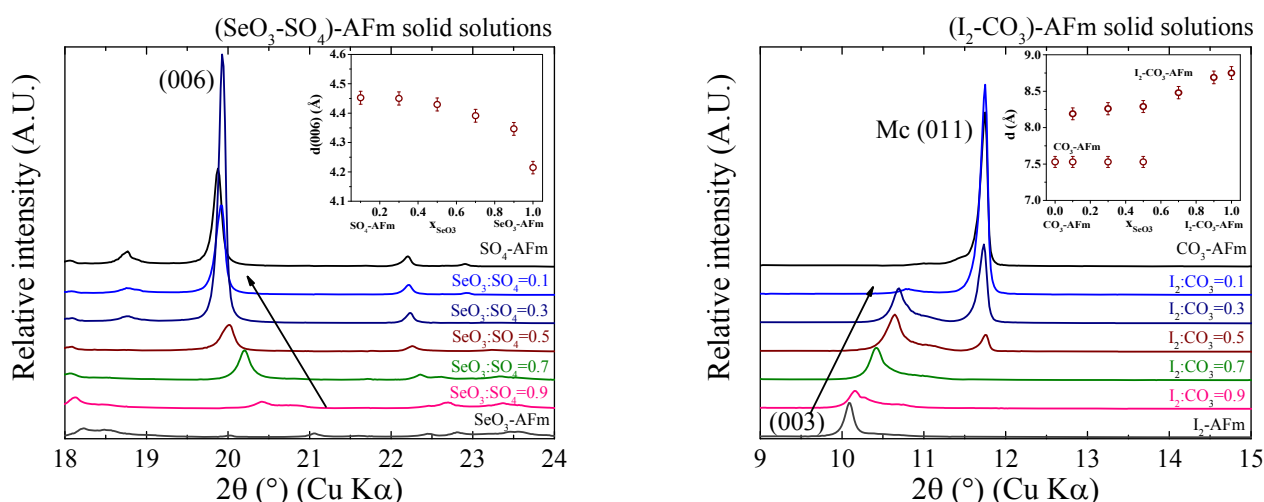


Fig. 3.6: XRD patterns of SeO_3 - SO_4 -AFm solid solution series (a) and the I_2 - CO_3 -AFm solid solution series (b). Inlays represent the dependence of the d-spacing on the solid solution composition.

3.2.6 Mechanism of Fe incorporation in montmorillonite (PhD project of A. Keri)

Molecular mechanism of Fe uptake by clay minerals is investigated in the framework of a SNSF funded PhD project "Detailed understanding of metal adsorption on clay minerals obtained by combining atomistic simulations and X-ray absorption spectroscopy". Molecular dynamics (MD) simulations based on density functional theory (DFT+U) were applied to investigate the incorporated iron in bulk montmorillonite in structurally different positions in the octahedral sheet of montmorillonite and to derive theoretical Fe XAS spectra.

Using a linear combination fit a consistent interpretation of calculated and measured (EXAFS) and (XANES) spectra of iron incorporated Milos-montmorillonite could be obtained. Currently, the trajectories of iron incorporated in the surface sites of montmorillonite are being evaluated. The molecular dynamics trajectories are used to calculate theoretical spectra inner- and outer-sphere surface complexes and to interpret the experimental observations.

The analysis of the experimental data for Milos-montmorillonite and simulation results suggested that iron in bulk montmorillonite is preferentially incorporated as Fe^{3+} into the octahedral layer and it equally occupies cis- and trans-octahedral sites of bulk Milos-montmorillonite (Fig. 3.7) (KÉRI et al. 2017).

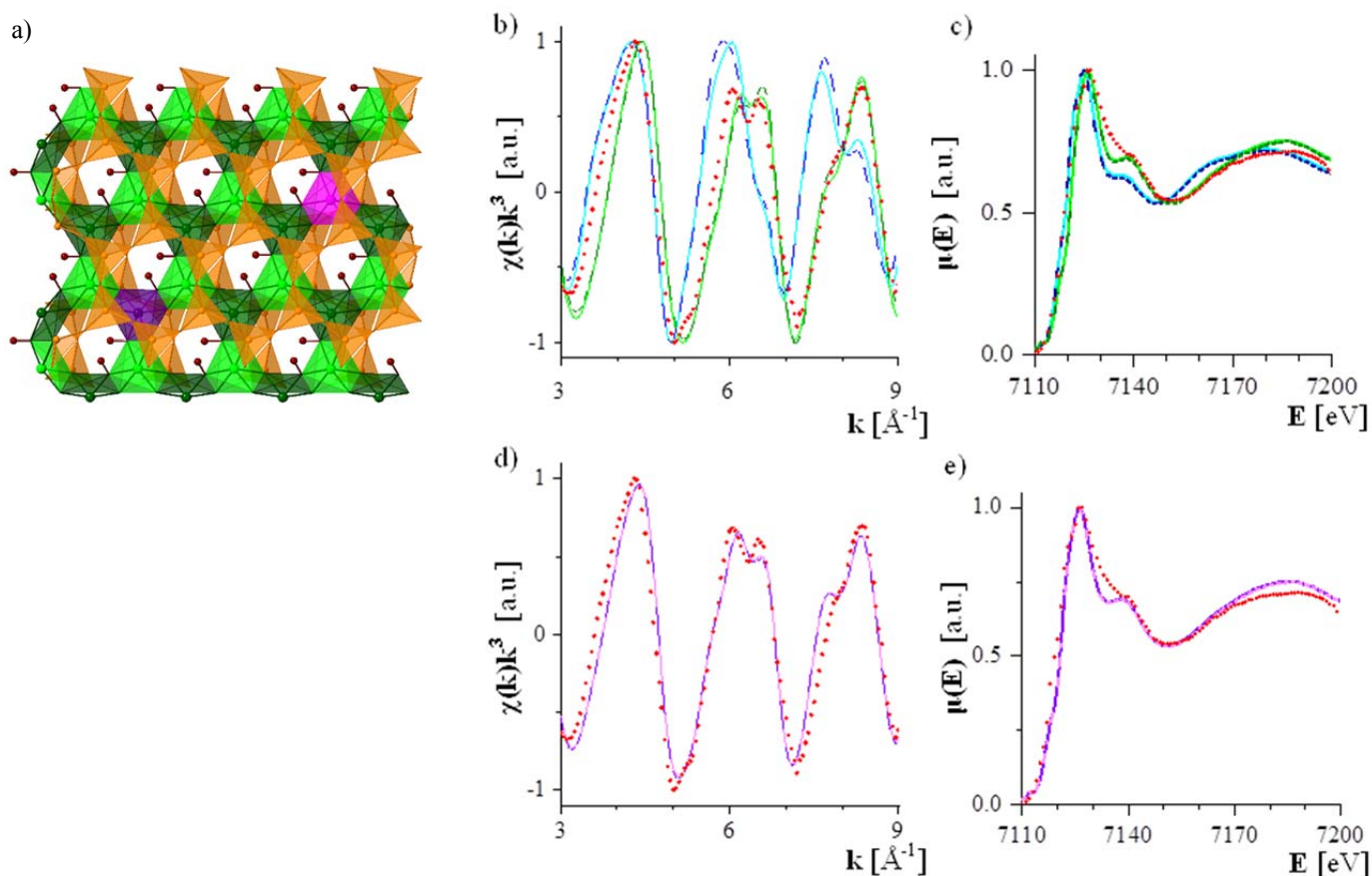


Fig. 3.7: Schematic structure of cis-vacant montmorillonite (a) Orange colour represents Si tetrahedra, Al octahedra are shown with green colour, while Fe incorporation is marked with pink and purple colours. Light colours in the octahedra layer represent cis- while dark colours show trans-occupational sites in respect to the relative positions of the hydroxyl groups. The calculated EXAFS and XANES spectra of Fe substitution in bulk montmorillonite for ferrous and ferric ions are shown with blue and green lines in insert (b) and (c), respectively. Light colours represent cis- while dark colours show trans-occupational sites of the iron incorporation. The measured spectrum of Milos-montmorillonite is denoted with red dots and orange triangles. The linear combination fits of the calculated EXAFS and XANES spectra (shown with pink and purple lines) to the measured ones are represented in insert (d)—(e), respectively (KÉRI et al. 2017).

3.2.7 Microscale distribution and speciation of thallium in contaminated soils

Thallium (Tl) is a highly toxic trace metal classified as a priority pollutant by the US EPA. However, the processes that control the retention and impact of Tl in soils and sediments have not been studied in detail to date. In the environment, Tl occurs mainly as monovalent Tl^I , to a lesser extent as trivalent Tl^{III} (VOEGELIN et al. 2015). Due to its similar ionic radius, Tl^I can substitute K in minerals such as feldspar or phyllosilicates (see section 3.2.4). Tl^{III} can be stabilized by formation of poorly soluble avicennite (Tl_2O_3) or by complexation on Mn-oxides (PEACOCK & MOON 2012). Recently, VOEGELIN et al. (2015) provided first spectroscopic evidence that Tl^I adsorbed onto illite and Tl^{III} bound in Mn-oxides represent key Tl species in geogenically Tl-rich soils.

Soil Mn concretions are accumulations of Mn-oxides in the soil matrix. Biogenic Mn-oxides readily sorb many trace elements and are highly redox reactive (TEBO et al. 2004). They structurally resemble δ - MnO_2 , a synthetic hexagonal birnessite (TEBO et al. 2004), and may transform into triclinic birnessite or todorokite (ATKINS et al. 2014). It has been shown that δ - MnO_2 can bind Tl by Tl^I oxidation and Tl^{III} complexation on top of vacancy sites, whereas triclinic birnessite only sorbs Tl^I as an outer-sphere complex (PEACOCK & MOON 2012). The mechanism of Tl uptake is thus expected to depend on Tl loading

and on the Mn-oxide phase, impacting the solubility of Tl in soil porewater.

Recently, we have conducted our first experiment at beamline I18 at the Diamond Light Source, UK, on soil thin-sections prepared on 250- μ m thin Si wafers to optimize thermal conductance and sample cooling in a cryostat at 10 K. Even at 10 K, XANES spectroscopy with a 5 x 5 μ m beam on Tl-rich Mn concretions showed radiation-induced Tl and Mn redox changes within the first scan (10 min exposure time). However, μ -XRF maps collected at 5 energies across the Tl L_{III} -edge (diagnostic of Tl^I or Tl^{III}) with 0.2 sec exposure time per pixel per map allowed to map the distribution of Tl^I and Tl^{III} within Mn concretions (Fig. 3.8), and repeated mapping up to 5 sec total exposure time per pixel showed no evidence of beam-induced Tl redox changes. The data revealed that Tl redox state can vary within a single Mn concretion (and between concretions), presumably due to variations in Mn-oxide type and/or Tl loading. Because diagnostic features of different types of Mn^{IV} -oxides are located in the EXAFS (MANCEAU et al. 2004), we were not able to reliably differentiate the Mn^{IV} -oxides without radiation-induced artefacts. For Tl, on the other hand, we found that XANES mapping at 70 energies across the Tl L_{III} -edge allowed us to resolve Tl speciation beyond oxidation state. The results from this experiment will be submitted for publication in a manuscript addressing methodological aspects and first results on Tl and Mn.

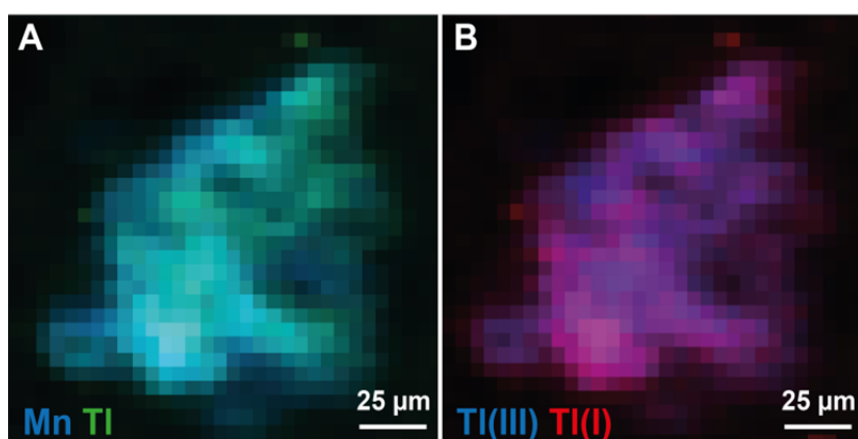


Fig. 3.8: (a) distribution of Mn (blue) and Tl (green) in a Tl-rich Mn concretion; (b) distribution of Tl^{III} (blue) and Tl^I (red) in the concretion in \AA .

3.3 References

- ATKINS A.L., SHAW S., PEACOCK C.L. (2014)
Nucleation and growth of todorokite from birnessite: Implications for trace-metal cycling in marine sediments: *Geochim. Cosmochim. Acta* 144, 109-125.
- BAEYENS B., BRADBURY M. H. (2017)
The development of a thermodynamic sorption database for montmorillonite and the application to bentonite rocks. PSI Bericht Nr. 17-05 and Nagra Tech. Rep. NTB 17-13.
- BAEYENS B., THOENEN T., BRADBURY M., MARQUES FERNANDES M. (2014)
Sorption data bases for the host rocks and lower confining units and bentonite for provisional safety analysis for SGT-E2: Nagra Tech. Rep. NTB 12-04.
- BRADBURY M.H., BAEYENS B. (1997)
A mechanistic description of Ni and Zn sorption on Na-montmorillonite Part II: modelling: *J. Contamin. Hydrol.* 27, 223-248.
- BRADBURY M.H., BAEYENS B. (2000)
A generalised sorption model for the concentration dependent uptake of caesium by argillaceous rocks: *J. Contamin. Hydrol.* 42, 141-163.
- BRADBURY M.H., BAEYENS B. (2003)
Far field sorption data bases for performance assessment of a high-level radioactive waste repository in an undisturbed Opalinus Clay host rock. PSI Bericht Nr. 03-08 and Nagra Tech. Rep. NTB 02-18.
- BRADBURY M.H., BAEYENS B. (2005)
Experimental and modelling investigations on Na-illite: Acid-base behaviour and the sorption of strontium, nickel, europium and uranyl. PSI Bericht Nr. 05-02 and Nagra Tech. Rep. NTB 04-02.
- BRADBURY M.H., BAEYENS B. (2009)
Sorption modelling on illite Part I: Titration measurements and the sorption of Ni, Co, Eu and Sn. *Geochim. Cosmochim. Acta* 73, 990-1003.
- BRADBURY M.H., BAEYENS B. (2017)
The development of a thermodynamic sorption database for illite and the application to argillaceous rocks. PSI Bericht Nr. 17-06 and Nagra Tech. Rep. NTB 17-14.
- BRADBURY M.H., MARQUES FERNANDES M., BAEYENS B. (2017)
Estimates of the influence of radionuclide solubility limits and sorption competition on the sorption values in the SDBs of MX-80 bentonite and Opalinus Clay: PSI Bericht Nr. 17-11 and Nagra Tech. Rep. NTB 17-04.
- BROUWER E., BAEYENS B., MAES A., CREMERS A. (1983)
Cesium and rubidium ion equilibria in illite clay: *J. Phys. Chem.* 87, 1213-1219.
- JENKINS H.D.B., THAKUR K.P. (1979)
Reappraisal of thermochemical radii for complex ions. *J. Chem. Education* 56, 576-577.
- KÉRI A., DÄHN R., KRACK M., CHURAKOV S.V. (2017)
Combined XAFS spectroscopy and ab initio study on the characterization of iron incorporation by montmorillonite. *Environ. Sci. Technol.* 51, 10585-10594.
- MANCEAU A., MARCUS M.A., TAMURA, N., PROUX O., GEOFFROY N., LANSON B. (2004)
Natural speciation of Zn at the micrometer scale in a clayey soil using X-ray fluorescence, absorption, and diffraction. *Geochim. Cosmochim. Acta* 68, 2467-2483.
- PEACOCK C.L., MOON E.M. (2012)
Oxidative scavenging of thallium by birnessite: Explanation for thallium enrichment and stable isotope fractionation in marine ferromanganese precipitates: *Geochim. Cosmochim. Acta* 84, 297-313.
- ROSSBERG A., REICH T., BERNHARD G. (2003)
Complexation of uranium(VI) with protocatechuic acid - application of iterative transformation factor analysis to EXAFS spectroscopy. *Anal. Bioanal. Chem.* 376, 631-638.
- TEBO B.M., BARGAR J.R., CLEMENT B.G., DICK G. J., MURRAY K. J., PARKER D., VERITY, R., WEBB S. M. (2004)
Biogenic manganese oxides: Properties and mechanisms of formation. *Ann. Rev. Earth Planetary Sci.* 32, 287-328.
- VOEGELIN A., PFENNINGER N., PETRIKIS J., MAJZLAN J., PLÖTZE M., SENN A.-C., MANGOLD S., STEININGER R., GÖTTLICHER J. (2015)
Thallium speciation and extractability in a thallium- and arsenic-rich soil developed from mineralized carbonate rock. *Environ. Sci Technol.* 49, 5390-5398.
- WICK S., BAEYENS B., MARQUES FERNANDES M., VOEGELIN A. (2017)
Thallium adsorption onto illite. *Environ. Sci Technol.* 52, 571-580.

4 ^{14}C SPECIATION AND TRANSPORT IN REPOSITORY

E. Wieland, M.A. Glaus, J. Tits, L.R. Van Loon, P. Bunic, S. Frick, D. Kunz, A. Laube, Y. Chen (PhD), B.Z. Cvetković (Postdoc)

4.1 Introduction

Carbon-14 has been identified as a key radionuclide in safety assessment and a major contributor to the long-term activity release rate (mSv per year) from the cement-based repositories for low- and intermediate-level waste (L/ILW) into the host rock. Activated (or irradiated) steel is the main source of ^{14}C in the radioactive waste produced in Switzerland. The current situation is that the chemical form of the ^{14}C -bearing compounds produced during the anoxic corrosion of activated steel is only poorly known while the overall ^{14}C inventory in the radioactive waste is well known. Thus, the aim of this project is to investigate i) the release of ^{14}C -bearing compounds from waste materials (e.g. during the corrosion of activated steel) and their speciation, ii) the chemical stability of ^{14}C -bearing organic compounds in repository relevant conditions, and iii) the retardation and migration of the ^{14}C -bearing in the near field of a repository for radioactive waste and in the host rock. To this end, both experimental and modelling studies are carried out.

In 2017 the main activities related to the task "release and speciation" were devoted to further sampling the corrosion experiment with activated steel and identify the ^{14}C -bearing aqueous organic compounds. Investigations carried out in conjunction with the task "chemical stability of organic corrosion products in a cement-based repository" focused on testing the experimental set-up previously developed and the analytical methods needed. Furthermore, a set of reproducible experimental data was successfully acquired. The work conducted in connection with the task "retardation and migration of ^{14}C -bearing molecules" comprises investigations of the transport of small organic molecules in dense clay systems (ROLOC) carried out in the framework of a PhD project and experimental studies on the migration of inorganic carbon in the Opalinus clay (OPA) host rock. The ROLOC project was finalised in 2017.

4.2 Release and speciation of ^{14}C -bearing compounds

A corrosion experiment with activated steel was started in May 2016 with the aim to identify and quantify the ^{14}C -bearing compounds present in the gas and aqueous phase using compound-specific ^{14}C accelerator mass spectrometry (^{14}C AMS). Scoping calculations performed in an earlier phase of the project and carried out to optimize the design of the

corrosion experiment revealed that, for a set-up viable in the PSI HOTLAB, the concentration of the ^{14}C -bearing compounds would be very low and require the development of a very sensitive analytical method capable of identifying and quantifying individual ^{14}C -bearing compounds. This method is based on the separation of individual compounds, both aqueous and gaseous species, by using liquid and gas chromatography and ^{14}C quantification by using ^{14}C AMS, in brief compound-specific ^{14}C AMS. In 2017 substantial progress has been made in the two sub-tasks which are briefly summarized in the following paragraphs.

Corrosion experiment with activated steel. The corrosion experiment was started by immersing two 1 g segments of an activated steel nut in $\text{Ca}(\text{OH})_2$ -saturated alkaline solution (artificial cement pore water (ACW) with $\text{pH} = 12.5$) in the in-house developed reactor (LES PROGRESS REPORT 2015). The steel nut was obtained from the nuclear power plant Gösgen (Switzerland) and characterized prior to use in the corrosion experiment (LES PROGRESS REPORT 2013; SCHUMANN et al. 2014). To ensure anoxic conditions the reactor was closed and purged with N_2 after mounting the steel segments. ACW was prepared in the glove box with a N_2 atmosphere by using degassed Milli-Q water and freshly prepared CaO , and injected into the reactor by using the in-house developed sampling system installed with the reactor. An overpressure of 4 bar N_2 inside the reactor is maintained during the experiment. Temperature, pressure and the concentration of dissolved oxygen are continuously recorded throughout the experiment (LES PROGRESS REPORT 2016).

Since the start of the experiment several samplings have been performed, i.e. after 1, 15, 29, 93, 286, 412 days reaction time. For the sampling, 50 mL gas phase and 7 mL aqueous phase were withdrawn from the reactor during each sampling followed by a readjustment of the liquid volume by injecting 7 mL of O_2 -free fresh ACW and a readjustment of the N_2 overpressure. An extensive analytical protocol was applied to determine several parameters that are related to the identification and quantification of the organic compounds, e.g. individual ^{12}C compounds dissolved in the liquid phase by ion chromatography (IC) and in the gas phase by gas chromatography (GC) both with mass spectrometry detection (MS), total organic carbon (TOC) of the liquid phase, and the total content of ^{14}C -bearing organic compounds (TO^{14}C).

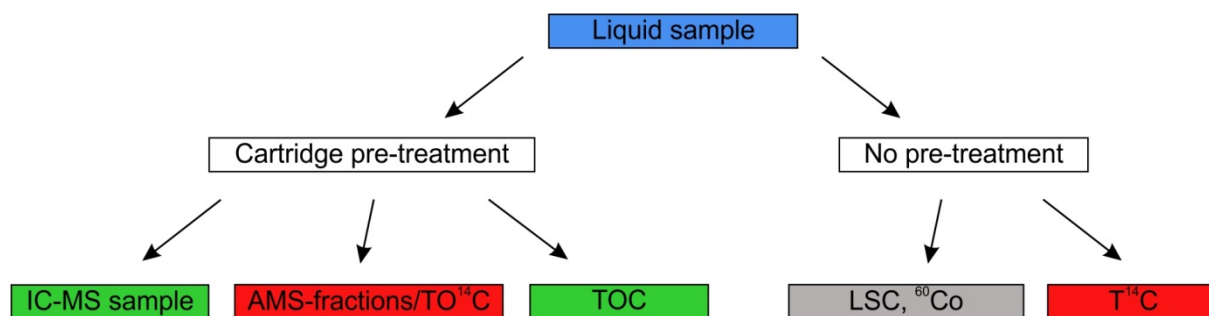


Fig. 4.1: Schematic presentation of the analytical protocol (green: ^{12}C analytics, red: ^{14}C analytics and grey: radioanalysis) for the analysis of the aqueous phase.

Furthermore, radioanalytical parameters were quantified, in particular total ^{14}C by liquid scintillation counting (LSC, β counting) and the ^{60}Co activity by gamma counting. A schematic presentation of the analytical approach is shown in Fig. 4.1.

Analysis of the first series of samples between 1 and 93 days showed that the concentrations of the individual organic compounds in the aqueous and gas phases are below or close, respectively, to the detection limit of IC-MS and GC-MS. In the gas phase only methane was identified as carbon species after 93 days reaction time. In the aqueous phase formate and lactate were clearly identified at concentrations significantly above the detection limit. Oxalate and glycolate were identified at concentrations close to the detection limit. Furthermore, we were able to quantify the ^{60}Co activity by γ counting (Fig. 4.2a) and the TO^{14}C content by using compound-specific ^{14}C AMS (Fig. 4.2b).

Note that the ^{60}Co activity is relatively high due to the large ^{60}Co inventory of activated steel ($61'670 \pm 2158$ kBq/g; SCHUMANN et al. 2014). In contrast, the TO^{14}C content is extremely low due to the very low ^{14}C inventory ($17'841 \pm 2017$ Bq/g; SCHUMANN et al. 2014) of activated steel and the very low corrosion rate of steel in alkaline solution (few nanometers per year) (Fig. 4.2b). The release of ^{60}Co and total ^{14}C to the solution during the corrosion of the activated steel nut segments can be calculated on the basis of the experimentally determined inventories and by assuming plausible corrosion rates (Fig. 4.2). In the case of ^{14}C it was further assumed that all ^{14}C released from activated steel will be present in the organic

chemical form (i.e. TO^{14}C). Hence, the formation of gaseous ^{14}C and inorganic ^{14}C compounds has been ignored. Fig. 4.2 shows that in the first stage of the corrosion process, i.e. over the first ~ 30 days, the release of ^{60}Co and ^{14}C as organic compounds is fast and can be modelled in accordance with an initial corrosion rate of ~ 100 nm/a. Thereafter, the corrosion process significantly decelerates and further release of ^{60}Co and ^{14}C to solution can be modelled by assuming a corrosion rate of 2 nm/a. It should be noted that although the release of ^{60}Co seems to be in line with progressing corrosion at 2 nm/a it is presently not clear whether or not the ^{60}Co activity is an adequate measure of the corrosion rate. For example, the ^{60}Co data may be erroneous due to loss of ^{60}Co activity by sorption processes during sampling and/or sorption onto the surface layer of steel which would explain the steady decrease of the ^{60}Co activity after ~ 30 days reaction time. A series of tests are ongoing with the aim to address this issue.

Fig. 4.2 further shows that the detection limit of compound-specific ^{14}C AMS is very low and, therefore, TO^{14}C concentrations ranging between $2.4 \cdot 10^{-14}$ and $6.9 \cdot 10^{-13}$ M could be detected. The increase in the aqueous ^{14}C concentration with time indicates that the production of ^{14}C -bearing organic compounds is related to the corrosion process in line with a corrosion rate of ~ 100 nm/a over the first ~ 30 days. After 92 days, however, the TO^{14}C content seems to decrease with time, suggesting degradation of the dissolved compounds and/or a decrease in the corrosion rate. At present, it is not clear whether or not this decrease is statistically significant, i.e. outside the uncertainty range of the experiments. Future samplings will enable us to further clarify this issue.

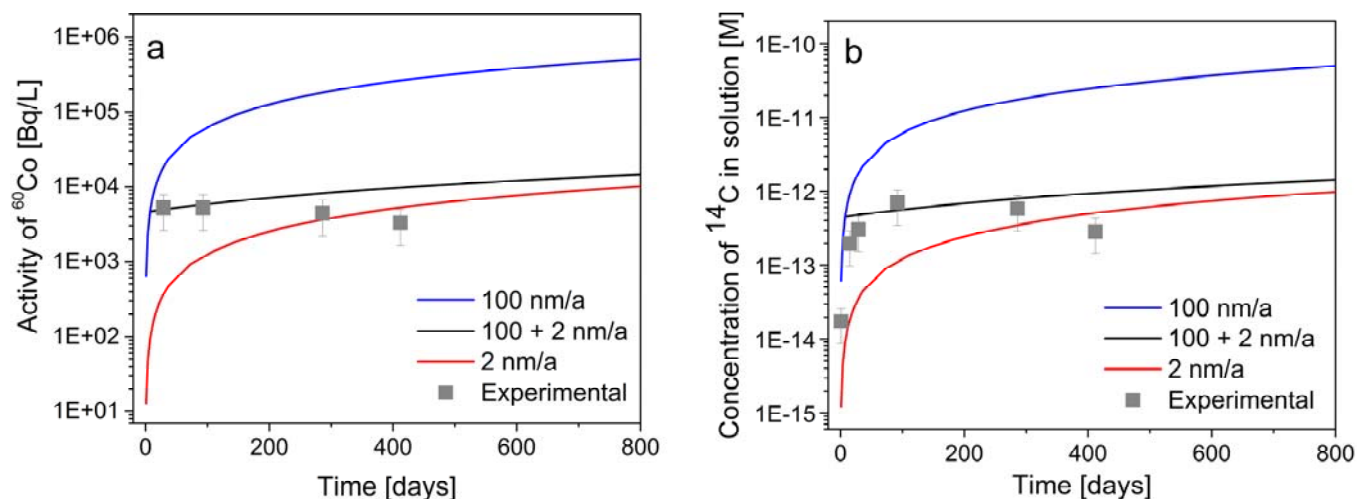


Fig. 4.2: Data: Measurements of a) total ^{60}Co activity and b) the total organic ^{14}C content (TO^{14}C) at different reaction times. Lines: Modelling of the total ^{60}Co activity and b) the TO^{14}C content based on estimated corrosion rates and measured ^{60}Co and ^{14}C inventories.

Table 4.1: Concentration of ^{14}C -bearing formate (FA), acetate (AA), and lactate (LA) determined by AMS after pre-concentration.

Fraction	Concentration		Dilution and background corrected concentration	
	[M]	Error [M]	[M]	Error [M]
LA	$1.7 \cdot 10^{-15}$	$4.3 \cdot 10^{-16}$	$8.7 \cdot 10^{-14}$	$1.7 \cdot 10^{-14}$
FA	$3.0 \cdot 10^{-15}$	$4.3 \cdot 10^{-16}$	$1.3 \cdot 10^{-13}$	$1.3 \cdot 10^{-14}$
AA	$3.0 \cdot 10^{-15}$	$8.7 \cdot 10^{-16}$	$1.0 \cdot 10^{-13}$	$3.5 \cdot 10^{-14}$
LA + FA + AA = TO^{14}C	-	-	$3.2 \cdot 10^{-13}$	$4.1 \cdot 10^{-14}$

The concentration of the individual ^{14}C -bearing organic compounds was determined in solution sampled after 412 days (Table 4.1). In the preceding samplings we were not able to quantify the individual ^{14}C -bearing organic compounds by compound-specific ^{14}C AMS because their concentration was below the detection limit of the analytical method. As a consequence, a freeze-drying process was developed to pre-concentrate ^{14}C in the fractions collected after chromatographic separation with the aim to achieve ^{14}C concentrations above the detection limit of the AMS (average pre-concentration by a factor 15). The concentrations of both ^{14}C -bearing acetate and formate were determined to be $3.0 \cdot 10^{-15}$ M (= 0.007 Bq/L) demonstrating the necessity to perform the pre-concentration step for quantifying the very low concentrations of ^{14}C -bearing organic compounds (Table 4.1). In addition traces of ^{14}C -bearing lactate were detected, i.e. $1.4 \cdot 10^{-15}$ M or 0.003 Bq/L, respectively (Table 4.1). The TO^{14}C content

corresponds to the total of the three analysed fractions, which was estimated at $(3.2 \pm 0.6) \cdot 10^{-13}$ (0.74 Bq/L) by taking into account the dilution caused by chromatographic separation. The value agrees well with that resulting from the direct measurement of the TO^{14}C content ($3.3 \cdot 10^{-13}$ M; Fig. 4.2b), suggesting that the TO^{14}C content can be attributed to the presence of ^{14}C -bearing formate, acetate and lactate in solution.

Development of compound-specific ^{14}C AMS for gaseous compounds. At present, the concentration of the ^{14}C -bearing gaseous compounds in the corrosion experiment cannot be determined using standard GC-MS as their concentration is below the detection limit of the analytical technique. Therefore, a compound-specific ^{14}C AMS methodology for the detection of gaseous ^{14}C -bearing compounds is currently under development. The LES owned GC system operated in the PSI HOTLAB was modified to allow the

separation and quantification of the individual gaseous ^{14}C -bearing compounds. The GC-based system consists of a combustion reactor which oxidizes the organic compounds to $^{14}\text{CO}_2$, and a CO_2 sampling system (Fig. 4.3). Target analytes are separated (separation column 1) and directly oxidized online to CO_2 inside the oxidation reactor. The oxidation products (ideally only CO_2) are then passed through a water separator to remove residual water and a reduction oven to remove traces of oxygen and nitrous oxides. The oxidation products pass through a short second separation column that was installed to separate CO_2 from the rest of the gaseous compounds, e.g. hydrocarbons that were not oxidized. The analytes are detected by a non-destructive method with thermal conductivity detection (TCD) and, based on their retention times, they are eventually collected as separate fractions by the fraction collector.

After installing the TCD in 2016 and the oxidation oven in 2017 we carried out a series of tests to check performance of the system. The second separation column allows the efficiency and the maximum capacity of the oxidation oven to be determined after consecutive injections by calculating the ratio of oxidized to unoxidized species (Fig. 4.4). The tests were performed by using a mixture of methane and ethane. The results are displayed for the tests with (black) and without (red) oxidation in operation. The shift in retention times caused by the second separation column allows a comparison between the initial compound and the oxidized one and, consequently, the oxidation process to be quantified. The tests show that complete oxidation was achieved.

For the AMS measurements a total amount of $20\ \mu\text{g}$ ^{12}C is required in each fraction trapped in the fraction collector. It was planned that the required amount of ^{12}C would be added during injection of the samples into the GC.

Gas chromatography (GC) + Oxidation

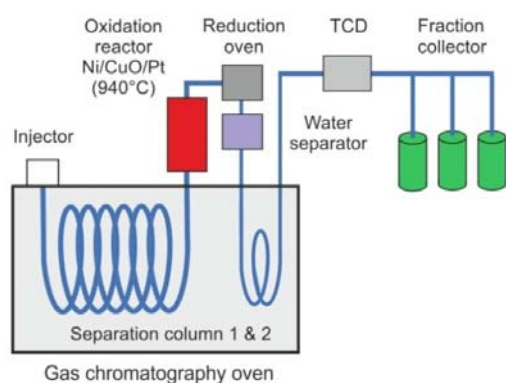


Fig. 4.3: Schematic presentation of the modified GC system to be used for the compound-specific ^{14}C AMS analysis of gaseous species.

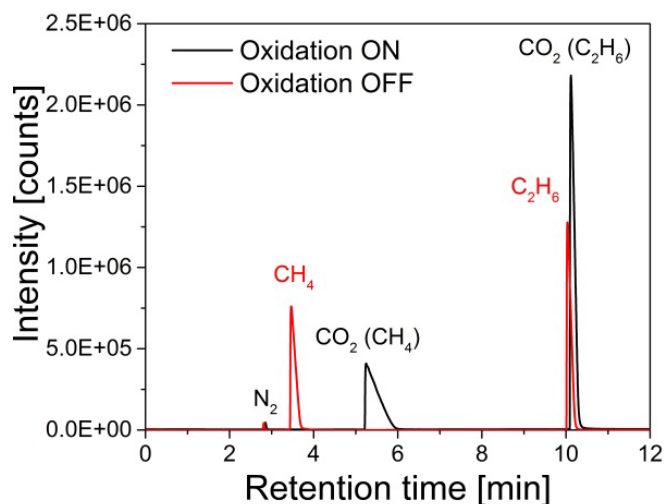


Fig. 4.4: GC-TCD chromatograms of a mixture of methane and ethane with (black) and without (red) oxidation.

To this end, the efficiency and the maximum capacity of the online oxidation had to be tested by sequentially injecting $20\ \mu\text{g}$ methane into the system. Conversion of methane to CO_2 was monitored and quantified (Fig. 4.5). 100% of $20\ \mu\text{g}$ methane was converted to CO_2 in a single injection, thus clearly demonstrating that complete oxidation of CH_4 occurred and the procedure considered for ^{12}C addition is technically feasible. The efficiency of conversion was further tested for up to 60 consecutive injections. It was observed that the efficiency of the oxidation reactor starts to decrease after 50 injections of $20\ \mu\text{g}$ methane. The above findings show that the oxidation reactor converts gaseous compounds into CO_2 very efficiently and has, in addition, a very high capacity.

With these developments at hand we will move on to the next step toward compound-specific ^{14}C AMS for gaseous species in the coming months which will involve tests with the recently installed fraction sampling system. The first test aimed at assessing the concept will already be performed in 2017 followed by recovery tests and final optimization of the entire system in 2018.

Partial financial support for this sub-project was provided by swissnuclear (Project title: "Investigation of the chemical speciation of ^{14}C released from activated steel"), by the EU FP7 collaborative project "CAST" (CARBON SOURCE TERM) and by Nagra. Specific tasks within this sub-project have been developed in co-operation with PD Dr. S. Szidat and Dr. G. Salazar (Department of Chemistry & Biochemistry at the University of Bern, Switzerland), and Brechtbühler AG (Schlieren, Switzerland), the commercial partner in the project.

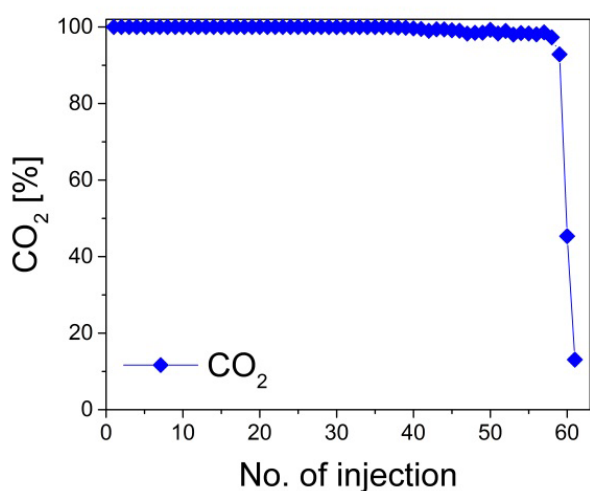


Fig. 4.5: Conversion efficiency to CO₂ for consecutive injections of 20 µg methane.

4.3 Chemical stability of organic compounds in repository relevant conditions

¹⁴C-bearing low molecular weight (LMW) organic molecules released during the corrosion of activated steel may be chemically unstable under the hyper-alkaline, reducing conditions prevailing in a cement-based L/ILW repository. In case of complete thermodynamic equilibrium, decomposition of LMW organics is predicted while the predominant species are CH₄ and CO₂ (and its bases) (WIELAND & HUMMEL 2015). However, complete thermodynamic equilibrium is rarely achieved in the C-H-O system at moderately elevated temperatures. In case partial thermodynamic equilibrium (metastability) prevails, it is still unclear what organic compounds will predominate in the repository. In the near field of a L/ILW repository temperatures up to 80°C and H₂ partial pressures up to 100 atm can be reached (XU et al. 2008).

The chemical stabilities of formate and acetate in hyper-alkaline, anoxic and reducing conditions are currently being studied with the aim to obtain a better insight into the degradation kinetics of LMW organic molecules under cementitious near-field conditions. In previous years, an experimental methodology was developed to perform stability tests with organics and a first series of stability experiments with formate and acetate were carried out in Milli-Q water in pressurized reactors in anoxic conditions at an overpressure of 4 bar N₂. In these experiments degradation of formate and acetate was not observed over time periods up to 8 months. Contact with a stainless steel surface as a catalyst and temperatures up to 150°C did not induce any detectable degradation.

In 2017 degradation tests with formate were continued. In contrast to the previous stability tests, the new series of experiments was carried out in reducing conditions and at elevated temperature and pressure, either in the presence of Fe powder as a reducing agent or in the presence of 2 atm forming gas (95% N₂/5% H₂).

In a first experiment the degradation of 3·10⁻⁴ M ¹³C-labelled formate was investigated in Milli-Q water and in ACW (Ca(OH)₂-saturated ACW with pH = 12.5) in the presence of 25 g L⁻¹ Fe powder (Carbonyl iron powder BASF-HQ, BASF, Ludwigshafen Germany). The degradation experiments were carried out in batch-type closed autoclaves which were stored in an oven at 200°C to accelerate potential decomposition reactions. The maximum pressure was estimated to be 85.5 atm by assuming that the total amount of Fe powder was corroded, thus producing H₂. At regular time intervals one of the autoclaves was taken out of the oven, let cool down, opened, and the aqueous phase was sampled to determine the concentration of ¹³C-labelled formate. The concentration of ¹³C-labelled formate was found to decrease steadily with reaction time over a period of 60 days both in Milli-Q water and in ACW (Fig. 4.6a). After 60 days, the aqueous concentration of ¹³C-labelled formate was reduced by 95% in Milli-Q water and 80% in ACW compared to the initial concentration. We checked whether or not ¹³C-labelled formate was sorbed on the Fe powder at the end of the experiment. To this end, the Fe powder was immersed overnight in Milli-Q water. No ¹³C-labelled formate was observed in solution, indicating that sorption was not an important process and that ¹³C-labelled formate was slowly decomposed in these experiments.

Subsequent degradation experiments with ¹³C-labelled formate were performed in gas-tight pressurized reactors to allow for a better control of the experimental conditions such as sampling of both aqueous and gas phase. To this end, 5·10⁻⁵ M formate solution, containing both ¹³C-labelled and ¹⁴C-labelled formate, was prepared either in Milli-Q water or in different alkaline media (0.01 M NaOH, 5·10⁻³ M and 2·10⁻² M Ca(OH)₂, respectively). The formate-containing solutions were then aged over a time period up to 2 months at a temperature of 150°C. The total pressure amounted to 5.5 bar (2 bar forming gas + 3.5 bar vapour pressure at 150°C). Both liquid and gas phase were sampled regularly. For the sampling, the reactors were cooled down to ambient temperature. Then, 50 mL gas phase and 7 mL aqueous phase were withdrawn from the reactor. The liquid volume was re-adjusted by injecting 7 ml formate-free alkaline solution and the overpressure

was re-adjusted with forming gas. After sampling and re-adjustments had been completed the temperature was again raised to 150°C. The compositions of aqueous and gas phases were determined by IC-MS (carboxylic acids: acetate, formate, lactate) and GC-MS (mainly hydrocarbons), respectively. Note that analytical methods for ^{13}CO , $^{13}\text{CO}_2$ and H_2 detection have not yet been elaborated.

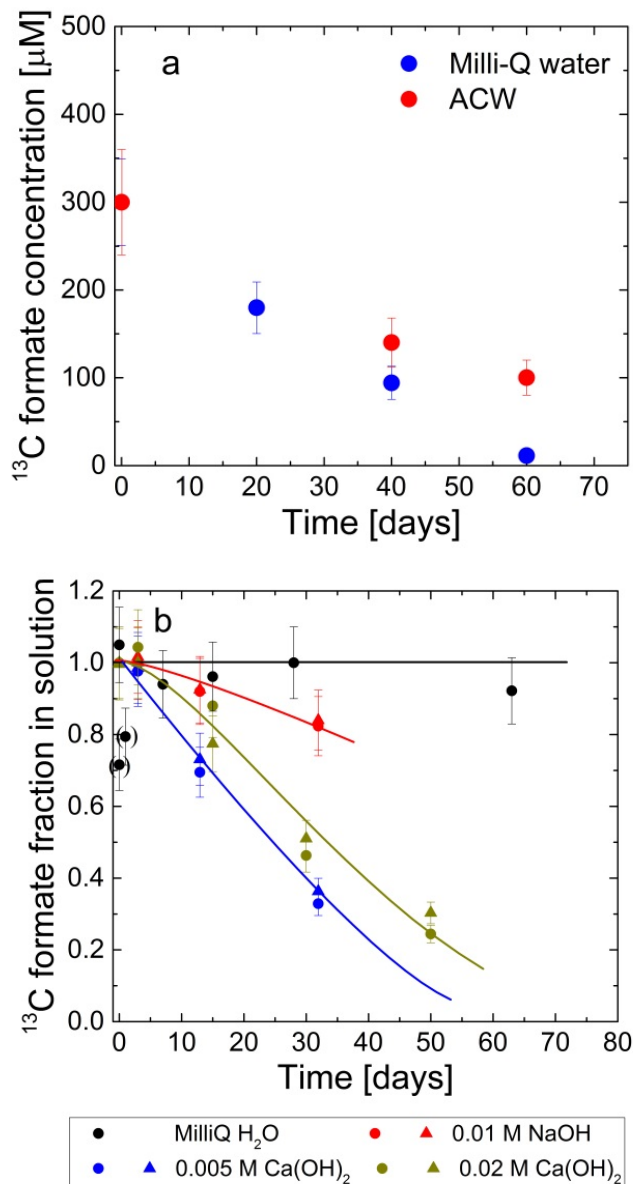


Fig. 4.6: Degradation of ^{13}C -labelled formate in Milli-Q water and in various alkaline solutions under reducing conditions shown as a function of time : a) In batch-type autoclaves in the presence of 25 g L^{-1} Fe powder under N_2 atmosphere ($T = 200^\circ\text{C}$, $P_{\text{max}} = 85.5 \text{ atm}$ ($\text{N}_2 + \text{H}_2$)). b) In gas-tight pressurized reactors at a temperature of 150°C and 2 atm forming gas (95% $\text{N}_2/5\%$ H_2). Dots: Fraction of total ^{13}C -labelled formate concentration in solution; triangles: Fraction of total ^{14}C activity in solution (not necessarily ^{14}C -labelled formate).

Under these experimental conditions, $^{13/14}\text{C}$ -labelled formate was found to be stable over a time period up to 60 days in Milli-Q water at enhanced H_2 partial pressure (Fig. 4.6b). However, in alkaline conditions the aqueous concentration of $^{13/14}\text{C}$ -labelled formate decreased significantly with time. This decrease was more pronounced in the presence of Ca (up to 80% of $^{13/14}\text{C}$ -labelled formate has disappeared after 50 days) than in the presence of Na. In addition, the fraction of ^{14}C -labelled formate, determined by the ^{14}C activity in solution, was observed to decrease at the same rate as the fraction of ^{13}C -labelled formate. This shows that the degradation products are not dissolved species. Rather, they must be either present in the gas phase or precipitate as solid phase. Rinsing the reactor with 0.1 M HCl at the end of the experiments did not lead to the recovery of any significant ^{14}C activity. This finding allows wall sorption or precipitation as potential sinks for $^{13/14}\text{C}$ -labelled formate to be excluded. So far, however, we have not been able to detect any ^{13}C -labelled organic compounds in the gas phase.

The above findings are unexpected and in contrast to literature data which suggest that formate degradation is slower at high pH (MCCOLLOM & SEEWALD 2003) than at near-neutral pH. Furthermore, literature suggests that $\text{Ca}(\text{HCOO})_2$ (the formic acid salt present in the $\text{Ca}(\text{OH})_2$ solutions) should be more stable than HCOONa (present in 0.01 M NaOH solution), thus requiring higher temperature for decomposition (ONWUDILI & WILLIAMS 2010).

The reason for these inconsistencies between our results and literature data is presently unknown. In the next step of this project, the analytical procedure for the gas phase will be improved with the aim to analyse not only the hydrocarbons in the gas phase but also the oxidized species CO and CO_2 . They have been reported in literature as possible degradation products.

4.4 Retardation and migration studies

Retardation and migration of organics in clay system: The study on the transport of LMW, potentially ^{14}C -bearing organic compounds in dense clay systems (ROLOC) has demonstrated unambiguously that some of the small organic compounds used in the study, i.e. aliphatic or hydroxylated carboxylic acids and alcohols, are retarded in pure clay minerals and their mixtures to an extent that would actually lead to a considerable reduction of the predicted radiation dose. The analysis of relationships between the observed retardation and structural properties of the test compounds suggested that ligand exchange at aluminol sites are most probably involved in the binding of hydroxylated carboxylic acids and dipole

interactions in the uptake of alcohols. The results observed in single-clay systems (kaolinite or illite, respectively) could be successfully used to predict the behaviour of the test compounds in kaolinite/illite mixtures. However, transferability of the results from single-clay minerals to clay rock by means of the component additivity ("bottom-up") approach was inherently associated with difficulties, which may challenge the assumption of a generically positive sorption distribution value for organic ^{14}C -bearing compounds in performance assessment for the OPA far field. The submission process of three manuscripts to scientific journals is presently ongoing (CHEN et al. 2018a,b;c).

The possibility of a follow-up project is currently under discussion. Possible strategies for such a project could either involve a more in-depth investigation of the molecular mechanisms of the uptake of LMW organic compounds by argillaceous media, or extending the scope by investigating the general reactivity of such compounds, such as mineralisation reactions, instead of focussing on sorption only. Indications for the latter processes being relevant were found during the course of the ROLOC project in the percolation experiments with OPA samples. For this reason and in view of the prospect of a more generic picture of the relevant processes, we would opt for a broader view on the reactivity of organic compounds in Opalinus Clay.

Diffusion and retention of $\text{H}^{14}\text{CO}_3^-$ in OPA. The diffusion and retention of $\text{H}^{14}\text{CO}_3^-$ in Opalinus Clay was studied on samples originating from the BMA-A1 borehole in the Mont Terri Underground Research Laboratory (URL). The samples were taken at a depth of 10.12 - 10.42 m below the floor level of the tunnel. The samples were mounted in a diffusion cell (VAN LOON et al. 2003) and equilibrated with artificial pore water for about 4 weeks before starting the diffusion experiments. Diffusion experiments with HTO resulted in an effective diffusion coefficient of $(1.4 \pm 0.1) \cdot 10^{-11} \text{ m}^2 \text{ s}^{-1}$ and a total porosity of 0.15 ± 0.02 . These values are comparable with values determined earlier by VAN LOON et al. (2004) and JOSEPH et al. (2013) and show a diffusion behaviour of HTO as expected for OPA from Mont Terri. After diffusion of HTO, diffusion of $\text{H}^{14}\text{CO}_3^-$ was started. The measurements are still ongoing. Analysis of the concentration of $\text{H}^{14}\text{CO}_3^-$ in the source reservoir shows a fast decrease (Fig. 4.7). On the other hand, no break-through of the $\text{H}^{14}\text{CO}_3^-$ could be observed so far. This indicates that $\text{H}^{14}\text{CO}_3^-$ strongly interacts with the Opalinus Clay.

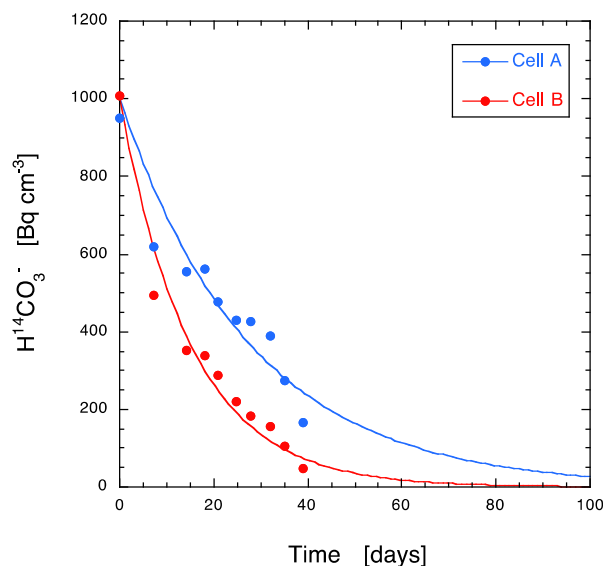


Fig. 4.7: Evolution of the concentration of $\text{H}^{14}\text{CO}_3^-$ in the source reservoir of the diffusion experiment. A strong decrease indicates a strong interaction with the Opalinus Clay. No break-through of $\text{H}^{14}\text{CO}_3^-$ was observed after 30 days (data not shown).

Because adsorption of $\text{H}^{14}\text{CO}_3^-$ on the clay phase is highly unlikely (SHEPPARD et al. 1998), incorporation of $\text{H}^{14}\text{CO}_3^-$ in the calcite phase is more likely (GONFIANTINI & ZUPPI 2003, AVRAHAMOV et al. 2013, LEMPINEN & LEHTO 2016).

This mechanism is schematically represented in Fig. 4.8. The decrease of the $\text{H}^{14}\text{CO}_3^-$ in solution as a function of time can be described by an exponential function (GONFIANTINI & ZUPPI 2003):

$$\frac{A(t)}{A_0} = \exp(-k \cdot t)$$

where $A(t)$ is the activity in solution at time t (Bq cm^{-3}), A_0 is the initial activity in solution at $t=0$ (Bq cm^{-3}), t is time (d) and k is an isotopic exchange constant (d^{-1}). Similar experiments were performed on illite from le Puy. Systems with and without addition of calcite were used to explore the role of calcite on the retention of $\text{H}^{14}\text{CO}_3^-$. Also in the case of illite a strong decrease of the concentration of $\text{H}^{14}\text{CO}_3^-$ in the source reservoir was observed. Unlike Opalinus Clay, however, a break-through of ^{14}C was observed after ~ 5 days, reaching a steady state after 15 days (Fig. 4.9). No significant effect of the addition of calcite could be observed.

The modelling of the results is ongoing. To this end, an isotopic exchange model has to be introduced in the existing transport/speciation codes (e.g. PHREEQC). Important parameters to be evaluated are the specific surface area and the recrystallization rate of calcite, and the transport porosity and effective diffusion coefficient of $\text{H}^{14}\text{CO}_3^-$ in the clay system.

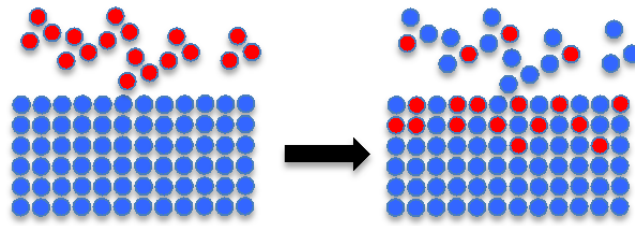


Fig. 4.8: Cartoon picture showing the sorption of $H^{14}CO_3^-$ on calcite by an isotopic exchange process. The system is in equilibrium as soon as the molar ratio of $H^{14}CO_3^-$ (red symbols) to $H^{12}CO_3^-$ (blue symbols) in the liquid phase equals that in the solid phase.

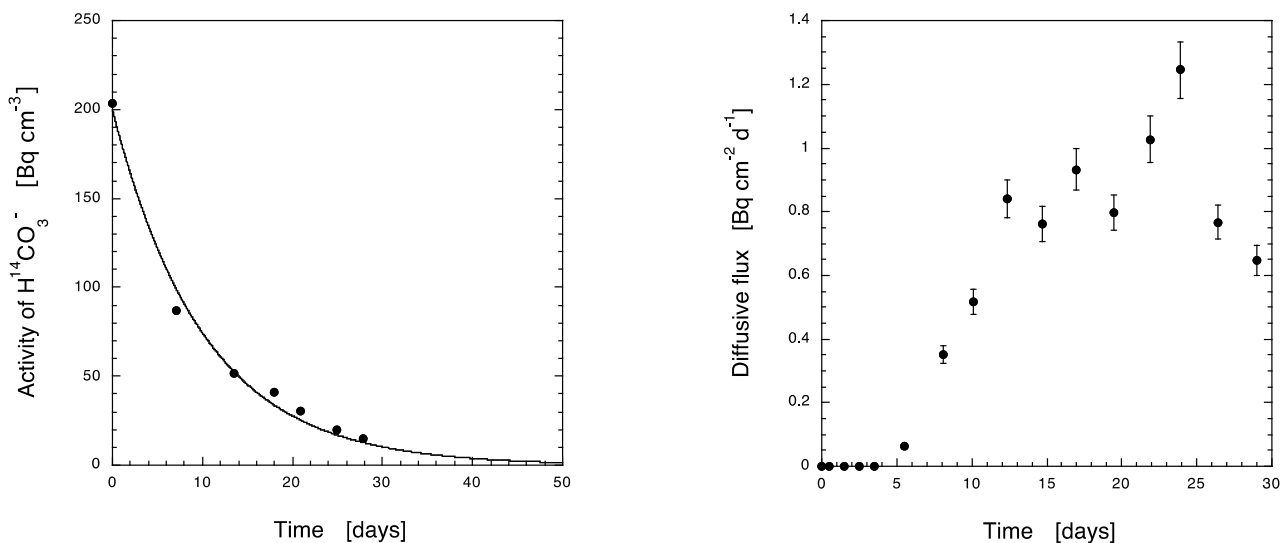


Fig. 4.9: Evolution of the concentration of $H^{14}CO_3^-$ in the source reservoir of the diffusion experiment with native illite (left) and the corresponding diffusive flux as a function of time (right).

4.5 References

AVRAHAMOV N., SIVAN O., YECHIELI Y., LAZAR B. (2013)

Carbon isotope exchange during calcite interaction with brine: implications for ^{14}C dating of hypersaline groundwater. *Radiocarbon* 55, 81-101.

CHEN Y., GLAUS M.A., VAN LOON L.R., MAEDER U., (2018a)

Transport behaviour of low molecular weight organic compounds in multi-mineral clay systems. A comparison between measured and predicted values. to be submitted to *Appl. Geochem.*

CHEN Y., GLAUS M.A., VAN LOON L.R., MAEDER U., (2018b)

Stereo-specific adsorption of lactate on compacted Na-illite measured in percolation experiments. to be submitted to *J. Am. Chem. Soc.*

CHEN Y., GLAUS M.A., VAN LOON L.R., MAEDER U., (2018c)

Transport of low molecular weight organic compounds in clay minerals. A study on compacted illite and kaolinite. to be submitted to *Geochim. Cosmochim. Acta.*

MCCOLLOM T.M., SEEWALD J.S. (2003)

Experimental constraints on the hydrothermal reactivity of organic acids and acid anions: I. Formic acid and formate. *Geochim. Cosmochim. Acta* 67, 3625 - 3644.

GONFIANTINI R., ZUPPI G.M. (2003)

Carbon isotope exchange rate of DIC in karst groundwater. *Chem. Geol.* 197, 319-336.

JOSEPH C., VAN LOON L.R., JAKOB A., STEUDTNER R., SCHMEIDE K., SACHS S., BERNHARD G. (2013) Diffusion of U(VI) in Opalinus Clay: Influence of temperature and humic acid. *Geochim. Cosmochim. Acta* 109, 74-89.

LEMPINEN J., LEHTO J. (2016)

Rate of radiocarbon retention onto calcite by isotope exchange. *Radiochim. Acta* 104, 663-671.

ONWUDILI J.A., WILLIAMS P. (2010)

Hydrothermal reactions of sodium formate and sodium acetate as model intermediate products of the sodium hydroxide-promoted hydrothermal gasification of biomass. *Green Chem.* 12, 2214 - 2224.

SCHUMANN D., STOWASSER T., VOLMERT B., GÜNTHER-LEOPOLD I., LINDER H.-P., WIELAND E. (2014)

Determination of the ^{14}C content in activated steel components from a neutron spallation source and a nuclear power plant. *Anal. Chem.* 86, 5448-5454.

SHEPPARD S.C., TICKNOR K.V., EVENDEN W.G. (1998)

Sorption of inorganic ^{14}C on to calcite, montmorillonite and soil. *Appl. Geochem.* 13, 43-47.

VAN LOON L.R., SOLER J.M., MÜLLER W., BRADBURY M.H. (2004)

Anisotropic diffusion in layered argillaceous rocks: A case study with Opalinus Clay. *Environ. Sci. Technol.* 38, 5721-5728.

WIELAND E., CVETKOVIĆ B.Z. (2016)

Development of a compound-specific carbon-14 AMS technique for the detection of carbon-14 labelled organic compounds. EU Project "CAST" report D 2.3.

WIELAND E., HUMMEL W. (2015)

Formation and stability of carbon-14 containing organic compounds in alkaline iron-water-systems: Preliminary assessment based on a literature survey and thermodynamic modelling. *Mineral. Mag.* 79, 1275-1286.

XU T., SENGER R., FINSTERLE S. (2008)

Corrosion-induced gas generation in a nuclear waste repository: Reactive geochemistry and multiphase flow effects. *Appl. Geochem.* 23, 3423-3433.

4.6 Personnel

Dr. Y. Chen has successfully defended her PhD thesis "Retardation of low-molecular weight organic compounds in clays" at the University of Bern (defence date: June 1, 2017).

5 RADIONUCLIDES TRANSPORT AND RETENTION IN COMPACTED SYSTEMS AT FULL AND PARTIAL SATURATION

L.R. Van Loon, M. A. Glaus, W. Pfingsten, C. Wigger, B. Baeyens, M. Marques Fernandes, S. Frick, P. Bunic, T. Gimmi, S.V. Churakov, Ph. Krejci (PhD)

5.1 Introduction

The sorption of radionuclides on clay minerals in engineered and geological barrier systems is a key safety function in the deep geological disposal of radioactive waste. Reliable sorption data (R_d values) and a mechanistic understanding of sorption processes are thus mandatory for a proper evaluation of this safety function. Sorption studies are mainly performed in batch systems using dispersed clay with a low solid to liquid ratio. In such systems the composition of the solution can be well controlled (e.g. pH, E_h , concentrations of anions and cations, organic and inorganic ligands) and/or varied in order to study their effect on the sorption.

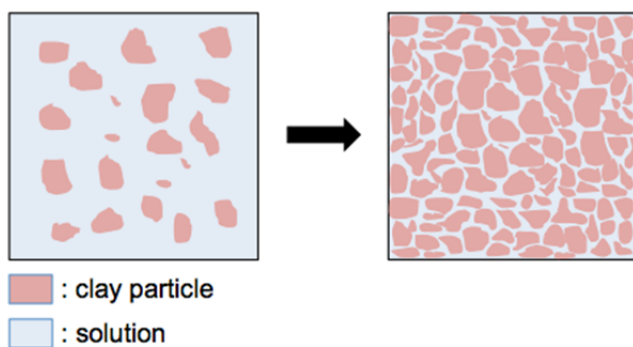


Fig. 5.1: Transferability of sorption data from dispersed to compact systems is a crucial factor in safety analysis of deep geological repositories. Compaction results in confinement of water in narrow spaces, potentially resulting in water with deviating (thermodynamic) properties.

Real clay systems, however, are very dense and are characterised by a high solid-to-liquid ratio (Fig. 5.1). It is still an unanswered question whether data and models evaluated from dilute dispersed systems can be transferred to the real, compact system. The aim of this project is to give a clear answer on this open question of transferability. Because of the diverse nature of the microstructure of clay minerals and clay rocks, answers to this question have probably to be given on a case-by-case basis. Generally speaking, the effect of compaction on the sorption behaviour can be subdivided mainly into the following items:

- sterical effects: accessibility of sorption sites in compact and dispersed systems

- specific surface area aspects: difference in specific surface area between dispersed and compact systems
- thermodynamic aspects: properties of confined versus bulk water and their consequences for sorption processes in confined systems.

A second aim of the project is to improve the fundamental understanding of transport and sorption mechanisms in clay. The focus is mainly on experimental work on the diffusion of strongly sorbing radionuclides in illite and Opalinus Clay, and on extending existing transport codes to model the transport of ions in clays. To this end a new method was introduced to simulate Donnan equilibria based on the Nernst-Planck equation and was tested for various cases. In addition, within an SNSF PhD project "Transport of sorbing ions in clays" (Ph. Krejci) the multispecies cation transport model in compacted clays was extended by taking into account the variable mobility of sorbed species on different sorption sites.

5.2 Desktop study: status report on "transferability"

A desktop study on the transferability was initiated. A draft report giving an overview of the state of the art of the transferability of sorption data and models from dilute to compact systems was prepared, based on existing knowledge from the literature. Moreover, still unresolved questions are highlighted and recommendations w.r.t. additional studies are given (VAN LOON 2017).

5.3 Sorption/diffusion studies on compacted illite

The question of potential differences in the sorption behaviour of compacted and dispersed clay systems was addressed by comparing the results of in-diffusion experiments of Eu(III) in compacted illite with those of batch sorption experiments. In the in-diffusion technique, a compacted clay sample is contacted with a tracer-containing background electrolyte solution. The time-dependent tracer depletion in the solution reservoir and the subsequently measured tracer profile in the clay, provide unambiguous information on the diffusion and sorption properties of the tracer. A broad variety of bounding parameters, such as pH, ionic strength, added concentration of stable Eu(III) and

concentration of a representative ligand (oxalate) were tested. Two different preparations of illite were used. Most experiments were carried out using a preparation, which has undergone a weak acid pretreatment and concomitant equilibration to the homo-ionic Na^+ form (Na-IdP-A). Additional experiments were carried out using a homo-ionic size-fractionated illite preparation that has undergone a strong acid pretreatment (Na-IdP-B). The latter procedure removes substantial amounts of feldspar, which is well-known to induce changes in the sorption behaviour in the pH region around 6.

The evaluation of the experimental data was performed by a combined approach using Comsol Multiphysics® for the purpose of single species transport calculations in a 2-D axisymmetric geometry. The latter option was required in view of the difference between the aperture of the diffusion cell and the thickness of the clay sample. 1-D transport calculations in PHREEQC are not appropriate for such purposes. As demonstrated in previous diffusion studies for illite (GLAUS et al. 2015), the speciation of bi-valent test cations has effects on both the effective diffusion coefficient (D_e) and the sorption distribution coefficient (R_d). Such functional dependencies, like the effect of the stable isotope background concentration on D_e and R_d , were defined in the Comsol Multiphysics® transport model according to the results of speciation calculations performed in PHREEQC.

Figure 5.2a shows the comparison of R_d values measured in dispersed suspensions of Na-IdP-B with the results obtained from in-diffusion experiments as a function of pH ("sorption edge") at a constant background electrolyte concentration of 0.1 M. The results demonstrate that no significant difference between the two test systems exist. The model curves were calculated using a modified 2 site protolysis non electrostatic surface complexation and cation exchange (2SPNE SC/CE) model using published thermo-dynamic data for the surface complexes (MARQUES FERNANDES et al. 2015). The modification consisted of using an electrical double layer (EDL) for the description of the interaction between cations and the negatively charged planar surface sites instead of cation exchange. The EDL species comprise Stern-layer species assumed to be immobile and diffuse layer species assumed to be mobile. Figure 5.2b

shows model predictions and experimental D_e values (Na-IdP-A) as a function of pH. The decrease of D_e at pH values <5 and >7 can be explained by competitive effects in the EDL between Eu^{3+} and other cations (e.g. Ca^{2+} and Al^{3+}) and by the formation of hydrolysed Eu^{3+} species, respectively. The comparison of the model curves shown in Figures 5.2a and 5.2b shows that D_e and R_d values for Eu(III) are not linearly correlated. This is in clear contrast to the observations made for the diffusion and sorption of cations preferentially bound to the planar sites in illite or montmorillonite (GLAUS et al. 2007; GLAUS et al. 2010) and has an important consequence for performance assessment calculations. The use of apparent diffusion coefficients, which are directly proportional to the ratio of D_e/R_d for strongly sorbing species, determined for a particular set of bounding conditions (pH, ionic strength, etc.) may not be necessarily representative for other bounding conditions. A careful analysis of the dependence of apparent diffusion coefficients with the time-dependent evolution of the chemical conditions in the liquid phase may therefore be required.

The robustness of the EDL diffusion and sorption model used here is noteworthy. The only parameter adjusted for the experiments with Eu(III) was the relative surface mobility of these species in the diffuse layer. Otherwise all parameters were identical with those previously used for modelling diffusion of bivalent cations (Sr^{2+} , Co^{2+} and Zn^{2+} , (GLAUS et al. 2015)) and no further adjustments were made for the simulation of the observed dependencies of D_e and R_d values on ionic strength, stable isotope background concentration or the concentration of oxalate. Without the assumption of mobile surface species, it was not possible to produce a consistent description of the tracer depletion in the reservoir solution and the tracer profiles in the clay. The results clearly demonstrate that the diffusion length is systematically and strongly underestimated when neglecting the mobility of the diffuse layer species. It can therefore be concluded that the use of effective diffusion coefficients derived from proportionalities of bulk-water diffusion coefficients will not lead to conservative predictions of dose rates in performance assessment for such elements.

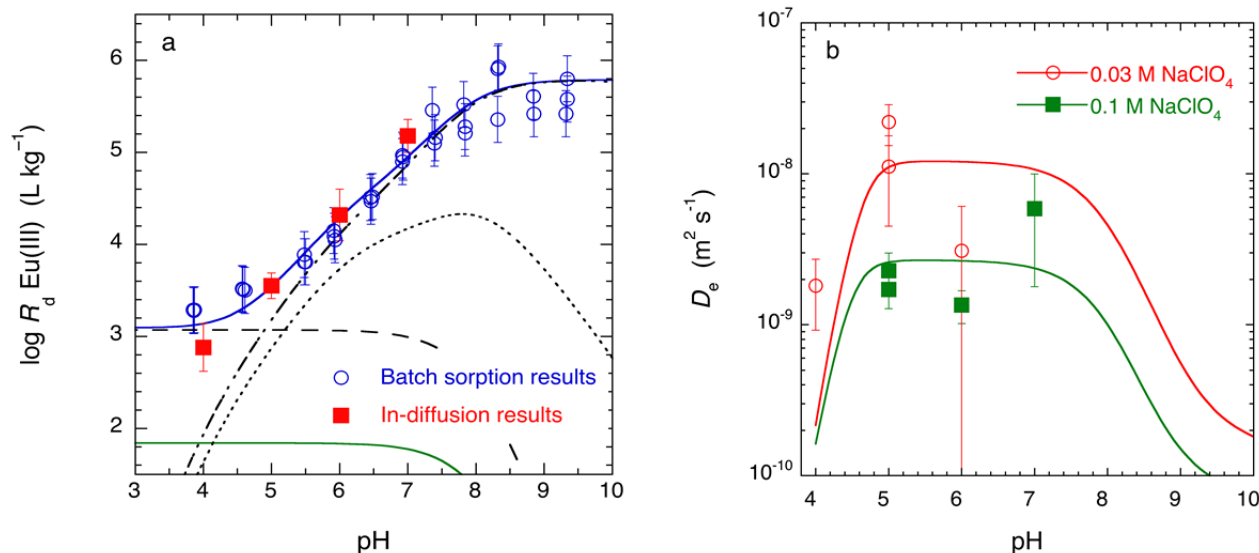


Fig. 5.2: pH dependence of $^{152}\text{Eu}(\text{III})$ sorption data at 0.1 M NaClO_4 and $1 \mu\text{M Eu}(\text{III})$ stable isotope concentration using Na-IdP-B (plot a). The blue overall model curve was calculated using the modified 2SPNE SC/CE model (see text) implemented in PHREEQC using contributions from surface complexes at strong sites (black dash-dotted), weak sites (black dotted) and Stern layer species (black dashed). All these species are assumed to exhibit no surface mobility. The green solid model curve represents the contribution of mobile diffuse layer species. The right-hand plot (b) shows experimental data for D_e obtained with Na-IdP-B and the respective PHREEQC simulations for two background concentrations of NaClO_4 .

5.4 Sorption/diffusion studies on intact Opalinus Clay

Different existing diffusion/retention measurements of $^{60}\text{Co}(\text{II})$ on intact Opalinus Clay (OPA) were revisited and compared with data measured on crushed OPA (e.g. BRADBURY & BAEYENS 2011). A summary of the data are given in Fig. 5.3. The sorption of $\text{Co}(\text{II})$ is non-linear as can be derived from the decrease of the K_d value with increasing equilibrium concentrations of $\text{Co}(\text{II})$ in the pore water. It can further be observed that sorption measurements on intact OPA samples give similar results as on crushed OPA, independent whether the diffusion or batch sorption technique was used.

The curve in Fig. 5.3 is a model curve calculated by the sorption model described in BRADBURY & BAEYENS (2011). It is clear that the models overpredict sorption in the lower concentration range and underestimate sorption in the higher concentration range. In the medium concentration range (10^{-5} - 10^{-6} M) the agreement with measured data is good. It has to be noted that the curve is not an optimised fit, but represents a blind prediction using the "bottom-up" approach (BRADBURY & BAEYENS 2011).

This set of data thus indicates that sorption data and models obtained in dilute systems can be transferred to compact systems in the case of $\text{Co}(\text{II})$, a transition element exhibiting a moderate sorption behaviour. Studies on other elements such as $\text{Eu}(\text{III})$ are currently ongoing.

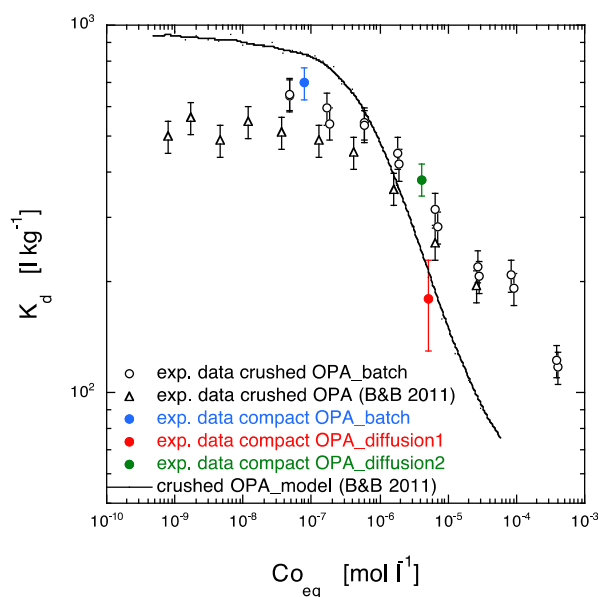


Fig. 5.3: Overview of sorption values of $\text{Co}(\text{II})$ measured on Opalinus Clay as a function of the equilibrium concentration of $\text{Co}(\text{II})$ in the pore solution. Open symbols represent measurements on crushed Opalinus Clay whereas filled symbols are measurements on intact Opalinus Clay, obtained from diffusion or batch sorption experiments.

5.5 Modelling the effect of surface diffusion on Cs transport in Opalinus Clay

The SNSF PhD project, "Transport of sorbing ions in clays" (Ph. Krejci), on modelling multispecies cation transport in compacted clays aims in expanding the capabilities of existing transport codes by taking into account variable mobility of sorbed species on different sorption sites. The need for a multi-site multi-mobility model for the description of cation transport in clays (e.g., diffuse layer, interlayer, outer-sphere complex, inner-sphere complex, strong site, weak site) is the outcome of several laboratory cation diffusion data in various clay samples. Such studies have shown that cation diffusion coefficients can be considerably larger than diffusion coefficients of water tracers, especially when sorption is high, as in the case of Cs. This discrepancy can be explained by surface diffusion, which accounts for a partial mobility of sorbed cations. Sorption of Cs in OPA can be described by a three site cation exchange model (BRADBURY & BAEYENS 2000) with planar, type II and frayed edge sites. In order to adequately model Cs transport in OPA a generalized multi-site surface diffusion model (GIMMI & KOSAKOWSKI, 2011) is implemented in the reactive transport code FLOTRAN (LICHTNER 2007). This model combines pore and surface diffusion in one single effective diffusion coefficient:

$$D_e = \frac{\varepsilon D_0}{\tau_p} + \rho_{bd} D_0 \sum_i \frac{K_{di} \mu_{si}}{\tau_{si}}$$

where ε is the porosity; τ_p, τ_{si} are the pore and surface tortuosities; ρ_{bd} the bulk density of OPA; D_0 is the diffusion coefficient in free water; K_{di} is the site-specific slope of the Cs isotherm and μ_{si} the site-specific surface mobility. The surface mobilities μ_{si} indicate how mobile sorbed cations are compared to those in bulk water and are not a priori known. Therefore, the μ_{si} were fitted to data of Cs in-diffusion experiments. In these experiments samples were pre-equilibrated for 2 months with different stable Cs concentrations (10^{-2} – $3.5 \cdot 10^{-8}$ M) and then spiked with ^{134}Cs tracer for another 7 days of diffusion. Figures 5.4 and 5.5 show the diffusion profiles of ^{134}Cs for the OPA samples with stable Cs background concentrations of 10^{-2} M and $3.5 \cdot 10^{-8}$ M. The solid blue curve represents the surface diffusion model and the dashed red curve an ordinary diffusion model with fitted D_e . Surface mobilities were determined to $4.7 \cdot 10^{-2}$ for the planar sites, 0 for the type II sites and $2 \cdot 10^{-3}$ for the frayed edge sites. For the ordinary diffusion model the D_e had to be raised by a factor of 3 for the high Cs concentration and by a factor of 18 for the low Cs concentration compared to diffusion of water tracers.

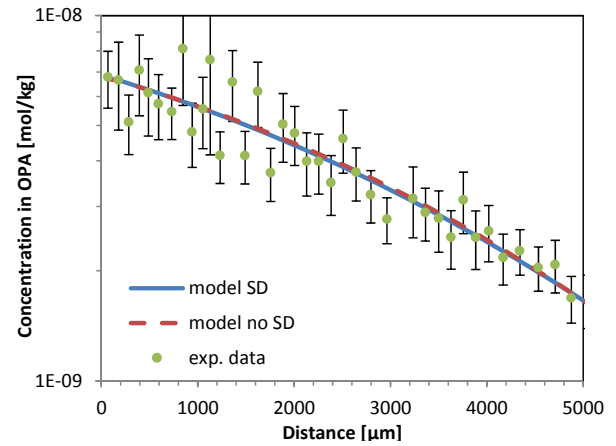


Fig. 5.4: Diffusion profile of ^{134}Cs for OPA pre-equilibrated with 10^{-2} M ^{133}Cs ; blue line: surface diffusion (SD) model, red line: ordinary diffusion model, green dots: experimental data with error bars.

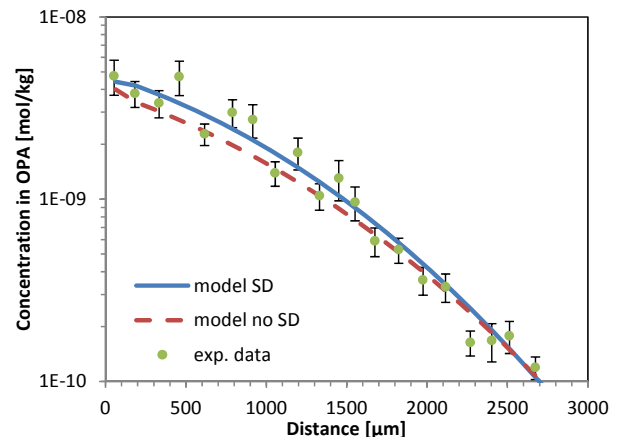


Fig. 5.5: Diffusion profile of ^{134}Cs for OPA pre-equilibrated with $3.5 \cdot 10^{-8}$ M ^{133}Cs ; blue line: surface diffusion (SD) model, red line: ordinary diffusion model, green dots: experimental data with error bars.

For the 3-site surface diffusion model, the tortuosity determined for a water tracer could be used. Both models fit the data very well. However, the ordinary diffusion model leads to too high D_e values and cannot describe both experiments with the same diffusion coefficient. The obtained surface mobilities are comparable to those in GIMMI & KOSAKOWSKI 2011. The surface diffusion model with the determined surface mobilities will now be tested against other experimental data.

5.6 Inter valent sorption competition between Eu(III) and Ni(II) during diffusion through bentonite

According to recent sorption studies (BRADBURY et al. 2017) trivalent cations (e.g. Eu, Am, ...) may show competitive sorption behaviour with respect to the sorption sites of montmorillonite and illite not only among each other but also with bivalent cations (e.g. Co, Ni, Zn, ...).

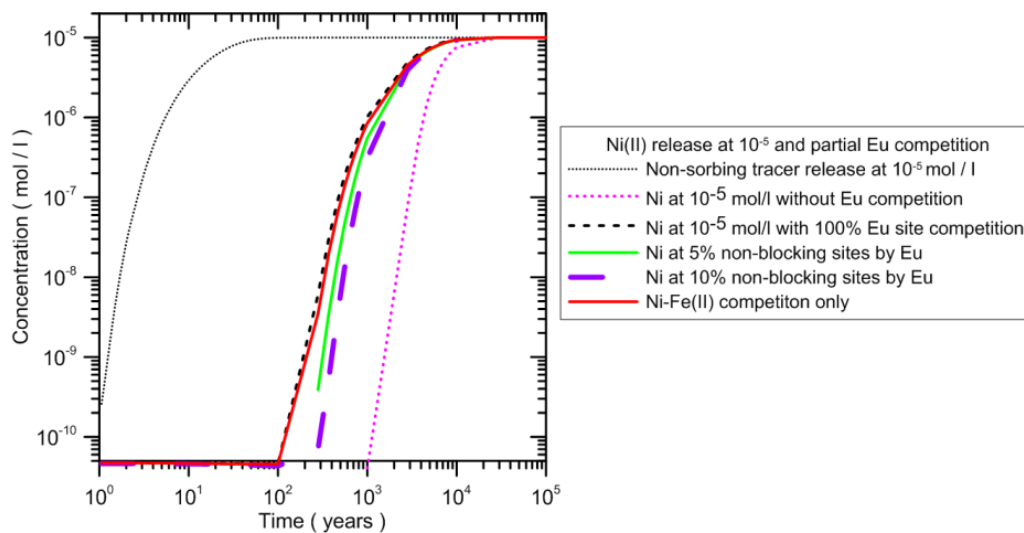


Fig. 5.6: Ni(II) sorption competition with Eu(III) at different levels of site blocking.

This is in contrast to all other combinations of differently valent cations where no sorption competition has been observed so far. In order to assess the potential influence of sorption competition between tri- and bivalent cations on radionuclide transport and to estimate the concentration of bi- and trivalent cations transported through the bentonite barrier into the Opalinus Clay, generic calculations have been performed for diffusion/sorption of tri- and bi-valent cations through bentonite using MCOTAC (PFINGSTEN, 2002) which includes the 2SPNE SC/CE sorption model from BRADBURY & BAEYENS (2002, 2005). A preliminary model set-up sums up all trivalent cations in solution at the "canister-bentonite-interface" after 10'000 years, i.e. an evolved bentonite porewater was assumed. A total source concentration of trivalent cations (Eu, Am, ...) was represented by Eu(III) at a constant concentration level (10^{-5} M) entering the bentonite at the interface with the (corroded) canister according to the set-up outlined in PFINGSTEN (2014). The total bivalent competing cation concentration was assumed to be $3 \cdot 10^{-5}$ M. Breakthrough curves for this set-up are shown in Fig 5.6.

If sorption competition between Ni(II) and Eu(III) is limited to a part of the sorption sites (e.g. 5% or 10%), as it was observed in batch experiments with dispersed clay (see section 3.2.1), the Ni(II) breakthrough is about a factor of two earlier as if blocking of sites by Eu(III) were 100%. The sorption competition effect of Eu(III) on Ni(II) is about the same as for bivalent sorption competition between Ni(II) and Fe(II) (not shown here). However, it seems that the sequence of occupation of sorption sites by different cations (bivalent Ni, Cu, Zn, Mn, Fe, ... and trivalent Eu, Am, ...) is important. It seems that Eu(III) is (partly) blocking/competing for Ni(II), but Ni(II) is not blocking/competing for Eu(III). For more

accurate predictions, the modelling has to be refined with respect to individual bi- and tri-valent cations concentrations as a function of leaching time from the canister and their individual transport and sorption parameters. In addition, kinetics of the individual sorption reactions or the related sequence of occupation of sorption sites at lab scale have to be investigated in more detail.

5.7 Anion accessible porosity in low porosity argillaceous rocks (ANPOR)

The work on anion accessible porosity in argillaceous rocks in the framework of a PhD project (ANPOR) could be successfully finished. The work was summarized in a PhD Thesis (WIGGER 2017). The defence, of the thesis took place on December 19th, 2017. One publication was accepted and published (WIGGER & VAN LOON 2017), and 4 publications were submitted and are currently under review.

The work has shown that anion behaviour in clay rocks is complex and cannot be generalised. Three kinds of pore spaces could be identified based on the diffusive behaviour of $^{36}\text{Cl}^-$. In the case of Opalinus Clay a significant part of the pore space (ca. 23%) is permanently accessible and independent on the composition (ionic strength) of the pore water, another part (ca. 40%) is permanently inaccessible and also independent on the composition of the pore water. The latter is assumed to represent interlayer equivalent pores (ILE) and/or bottleneck pores (BP). The rest of the porespace (ca. 37%) represents a Donnan space with pores having a size that is large enough so that diffuse double layers do overlap or do not overlap, depending on the ionic composition of the pore solution. The anion accessibility of the Donnan space is thus governed by the chemical composition of the pore solution (Fig. 5.7).

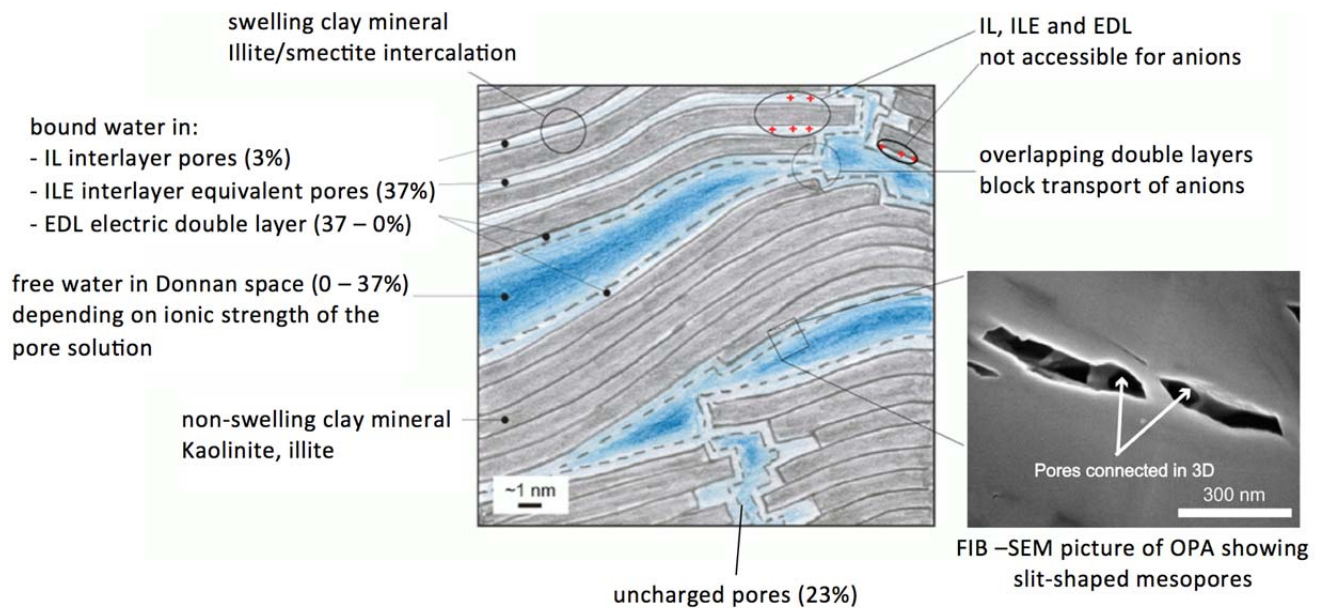


Fig. 5.7: Schematic picture of the pore structure in Opalinus Clay showing uncharged pores, ILE pores and a Donnan space (modified after APPELO *et al.* 2010). The FIB-SEM picture was taken from HOUBEN *et al.* (2013).

5.8 Ions transport in compacted clays at partially saturated conditions

Bentonite backfill and host rock may become partially saturated during the initial thermal pulse in a SF/HLW repository or due to gas ingress produced by the metal corrosion and degradation of organic matter in a L/ILW repository. Transport experiments at partially saturated conditions are challenging and time consuming. The effect of saturation on ion transport was evaluated by modelling based on previously developed clay structural maps (TYAGI *et al.* 2013) and pore scale ion diffusion coefficients derived from molecular simulations at various degree of water saturation (CHURAKOV 2013).

The pore saturation was modelled taking into account capillary forces and films of molecular water adsorption on clay surfaces, which were derived directly from molecular simulations. The integral effects of pore scale diffusivity and clay particle microstructure was evaluated based on a random walk simulation approach (CHURAKOV & GIMMI 2011). A good agreement between the simulated effective diffusion coefficient and the experimental data could be obtained for water and ions as a function of water saturation. Overall, the obtained effective diffusion coefficients broadly follow the empirical Archie's relation (GIMMI & CHURAKOV 2018).

5.9 References

- APPELO A.C.J., VAN LOON L.R., WERSIN P. (2010) Multicomponent diffusion of a suite of tracers (HTO, Cl, Br, I, Na, Sr, Cs) in a single sample of Opalinus Clay. *Geochim. Cosmochim. Acta* 74, 1201-1219.
- BRADBURY M.H., BAEYENS B. (2002) Sorption of Eu on Na- and Ca-montmorillonites: experimental investigations and modelling with cation exchange and surface complexation. *Geochim. Cosmochim. Acta* 66, 2325-2334.
- BRADBURY M.H., BAEYENS B. (2005) Modelling the sorption of Mn(II), Co(II), Ni(II), Zn(II), Cd(II), Eu(III), Am(III), Sn(IV), Th(IV), Np(V) and U(VI) on montmorillonite: Linear free energy relationships and estimates of surface binding constants for some selected heavy metals and actinides. *Geochim. Cosmochim. Acta* 69, 875-892.
- BRADBURY M.H., BAEYENS B. (2011) Predictive sorption modelling of Ni(II), Co(II), Eu(III), Th(IV) and U(VI) on MX-80 bentonite and Opalinus Clay: A "bottom-up" approach. *Appl. Clay Sci.* 52, 27-33.
- BRADBURY M.H., MARQUES FERNANDES M., BAEYENS B. (2017) Estimates of the influence of radionuclide solubility limits and sorption competition on the Sorption values in the SDBs of MX-80 bentonite and Opalinus Clay. PSI Bericht Nr. 17-04 and Nagra Tech. Rep. NTB 17-11 (2017).

- CHURAKOV S.V. (2013)
Mobility of Na and Cs on montmorillonite surface under partially saturated conditions. *Environ. Sci. Technol.* 47, 9816-9823.
- GIMMI T. & CHURAKOV S.V. (2018)
Water retention and solute diffusion in unsaturated clays: Connecting atomistic and pore scale simulations. *Appl. Clay Sci.* (submitted).
- GLAUS M.A., BAEYENS B., BRADBURY M.H., JAKOB A., VAN LOON L.R., YAROSHCHUK A. (2007)
Diffusion of ^{22}Na and ^{85}Sr in montmorillonite: Evidence of interlayer diffusion being the dominant pathway at high compaction. *Environ. Sci. Technol.* 41, 478–485.
- GLAUS M.A., FRICK S., ROSSÉ R., VAN LOON L.R. (2010)
Comparative study of tracer diffusion of HTO, $^{22}\text{Na}^+$ and $^{36}\text{Cl}^-$ in compacted kaolinite, illite and montmorillonite. *Geochim. Cosmochim. Acta* 74, 1999–2010.
- GLAUS M.A., AERTSENS M., APPELO C.A.J., KUPCIK T., MAES N., VAN LAER L., VAN LOON L.R. (2015)
Cation diffusion in the electrical double layer enhances the mass transfer rates for Sr^{2+} , Co^{2+} and Zn^{2+} in compacted illite. *Geochim. Cosmochim. Acta* 165, 376–388.
- HOUBEN M.E., DESBOIS G., URAI J.L. (2013)
Pore morphology and distribution in the Shaly facies of Opalinus Clay (Mont Terri, Switzerland): Insights from representative 2D BIB–SEM investigations on mm to nm scale. *Appl. Clay Sci.* 71, 82-97.
- MARQUES FERNANDES M., VER N., BAEYENS B. (2015)
Predicting the uptake of Cs, Co, Ni, Eu, Th and U on argillaceous rocks using sorption models for illite. *Appl. Geochem.* 59, 189-199.
- PFINGSTEN W. (2002)
Experimental and modelling indications for self-sealing of a cementitious low- and intermediate-level waste repository by calcite precipitation. *Nucl. Technol.* 140, 63–82.
- PFINGSTEN W. (2014)
The influence of stable element inventory on the migration of radionuclides in the vicinity of a high level nuclear waste repository exemplified for ^{59}Ni . *Appl. Geochem.* 49, 103-115.
- VAN LOON L.R. (2017)
Can sorption values and models for radionuclides measured on dispersed clay systems be transferred to compact clay systems? PSI Technical Report TM-44-17-03, Paul Scherrer Institut, Villigen PSI, Switzerland.
- WIGGER C., VAN LOON L.R. (2017)
The role of interlayer equivalent pores for anion diffusion in clay-rich sedimentary rocks. *Environ. Sci. Technol.* 51, 1998-2006.
- WIGGER C. (2017)
Anion Accessibility in Low Porosity Argillaceous Rocks. PhD Thesis, University of Bern, Bern, Switzerland.
- TYAGI M., GIMMI T CHURAKOV S.V. (2013)
Multi-scale micro-structure generation strategy for up-scaling transport in clays. *Adv. Water Res.* 59, 181–195.

6 THERMODYNAMIC MODELS AND DATABASES

W. Hummel, D.A. Kulik, D. Miron (Postdoc), T. Thoenen, L.R. Van Loon

6.1 Introduction

The aim of this project is to develop thermodynamic models and databases to be applied in the preparation of various reports for the general license applications (RBG). Solubility and sorption databases and synthesis reports are an important part of the documentation for RBG.

Particularly important is the timely finalisation of the thermodynamic database. These carefully selected thermodynamic data provide the basis for the solubility databases, the development of the sorption databases and simulation of the in situ conditions. The consistent and consequent use of the approved and "frozen" thermodynamic dataset throughout all types of thermodynamic calculations is of crucial importance.

The GEM Software (GEMS) code collection has been developed at PSI/LES since 2000 by a community team lead by D. Kulik. The current development focuses on the prediction of temperature trends with the new software tool ThermoMatch which facilitates the sharing of thermodynamic data with the GEMS package and external software.

6.2 Update of the Thermodynamic Data Base (TDB)

A high quality Thermodynamic Data Base (TDB) is currently in place. This database needs to be kept state-of-the-art and remaining gaps need to be filled where this is safety relevant. As the availability of a "frozen" TDB is an essential prerequisite for preparing solubility limits and sorption database reports for the next safety assessments related to Nagra's general license applications (RBG), updates and filling gaps of the TDB need to be finished before work on solubility and sorption databases commences. The latter work is planned to start in 2021. Hence, TDB update work has been planned for the period 2017 – 2019 (Table 6.1) with a final document to be published in 2020.

Updates for elements and ligand groups already included in the current or previous versions of our TDB are foreseen for: C_{org} (organics), Si (silicates), Fe, Nb, Mo, Pd, Sn and Eu (Table 6.1).

The list of new elements to be included into the TDB comprises Ti, Cu, Ag, Sm, Ho, Hg, Pb, Po, Ac, Pa and Cf (Table 6.1).

Thermodynamic data on Cu are needed to explore the geochemical effects of the option using copper-coated canisters instead of steel canisters in the planned high-level waste geological repository.

^{108m}Ag is a dose-relevant activation product in Ag control rods used in pressurised water reactors.

A number of long-lived dose-relevant radionuclides occur in research wastes from PSI and CERN:

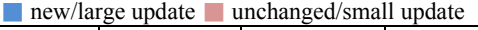
²⁶ Al	$T_{1/2} = 7.17 \cdot 10^5 \text{ y}$
³² Si	$T_{1/2} = 153 \text{ y}$
⁴¹ Ca	$T_{1/2} = 9.94 \cdot 10^4 \text{ y}$
⁴⁴ Ti	$T_{1/2} = 58.9 \text{ y}$
⁶⁰ Fe	$T_{1/2} = 2.62 \cdot 10^6 \text{ y}$
⁹¹ Nb	$T_{1/2} = 680 \text{ y}$
¹⁹⁴ Hg	$T_{1/2} = 520 \text{ y}$
²⁰² Pb	$T_{1/2} = 5.25 \cdot 10^4 \text{ y}$
²⁰⁹ Po	$T_{1/2} = 125.2 \text{ y}$

(Half-lives, $T_{1/2}$, from the Karlsruhe Nuclide Chart Online KNCO++, <https://www.nucleonica.com/>)

Almost all nuclides listed above originate solely from spallation reactions, with the exception of ⁴¹Ca which is also produced in nuclear reactors by neutron activation. Al, Si, Ca and Fe are already in our TDB, where Fe and Si (silicates) will be updated, while Ti, Hg, Pb and Po are new elements to be included into the TDB.

The TDB update has been started in 2017 with reviews of Fe, Cu, Hg, Pb and Po data and the review work will continue in 2018 and 2019 with the other elements mentioned above (Table 6.1). The reviews of individual elements will be published as PSI TMs and these TMs will be merged into a single document at the end of the project.

Table 6.1: Overview of previous and the ongoing updates of the PSI/Nagra TDB with respect to the dose-relevant radionuclides (drn).

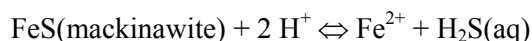
drn	TDB 05/92	TDB 01/01	TDB 12/07	TDB 2020	Basis for Update 2020	Comments	Date
	NTB 91-17 NTB 91-18	NTB 02-16	NAB 14-49	on-going			
							
C _{anorg}						carbonate: implicit update	
C _{org}					NEA TDB ⁴		2019
Al							
Si					own review	silicates	2019
(S) ¹						sulfides	
Cl							
Ca							
Ti					own review, Yucca Mountain		2018
Fe					NEA TDB ⁵		2017
Ni							
(Cu) ²					IUPAC ⁶		2017
Se							
Sr							
Zr							
Nb					own review		2018
Mo					NEA TDB ⁷		2019
Tc					NEA TDB Update ⁸		
Pd					own review		2019
Ag					own review		2018
Sn					NEA TDB ⁹		2018
I							
Cs							
Sm					own review, lanthanide(III)-systematics		2019
(Eu) ³							2019
Ho							2019
Hg					IUPAC ¹⁰		2017
Pb					IUPAC ¹¹		2017
Po					own review		2017
Ra							
Ac					own review, actinide(III)-systematics		2018
Th					NEA TDB update ⁸		
Pa					own review		2018
U					NEA TDB update ⁸		
Np					NEA TDB update ⁸		
Pu					NEA TDB update ⁸		
Am					NEA TDB update ⁸		
Cm					NEA TDB update ⁸		
Cf					own review, actinide(III)-systematics		2018

¹ not dose relevant, but sulfides are important ground- and porewater constituents; ² not dose relevant, but a potential canister material; ³ not dose relevant, but important for lanthanide systematics; ⁴ HUMMEL et al. (2005); ⁵ LEMIRE et al. (2013); ⁶ POWELL et al. (2007); ⁷ ongoing review, NEA TDB Phase IV; ⁸ ongoing review, NEA TDB Phase V; ⁹ GAMSJÄGER et al. (2012); ¹⁰ POWELL et al. (2005); ¹¹ POWELL et al. (2009)

6.2.1 The solubility of FeS (mackinawite)

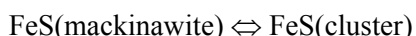
Our update of thermochemical data for iron was based on the NEA review by LEMIRE et al. (2013). The NEA reviews are recognised as very thorough, and the selected data are of high quality. In adapting the data recommended by NEA, however, it is not sufficient just to copy the data without a scrutinising review, as the example of mackinawite (FeS) solubility shows below.

LEMIRE et al. (2013) discussed various aqueous iron(II) sulfide complexes, some of which were derived from the interpretation of solubility data of FeS (mackinawite), which forms as a black precipitate when Fe(II) solutions are mixed at room temperature with sulfide solutions. The precipitate consists of mackinawite nanoparticles. As seen in Fig. 6.1 the solubility of mackinawite decreases with pH under acidic conditions and becomes constant under more basic conditions ($\text{pH} > 6$). The slope of the solubility curve under acidic conditions is well constrained and very close to -2, which is compatible with the dissolution reaction:



LEMIRE et al. (2013) accepted 5 equilibrium constants for this reaction from 5 different experimental studies and selected the weighted arithmetic mean with an increased uncertainty: $\log_{10} K_{s,0}^\circ(298.15 \text{ K}) = (3.8 \pm 0.4)$.

The solubility in the plateau region at higher pH is less well constrained. The experimental data by MEHRA (1986) and RICKARD (2006), see Fig. 6.1, indicate that the solubility in the plateau region is independent of the sulfide concentration. For the plateau region, RICKARD (2006) suggested the pH-independent reaction:



where FeS(cluster) is a monomeric representation of the aqueous cluster complex Fe_xS_x , whose presence was inferred by RICKARD (2006) from voltammetry.

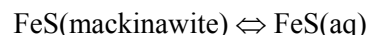
In contrast to the findings by RICKARD (2006), the experimental data by DAVISON et al. (1999) suggest a dependence of the solubility from the partial pressure of $\text{H}_2\text{S(g)}$, see Fig. 6.1, which they explained with the existence of the neutral complex $\text{Fe(HS)}_2\text{(aq)}$, leading to the pH-independent mackinawite solubility reaction:



LEMIRE et al. (2013) discussed data from the literature for various Fe(II) sulfide complexes: FeS(aq) , FeHS^+ , $\text{Fe(HS)}_2\text{(aq)}$, FeSHS^- , $\text{Fe}_2\text{(HS)}^{3+}$, and $\text{Fe}_3\text{(HS)}^{5+}$. They concluded that no good evidence was given for the

existence of any of these complexes. With respect to the discrepancy in the solubility at higher pH reported by DAVISON et al. (1999) and RICKARD (2006), LEMIRE et al. (2013) made the following comment: "Two seemingly very reliable papers report quite different solubility behaviour at higher pH values, and the reviewer cannot discern a reason for the difference. The difference in the crystallinity or in the surface condition, formation of a very small amount of surface FeS solid other than mackinawite, or differences in the rates of precipitation and dissolution at higher pH values may affect the solubility. The speciation of the soluble iron sulfide can be discussed only after reproducible and reliable solubility data in this pH region are obtained. So far, this review cannot recommend any speciation or formation constant in this pH region". Accordingly, no data are provided in the database.

Such a commitment to high quality, however, can be very dangerous when it comes to practical thermodynamic calculations. It is obvious from Fig. 6.1 that neglecting iron-sulfide complexes in geochemical models invariably leads to absurdly small Fe-solubilities at $\text{pH} > 6$. For practical calculation purposes, therefore, a pragmatic approach is required. Based on the data shown in Fig. 6.1, we decided to express the solubility of mackinawite in the pH-independent region according to the reaction



with the solubility constant $\log_{10} K_{s,1}^\circ(298.15 \text{ K}) = -(5 \pm 1)$. This value with its uncertainty covers the largest part of the experimental data points in the pH-independent region and belongs in our database to the supplemental dataset. We justify the choice of FeS(aq) as relevant Fe-sulfide species by noting that the explicit purpose of the experimental study by RICKARD (2006) was to investigate the pH-independent region and to decide whether the solubility was dependent on the sulfide concentration, with $\text{Fe(HS)}_2\text{(aq)}$ as dominant species, or not. The experimental data by RICKARD (2006) strongly suggest that the solubility is indeed independent of the sulfide concentration and the choice of an FeS-cluster, represented as FeS(aq), is the simplest one possible.

The experimental data by MEHRA (1968), not mentioned by LEMIRE et al. (2013), at $\text{pH} > 5$ support the assumption that the solubility of mackinawite is independent of pH and sulfide concentration. In addition, his data show that the plateau of constant Fe(II) concentration extends almost up to $\text{pH} = 14$, a strong indication that no other Fe-sulfide species become dominant under very basic conditions.

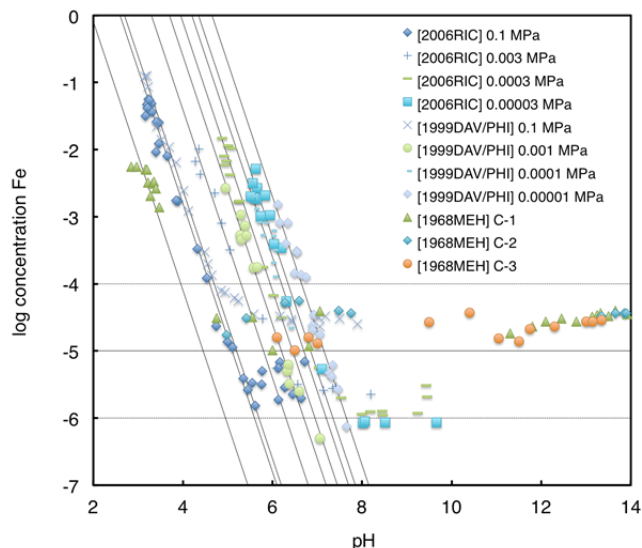


Fig. 6.1: Solubility of mackinawite as a function of pH and several partial pressures of $H_2S(g)$ or total sulfide concentrations (C-1: pS_{tot} between 1.31 and 1.61, C-2: pS_{tot} between 1.03 and 1.18, C-3: pS_{tot} between 1.62 and 1.76), with indicative slopes of -2 (fitted to the data by eye), corresponding to the reaction FeS (mackinawite) + $2 H^+ \Leftrightarrow Fe^{2+} + H_2S(aq)$. The solid horizontal line corresponds to the reaction $FeS(mackinawite) \Leftrightarrow FeS(aq)$, with $\log_{10}K_{s,1}(298.15 K) = -5$. The dotted horizontal lines represent the uncertainty ± 1 . Experimental data by MEHRA (1986), DAVISON et al. (1999), and RICKARD (2006).

6.3 Prediction of temperature trends of standard thermodynamic properties by isocoulombic reactions generated within the ThermoMatch code

In the framework of the joint project ThermAc, financed by the German Federal Ministry of Education and Research (BMBF), ThermoMatch – an advanced user-friendly code for managing thermodynamic data sets in the ThermoHub database – was developed as a replacement of our former PMATCHC code (PEARSON et al. 1999). Our motivation was that, in order to avoid errors and to speed up data collection and data evaluation processes, it is essential to use state-of-the-art data management tools, implemented using modern software best practices (MIRON et al., in preparation).

At the present stage of development ThermoMatch allows importing and exporting thermodynamic data from and into various external formats. One application of ThermoMatch was to generate an

LMA-type (Law of Mass Action) reaction-based database from the GEMS version of the Cemdata 18 database for cementitious systems (LOTHENBACH et al. 2017), and to export it into a PHREEQC.dat file readable with the PHREEQC geochemical modelling code (PARKHURST & APPELO 1991).

In order to automatically generate reactions based on the lists of selected master and product species, the Reaction Generator Module of ThermoMatch was implemented using an algorithm based on the method by SMITH & MISSEN (1982). The module is operated via a simple graphical widget. After selecting the source thermodynamic dataset (e.g. PSI/Nagra database, THOENEN et al. 2014) and the chemical elements of the chemical system to be considered, a list of all feasible species is produced, and the user may choose the desired master species ('M') from the list. With a mouse click, the list of reactions is then generated for all remaining product (dependent, 'D') species (Fig. 6.2).

An additional module implemented in ThermoMatch is the isocoulombic reaction generator, aimed at compiling all possible reactions having the same number of species with the same species charge for both products and reactants. This module is useful for systematic predictions of standard thermodynamic properties ($\Delta_r G^\circ$ etc.) of reaction at elevated temperatures based on the standard state properties of isocoulombic reactions, where little or no high temperature experimental data are available. The isocoulombic reaction generator derives all possible isocoulombic reactions by combining the chosen reaction of interest (with unknown temperature trend) with suitable model reactions having well-known temperature trends (Fig. 6.3). The predictions from the generated isocoulombic reactions can then be plotted and their quality can be checked within temperature and pressure intervals of interest. The standard properties ($\Delta_r G^\circ$ etc.) of isocoulombic reactions at elevated temperatures are calculated using either one-term ($\Delta_r G^\circ$ constant or $\log K^\circ$ constant), two-term or van't Hoff ($\Delta_r S^\circ$ constant, $\Delta_r Cp^\circ = 0$), or three-term ($\Delta_r S^\circ$ constant, $\Delta_r Cp^\circ$ constant) extrapolations. Predicted effects of the reaction of interest are retrieved at each temperature and pressure point, by subtracting the calculated properties of the model reaction from those of the isocoulombic reaction.

ThermoMatch ReactionSet Generator Dialog

Source TDB: OTHER MethodEOS: CTPM_REA
 Set Type: LMA MethodT: CTM_EK3
 Name: Ln(III) with F MethodP: CPM_OFF
 Symbol: Reaction Level: 0

Type	symbol	name	formula
0 M	Ce+3	Ce+3	Ce+3
1 M	Dy+3	Dy+3 ion	Dy+3
2 M	Er+3	Er+3 ion	Er+3
3 M	Eu+3	Eu+3 ion	Eu+3
4 M	Gd+3	Gd+3 ion	Gd+3
5 M	Ho+3	Ho+3 ion	Ho+3
6 M	La+3	La+3 ion	La+3
7 M	Lu+3	Lu+3 ion	Lu+3
8 M	Nd+3	Nd+3 ion	Nd+3
9 M	Pr+3	Pr+3 ion	Pr+3
10 M	Sm+3	Sm+3 ion	Sm+3
11 M	Tb+3	Tb+3 ion	Tb+3
12 M	Tm+3	Tm+3 ion	Tm+3
13 M	Yb+3	Yb+3 ion	Yb+3
14 M	F-	F-	F-
15 D	CeF+2	CeF+2	CeF+2
16 D	DyF+2	DyF+2	DyF+2
17 D	ErF+2	ErF+2	ErF+2

Reactions/Substances	Coeff	ISOC	logKr	dGr/G0	dHr/H0	dSr/S0	dCpr/Cp0
▼ R1 (Ce+3 + F- = CeF+2)			3.848	-21966	12006	113.946	417.953
Ce+3	-1			-676134	-700283	-205.016	-198.578
F-	-1			-281751	-335392	-13.18	-113.12
CeF+2	1			-979851	-1.02367e+06	-104.25	106.255
► R2 (Dy+3 + F- = DyF+2)			4.391	-25062	10900	120.62	131.251
► R3 (Er+3 + F- = ErF+2)			4.266	-24350	11716	120.97	145.452
► R4 (Eu+3 + F- = EuF+2)			4.259	-24309	9744.51	114.22	218.972
► R5 (Gd+3 + F- = GdF+2)			4.229	-24142	8843.89	110.64	212.908
► R6 (Ho+3 + F- = HoF+2)			4.281	-24434	11641	121	155.802
► R7 (La+3 + F- = LaF+2)			3.628	-20710	12037.8	109.84	429.503
► R8 (Lu+3 + F- = LuF+2)			4.244	-24225.4	13304.7	125.88	111.809
► R9 (Nd+3 + F- = NdF+2)			3.819	-21799	10850.2	109.51	396.441

Status: Reactions have been generated successfully

Fig. 6.2: ThermoMatch Reaction Generator widget. Example for generating fluorine complexation reactions with trivalent lanthanides.

ThermoMatch Isocoulombic Reactions Generator Dialog

Source TDB: OTHER Symbol: Reaction Level: 0
 Comment: La(III)F+2 Solvent Symbol: H2O@

Type	symbol	name	equation
0 I	ErF+2	ErF+2	Er+3 + F- = ErF+2
1 I	GdF+2	GdF+2	Gd+3 + F- = GdF+2
2 I	HoF+2	HoF+2	Ho+3 + F- = HoF+2
3 I	SmF+2	SmF+2	Sm+3 + F- = SmF+2
4 I	PrF+2	PrF+2	Pr+3 + F- = PrF+2
5 I	NdF+2	NdF+2	Nd+3 + F- = NdF+2
6 I	LaF+2	LaF+2	La+3 + F- = LaF+2
7 I	LuF+2	LuF+2	Lu+3 + F- = LuF+2

Reactions/Substances	Coeff	ISOC	logKr	dGr/G0	dHr/H0	dSr/S0	dCpr/Cp0	dVr/V0
Er+3 + F- = ErF+2								
▼ Er+3 + GdF+2 = ErF+2 + Gd+3		+	0.036	-208	2872.09	10.33	-67.456	-0.031
Er+3 + F- = ErF+2	1			-24350	11716	120.97	145.452	0.392
Gd+3 + F- = GdF+2	-1			-24142	8843.89	110.64	212.908	0.423
► Er+3 + HoF+2 = ErF+2 + Ho+3		+	-0.015	84	74.949	-0.03	-10.35	-0.016
► Er+3 + SmF+2 = ErF+2 + Sm+3		+	0.124	-710	1961.51	8.96	-125.341	-0.012
► Er+3 + PrF+2 = ErF+2 + Pr+3		+	0.41	-2342	-887.214	4.88	-226.088	-0.011
► Er+3 + NdF+2 = ErF+2 + Nd+3		+	0.447	-2551	865.773	11.46	-250.989	0.001
► Er+3 + LaF+2 = ErF+2 + La+3		+	0.638	-3640	-321.857	11.13	-284.051	-0.051
► Er+3 + LuF+2 = ErF+2 + Lu+3		+	0.022	-124.6	-1588.68	-4.91	33.643	0.023
► Er+3 + EuF+2 = ErF+2 + Eu+3		+	0.007	-41	1971.47	6.75	-73.52	-0.02
► CeF+2 + Er+3 = Ce+3 + ErF+2		+	0.418	-2384	-289.978	7.024	-272.501	0.012
► DyF+2 + Er+3 = Dy+3 + ErF+2		+	-0.125	712	815.944	0.35	14.201	-0.027
► Er+3 + TbF+2 = ErF+2 + Tb+3		+	-0.095	544	3006.79	8.26	-27.613	-0.033
► Er+3 + TmF+2 = ErF+2 + Tm+3		+	-0.015	84	-533.138	-2.07	15.866	-0.001
► Er+3 + YbF+2 = ErF+2 + Yb+3		+	-0.103	586	-320.35	-3.04	33.331	0.017
Gd+3 + F- = GdF+2								
► ErF+2 + Gd+3 = Er+3 + GdF+2		+	-0.036	208	-2872.09	-10.33	67.456	0.031

Status: The isocoulombic reactions were generated successfully

Fig. 6.3: The ThermoMatch Isocoulombic Reaction Generator widget: an example for generating isocoulombic reactions for Ln^{3+} and F^- complexation.

6.3.1 Systematic study of isocoulombic reactions for Ln(III)-fluoride complexation

The experimentally based thermodynamic dataset of MIGDISOV et al. (2009) on Ln(III) complexation with fluoride was used to investigate what kind of model reactions (with known temperature trend) can be combined with the reactions whose temperature trends

are unknown, in order to produce the best estimates for the unknown reaction properties at elevated temperatures. For the subsequent "blind testing", we excluded La, Eu, and Tm from the full Ln(III) dataset; the remaining species and their reactions were used as a "validation" dataset.

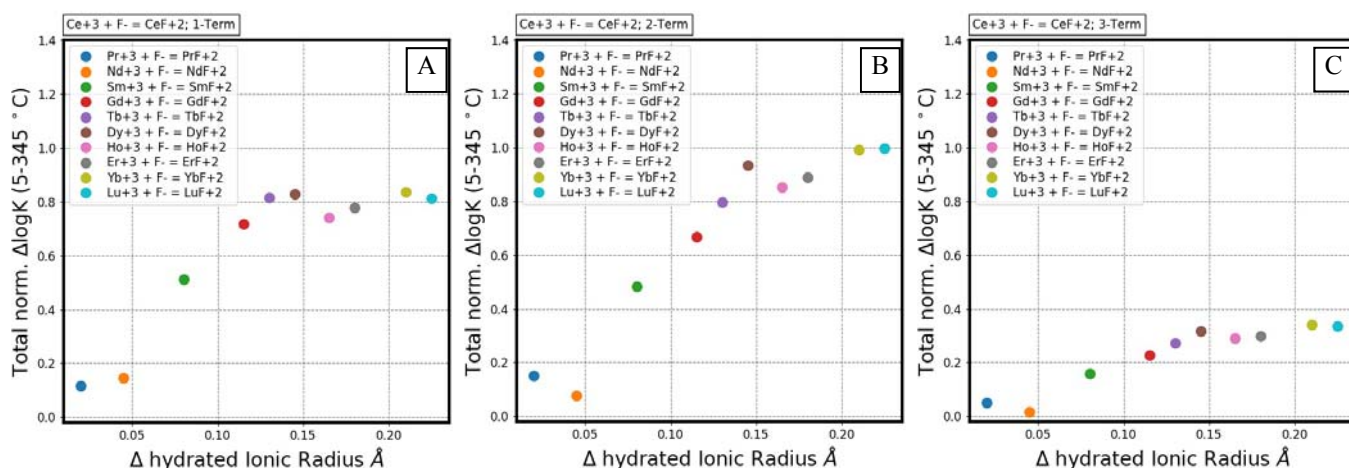


Fig. 6.4: Average deviations $\Delta \log K$ between experimentally measured and predicted $\log K^\circ$ values for the CeF^{2+} complex formation reaction, in the 5-345 °C temperature interval, against the differences in the hydrated ionic radii between Ce^{3+} and cations involved in the model reactions shown. CeF^{2+} complex formation reaction was combined with the shown model reactions into isocoulombic reactions. Predictions were done using (A) 1-term; (B) 2-term; (C) 3-term temperature extrapolation.

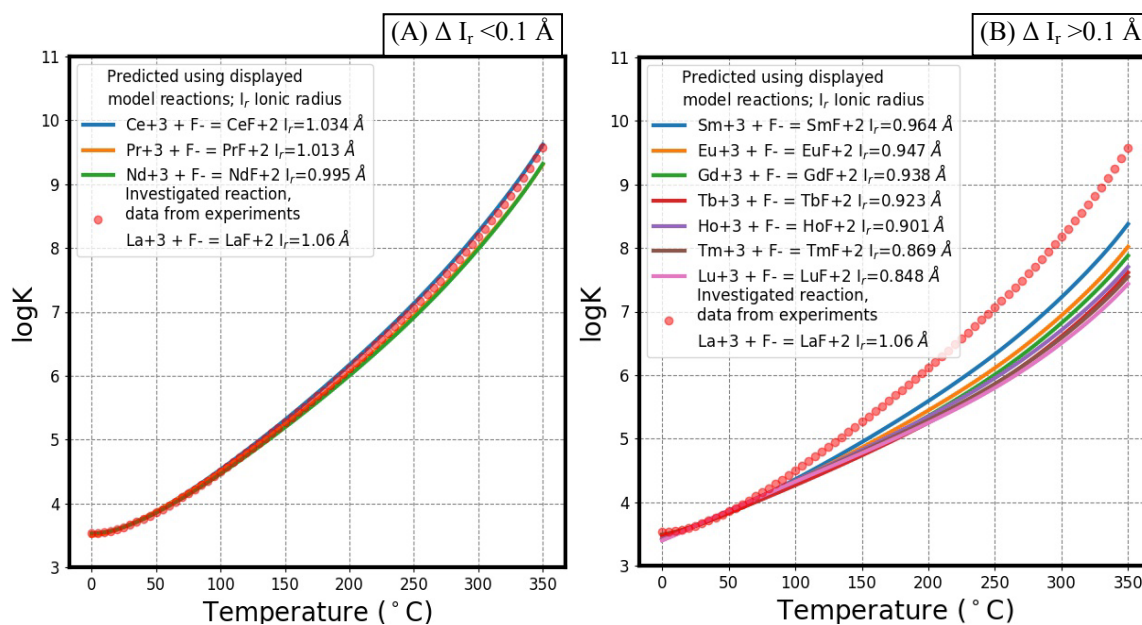


Fig. 6.5: Experimentally measured $\log K^\circ$ of the LaF^{2+} formation reaction (red circles) and the predicted properties from isocoulombic reactions approach (colored curves): (A) For model reactions with cations having hydrated ionic radii similar to that of La^{3+} ($< 0.1 \text{ \AA}$). (B) For model reactions with cations having ionic radii different from that of La^{3+} ($> 0.1 \text{ \AA}$).

The main observation from the learning stage is that the most accurate prediction of temperature trends of $\Delta_r G^\circ$ or $\log K^\circ$ for the reaction of interest can be obtained by using model reactions with Ln(III) ions having hydrated ionic radii similar to that of the cation in the reaction of interest (Fig. 6.4). The discovered regularity indicate that if the difference in the ionic radius is less than 0.01 nm the average deviation of predicted versus known $\log K^\circ$ of the reaction of

interest, is within less than 0.3 pK units over the temperature interval from 5 to 345 °C.

Based on the regularity discovered using the test dataset, we were then able to blindly predict reasonably well the standard properties ($\log K^\circ$) of La, Eu, and Tm fluoride complexation reactions at elevated temperatures. This was done successfully by using just $\log K^\circ$ values at 25 °C (i.e. using 1-term extrapolations with constant $\Delta_r G^\circ$) for the reaction of interest, and by using model reactions involving

Ln(III) ions with similar hydrated ionic radii (Fig. 6.5A). As seen in Fig. 6.5B, the usage of model reactions with cations having substantially different ionic radii leads to significant deviations of the 1-term extrapolation curves from the "experimental" data.

6.4 G-values for gas production (H₂) during irradiation of organic and inorganic materials present in a repository for low- and intermediate-level radioactive waste

Irradiation of organic and inorganic waste forms results in the production of gases. The most important gas is hydrogen. The amount of gas formed during the irradiation of materials is characterised by the so called G-values, representing the number of gas molecules per 100 eV absorbed energy. These G-values are used to estimate the amount of radiolytic gases produced in a repository for low- and intermediate-level radioactive waste. A number of G-values (G-values for α -irradiation, G_{α} , and G-values for γ -irradiation, G_{γ}) were reported in PANTELIAS GARCÉS & SCHWEINGRUBER (2014). The data summarized in that report are based on information dated back to 1992 and earlier and were not updated since then, although new data has been published. Values reported in PANTELIAS GARCÉS & SCHWEINGRUBER (2014) were - when possible - compared with values given in a recent overview published by AMEC FOSTER WHEELER (2015). If new or more recent data on G-values was available, it was integrated in the evaluation of alternative values. The results of the update are reported in VAN LOON (2017). For the organic compounds, 90% (for 30 different organic waste forms) of the reported data had to be revised, based on new information. In the case of inorganic compounds, 40% of the reported data (for 28 different waste compounds) had to be adapted.

6.5 References

- AMEC FOSTER WHEELER (2015)
Determination of G-values for use in SMOGG gas generation calculations. Amec/200615/001 Issue 3.
- DAVISON W., PHILLIPS N., TABNER B.J. (1999)
Soluble iron sulfide species in natural waters: Reappraisal of their stoichiometry and stability constants. *Aquat. Sci.*, 61, 23–43.
- GAMSIÄGER H., GAJDA T., SANGSTER J., SAXENA S.K., VOIGT W. (2012)
Chemical Thermodynamics of Tin. *Chemical Thermodynamics Series*, Vol. 12, OECD NEA, Paris, France, 609 pp.
- HUMMEL W., ANDEREGG G., PUIGDOMÈNECH I., RAO L., TOCHIYAMA O. (2005)
Chemical thermodynamics of compounds and complexes of U, Np, Pu, Am, Tc, Se, Ni and Zr with selected organic ligands. *Chemical Thermodynamics Series*, Vol. 9, OECD NEA, Paris, France, 1088 pp.
- LEMIRE R.J., BERNER U., MUSIKAS C., PALMER D.A., TAYLOR P., TOCHIYAMA O. (2013)
Chemical thermodynamics of iron, Part 1, *Chemical Thermodynamics Series*, Vol. 13a, OECD NEA, Paris, France, 1082 pp.
- LOTHENBACH B., KULIK D.A., MATSCHEI T., BALONIS M., BAQUERIZO L., DILNESA B., MIRON G.D., MYERS R.J. (2017)
Cemdata'18: A chemical thermodynamic database for hydrated Portland cements and alkali-activated materials. *Cem. Conc. Res.* (in prep.).
- MEHRA M.C. (1968)
Studies on the stabilities of some metal selenite, sulphide, and selenide complexes in solution. Ph.D. thesis, Laval University, Quebec.
- MIGDISOV A.A., WILLIAMS-JONES A.E., WAGNER T. (2009)
An experimental study of the solubility and speciation of the rare earth elements (III) in fluoride- and chloride-bearing aqueous solutions at temperatures up to 300 °C. *Geochim. Cosmochim. Acta* 73, 7087–7109.
- PANTELIAS GARCÉS M., SCHWEINGRUBER M. (2014)
MIRAM 14 (Basisszenarium) – Referenzgebinde. Erläuterungen zu radiologischen Kenndaten. Nagra Interner Bericht NIB 14-16, Nagra, Wettingen, Switzerland.
- PARKHURST D.J., APPELO C.A.J. (1999)
User's Guide to PHREEQC (version 2) - A computer program for speciation, batch reaction, one dimensional transport, and inverse geochemical calculations, Denver, Colorado.
- PEARSON F.J., THOENEN T., DMYTRIYEVA S., KULIK D.A., HUMMEL W. (2001)
PMATCHC: A Program to Manage ThermoChemical data, written in C++ (Version 1.1, 31-08-2001). PSI Technical Report TM-44-01-07, Paul Scherrer Institut, Villigen, Switzerland (<https://www.psi.ch/les/pmatchc>).
- POWELL K.J., BROWN P.L., BYRNE R.H., GAJDA T., HEFTER G., SJÖBERG S., WANNER H. (2005)
Chemical speciation of environmentally significant metals with inorganic ligands. Part 1: The Hg²⁺-Cl⁻, OH⁻, CO₃²⁻, SO₄²⁻, and PO₄³⁻ aqueous systems (IUPAC Technical Report). *Pure Appl. Chem.* 77, 739–800.

POWELL K.J., BROWN P.L., BYRNE R. H., GAJDA T., HEFTER G., SJÖBERG S., WANNER H. (2007)

Chemical speciation of environmentally significant metals with inorganic ligands. Part 2: The $\text{Cu}^{2+} - \text{OH}^-$, Cl^- , CO_3^{2-} , SO_4^{2-} , and PO_4^{3-} systems (IUPAC Technical Report). *Pure Appl. Chem.* 79, 895–950.

POWELL K.J., BROWN P.L., BYRNE R.H., GAJDA T., HEFTER G., LEUZ A.-K., SJÖBERG S., WANNER H. (2009)

Chemical speciation of environmentally significant metals with inorganic ligands. Part 3: The $\text{Pb}^{2+} + \text{OH}^-$, Cl^- , CO_3^{2-} , SO_4^{2-} , and PO_4^{3-} systems (IUPAC Technical Report). *Pure Appl. Chem.* 81, 2425–2476.

RICKARD D. (2006)

The solubility of FeS. *Geochim. Cosmochim. Acta*, 70, 5779–5789.

SMITH W.R., MISSEN R.W. (1991)

Chemical reaction equilibrium analysis: Theory and algorithms. Wiley-Interscience, New York, 1982. (reprinted with corrections by Krieger, Malabar, FL).

THOENEN T., HUMMEL W., BERNER U., CURTI E. (2014)

The PSI/Nagra Chemical Thermodynamic Data Base 12/07, PSI Report 14-04, Villigen PSI, Switzerland.

VAN LOON L.R. (2017)

G-values for the generation of gas by hydrolysis. PSI Technical Report TM-44-17-01, Paul Scherrer Institut, Villigen PSI, Switzerland.

7 CEMENT-WASTE INTERACTION AND UPSCALING TO THE FIELD SCALE

G. Kosakowski, E. Wieland, R. Dähn, G. Geng (Postdoc), A. Laube, A. Mancini (PhD), J. Tits

7.1 Introduction

A multi-barrier concept is foreseen to ensure safe disposal of spent fuel and high-level waste (SF/HLW), long-lived intermediate-level waste (ILW) and low- and intermediate-level waste (L/ILW) in Switzerland (NAGRA 2002). The barrier of the L/ILW repository includes the waste matrix, waste packages, emplacement containers, the cavern backfill and the host rock. For safety assessment it is of fundamental interest to understand the behaviour and performance of the barriers with the aim to assess the long-term isolation of radioactive waste and migration of radionuclides from the repository into the host rock. Cement-waste interaction processes are of particular importance because large amounts of cementitious materials are currently being used for the conditioning of L/ILW by the nuclear power plants, and, further, cementitious materials will be used to fabricate emplacement containers, tunnel support and backfills. The barrier function of the cementitious near field is expected to change over time due to various chemical processes that will take place, such as i) the (bio)chemical degradation of organic waste materials and the interaction of the main degradation product, CO₂ (and its bases), with hydrated cement, ii) the corrosion of the metallic waste materials and potential interaction of the corrosion products with hydrated cement, iii) the long-term degradation of hydrated cement due to interaction of highly alkaline cement pore water with silicate aggregates in concrete and backfill or by groundwater ingress from the host rock (KOSAKOWSKI et al. 2014). Cement-waste interactions may lead to the degradation of cementitious materials which could affect the long-term performance of the barrier.

The aim of this project is i) to assess the temporal evolution of the heterogeneous near field of the cement-based L/ILW repository, ii) to identify the physico-chemical processes controlling the temporal evolution of heterogeneities in the near field, iii) to model the interaction of waste sorts with the cement paste of the engineered barrier, iv) to study relevant cement-waste interaction processes and their consequences for the long-term evolution of the chemical conditions in waste sorts such as iron corrosion at the cement-iron interface and the reaction of concrete aggregates, v) to assess the impact of the cement-waste interactions on gas production, vi) to investigate mineralogical alterations and porosity

changes at the cement-clay interface, and vii) to assess the effect of porosity changes on diffusion processes. To this end, both experimental and modelling studies are carried out.

7.2 Geochemical modelling of the temporal evolution of waste packages

The study on the temporal evolution of the geochemical conditions in waste packages was launched last year (LES PROGRESS REPORT 2016) and continued in 2017 (WIELAND et al. 2017). The aim is to predict the chemical conditions within selected waste packages over the 100'000 year service life of a repository on the basis of thermodynamic modelling. After a thoughtful review provided by Nagra it was decided to also model the evolution of the volume of waste packages with time. The selected waste sorts were those previously considered for modelling the inventories of solids (waste materials, cement phases, minerals) and the composition of the aqueous phase, that is, three cement-stabilized operational waste sorts (BA-B-HP, BA-M-H, BA-PH-PF) and two decommissioning waste sorts (SA-PW-MX, SA-L-MX). The composition of these waste sorts is very different. For example, the operational waste sorts contain large amounts of organic materials, such as spent ion exchange resins or cellulose, respectively, while the decommissioning waste sorts are mostly metallic. The chemical reactions that are expected to progress with time inside the waste packages are i) metal corrosion, ii) degradation of organics, iii) dissolution of silicate aggregates and iv) carbonation of cementitious materials. These reactions are believed to control the degradation of the waste matrices and to be primarily responsible for cement-waste interactions as the degradation products can react with the solidifying concrete inside the waste packages. Two scenarios were taken into account for the modelling: limited and unlimited water availability. The first scenario is based on the assumption that the waste packages remain intact over a long time period ("closed system") while the second scenario implies that small openings (e.g. cracks, pit corrosion, etc.) exist in the walls of the waste packages already at the start of waste emplacement in the deep geological repository ("semi-open system"). The two scenarios were modelled, either allowing for the formation of thermodynamically stable zeolites or assuming that zeolite formation is inhibited, respectively.

The results for one of the cement-stabilized decommissioning waste sorts (denoted as SA-L-MX) are shown in Fig. 7.1, illustrating the complete set of information obtained from thermodynamic modelling, such as the initial composition of the solidifying concrete (Fig. 7.1b) and the evolution of mass and volume of the solid materials (waste, cement phases, minerals) (Fig. 7.1c). The results are shown for the scenario with unlimited water availability and absence of zeolites. The waste sort mainly contains metals and the initial inventory is as follows (NAGRA 2014): 4519 kg solidifying concrete including aggregates and pore solution, 12.9 kg low molecular weight (LMW) organics, 0.75 kg PVC, 4.5 kg urea, 5930 kg steel, 210 kg iron (cast), 3.2 kg aluminium, 124 kg brass, 139.1 kg copper, 0.56 kg zinc.

The composition of the solidifying concrete corresponds to a "low-pH"-type cement where portlandite is completely converted into calcium silicate hydrates (C-S-H) and pH of the pore solution is comparatively low (12.68). The buffer capacity of the cementitious system is very low due to the absence of portlandite. Nevertheless, temporal evolution does not lead to dramatic pH changes because carbonation is only a minor process. The inventory of organic materials is very low in this waste sort and, therefore, carbonation of the cementitious material by CO₂ resulting from the degradation of the organic materials is negligible. Corrosion of metals dominates the long-term

behaviour of this waste sort. Anoxic corrosion of aluminium, brass, iron, steel and zinc produces large volumes of H₂ (not shown) and magnetite as corrosion product (Fig. 7.1c).

Changes in the total volume of all selected waste sorts were modelled by assuming zeolite formation or absence of zeolites. As expected, the volume of waste materials decreases with time due to the degradation of organics and corrosion of metals (Fig. 7.2). As a consequence large volumes of CH₄ and CO₂ are produced (data not shown; see LES PROGRESS REPORT 2016). Corrosion products are formed with time, i.e. magnetite, which, in particular, increases the volume of the waste matrix in the decommissioning waste packages (Fig. 7.1c). In contrast, the volume of the waste matrix decreases in case of the operational waste sorts because the inventory of organic compounds is typically larger in these waste sorts than that of the metallic waste materials. The reduction of the volume of the operational waste sorts is caused by the degradation of the organic materials with time while the increase in the volume caused by the corrosion of metals is comparatively small. Fig. 7.2 further reveals that the total volume of the three operational and two decommissioning waste sorts increases with time for both modelling scenarios. The total increase in volume amounts to ~ 35 vol.%.

The modified report was re-submitted to Nagra for a review.

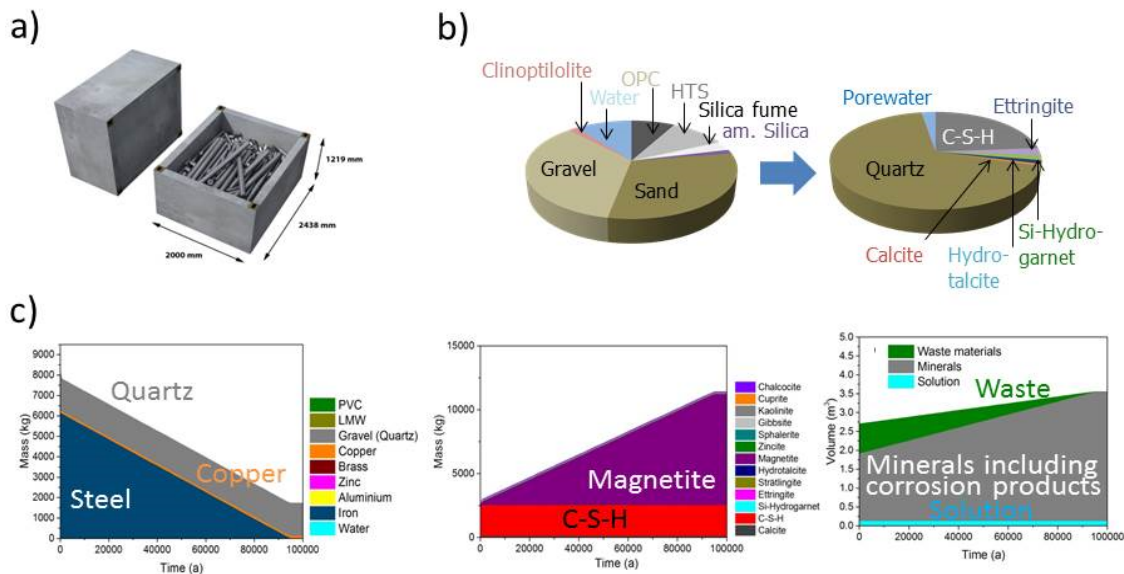


Fig. 7.1: Decommissioning waste sort SA-L-MX, a) image of the waste package, b) composition of the solidifying concrete: unhydrated (left) and hydrated, modelled cement mix (right), c) temporal evolution of the waste materials (left), mineral composition (centre) and the volume of waste materials and minerals (right). Modelling scenario: unlimited water and absence of zeolites.

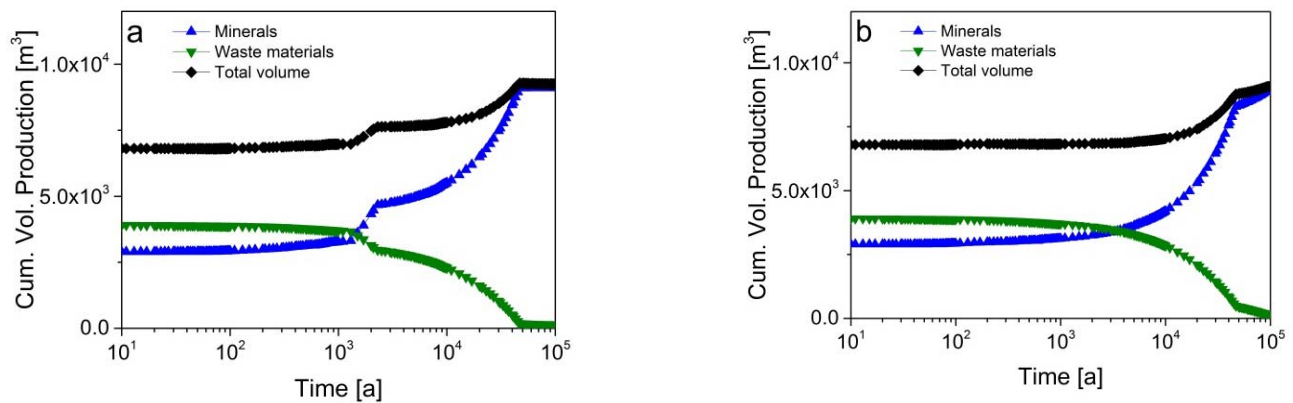


Fig. 7.2: Time-dependent changes in the total volume, and the volume of waste materials and minerals in the five waste sorts considered, a) with zeolite formation, b) absence of zeolites.

7.3 Multi-phase mass transport in waste-packages using a look-up table approach for description of cement degradation

Fully coupled thermo-hydraulic-chemical (THC) simulations of two-phase mass transport with complex chemistry in heterogeneous 2D and 3D systems are currently not feasible. We therefore developed a simplified look-up table based approach which substitutes numerically expensive calculation of complex chemical equilibria in reactive transport calculations and allows an efficient description of the degradation processes in heterogeneous cementitious systems. Degradation processes considered are the alkali-silica-reaction (ASR) and carbonation due to ingress of CO_2 . The look-up table approach provides a feedback mechanism for a reactive multi-phase multi-component transport model, if combined with kinetically controlled source terms for reaction products (Fig. 7.3). It defines source and sink terms for gases, specifically H_2 , CH_4 and CO_2 (gas consumption/production due to (bio-)chemical reactions), changes in porosity (due to mineral precipitation/dissolution reactions), and source and sink terms for water (water consumption/production due to (bio-)chemical reactions). The state of concrete degradation can be estimated based on the amount of CO_2 that is consumed in a specific concrete volume and the amount of SiO_2 -containing aggregate reacted within the same volume over time.

In cooperation with the Helmholtz Centre for Environmental Research – UFZ, Leipzig, Germany, the look-up table approach was implemented in a new multi-component multi-phase solver developed by Yonghui Huang and Haibing Shao within the OpenGeoSys-6 framework (HUANG et al. 2017).

In a first step we did extensive testing by comparing the new multi-phase model that approximates

chemical processes with a look-up table (OGS-MP-LT) and our reactive transport solver (OGS-GEM) that explicitly includes calculation of chemical reactions. Test cases were created for accelerated carbonation where CO_2 transport in the gas phase causes carbonation, for ASR only and for cases where carbonation (due to in-diffusion of CO_2) and ASR are competitive reactions. Fig. 7.4 shows the pH evolution with time for a case where very high concentrations of CO_2 , close to a pure CO_2 atmosphere, diffuse in gas and water phases into a 10 meter long partially water-saturated concrete structure. Initial pH in the concrete is about 13 and after full carbonation it drops to a value close to 6. The initial fast progress of the carbonation front slows down with time and it takes the front about 1500 years to reach a distance of 8 m. In the same time period, the concurrent reaction of cement phases with silica from the aggregates (ASR) will lower the pH to values near 10 in concrete not affected by carbonation. Fig. 7.4 is one example for the generally very good agreement between the model with look-up table and the full reactive transport model.

As an advanced test case the mass transport in a single cemented waste package was investigated. The goal was to explore the influence of feedback between chemical processes and multi-phase transport processes in a single generic low-level radioactive waste package during intermediate storage. The model set-up includes gas and water transport, gas generation and water consumption by metal corrosion or microbial degradation of organic wastes, water consumption (or release) by degradation of concrete due to carbonation or ASR, as well as feedback of water availability and concrete degradation state on (bio-)chemical reactions.

The modelling approaches strongly depend on a sound knowledge of the kinetics of the reactions and robust thermodynamic data sets for the involved reaction products. To this end, thermodynamic data of the reaction products formed during the course of the interaction of iron/steel with cement paste are essential as the inventory of metallic waste materials is substantial in the L/ILW repository (see e.g. Fig. 7.1). At present, the data basis for thermodynamic modelling of the interaction of iron (or steel) corrosion products with cement paste under reducing conditions is very limited. Magnetite (Fe_3O_4) and pyrite (FeS_2) are the only products currently considered in conjunction with iron corrosion in anoxic alkaline conditions. Furthermore, it is assumed that iron corrosion products do not interact with cement paste. A PhD project financed by the Swiss National Science Foundation (SNSF grant No 200021_162342) was started in 2016 with the aim to critically assess the current understanding.

In 2017 the study focused on the development of an experimental set-up for investigations on the interaction of Fe(II), which is an important species during anoxic corrosion of iron with cement phases. Fig. 7.5a illustrates that Fe(II) is chemically very unstable in alkaline solutions and readily oxidizes to Fe(III). Even the addition of high concentrations of commonly used reducing agents, such as Na_2SO_3 , did not significantly inhibit the oxidation process in alkaline media. From these experiments it was inferred that traces of oxygen are present in the solutions although de-aerated Milli-Q water was prepared by using the standard treatment reported in the literature, i.e. acidifying Milli-Q water to pH 4 with HCl and subsequent boiling for 60 min under continuous N_2 purge. Preliminary sorption experiments carried out with Fe(II,III) on (C-S-H) phases further corroborated the above finding (Fig. 7.5b). The distribution ratios (R_d) determined for Fe(II) uptake by the C-S-H phases (Ca/Si ratios = 0.8 and 1.5) agrees within the experimental uncertainties with the values determined for Fe(III) uptake by the same cement phases. Note that the R_d values were determined in batch-type sorption experiments carried out in the glove box with N_2 atmosphere using ^{55}Fe radiotracer at a total Fe concentration of $\sim 10^{-10}$ M. Thus, Fe(II) is readily oxidized to Fe(III) at the given concentration level and, further, oxidation cannot be suppressed in the hyper-alkaline C-S-H suspensions by using reducing agents. As a consequence, the experimental set-up for sorption studies with Fe(II) has to be modified and electrochemical cells will be used in the future to control the redox stability of Fe(II).

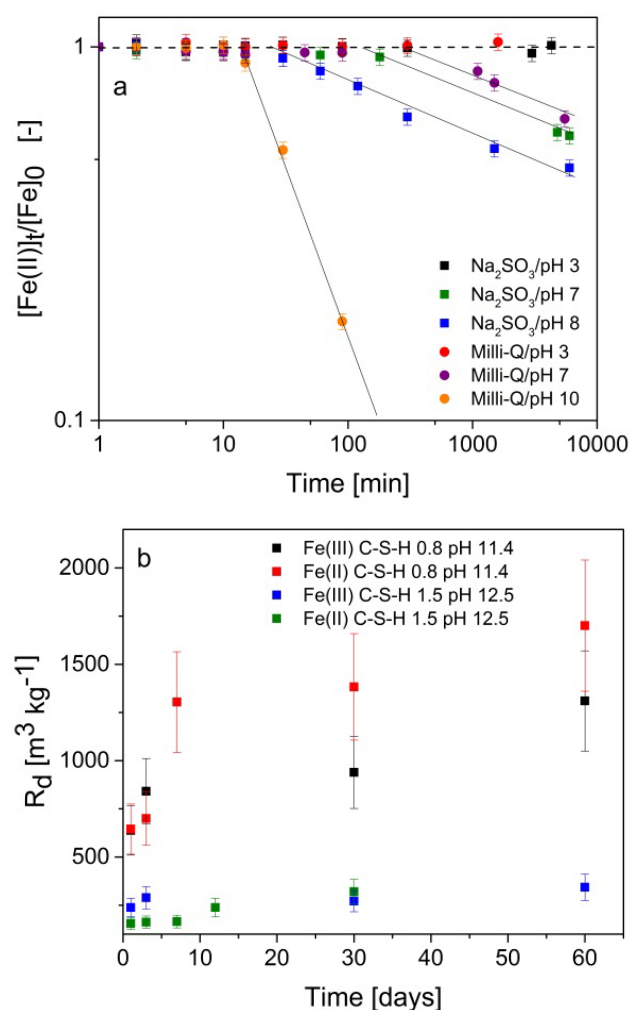


Fig. 7.5: a) Time-dependent changes in the aqueous Fe(II) concentration, b) Kinetics of Fe(II) and Fe(III) uptake by C-S-H phases.

In 2017 X-ray absorption spectroscopy (XAS) measurements were performed at the SAMBA beamline of the SOLEIL synchrotron (France) and the MicroXAS beamline of the Swiss Light Source (SLS) (Switzerland) with the aim to determine the oxidation state and coordination environment of Fe species in cementitious materials. X-ray absorption near edge spectroscopy (XANES) showed that Fe(II) was not stable in the X-ray beam at SOLEIL and was reduced to Fe(III) (Fig. 7.6).

However, Fe(II) was found to be stable in the beam on Fe(II) doped C-S-H samples if the measurements were conducted in cryogenic conditions (He cryostat, $T = 25$ K). The experiments further revealed that Fe(II) was already oxidized to Fe(III) during sample preparation in the C-S-H samples with the lowest loadings (~ 500 ppm) while a mixture of Fe(II)/Fe(III) oxidation states was observed on the samples with the higher loading (~ 3000 ppm).

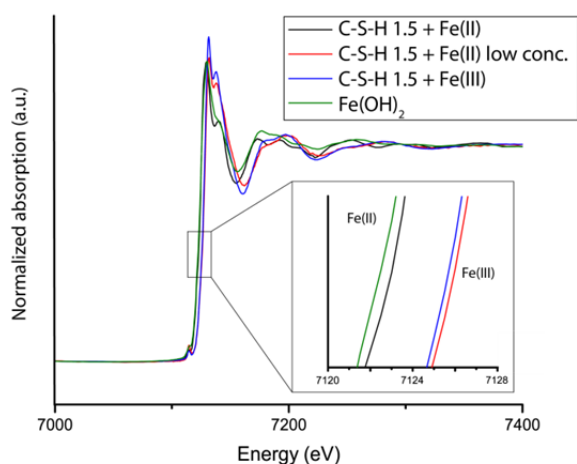


Fig. 7.6: XANES spectra of Fe(II, III) doped C-S-H samples and $\text{Fe}(\text{OH})_2$ as a reference.

Thus, this observation is in accordance with the conclusions drawn from the wet chemistry experiments that Fe(II) is not stable in hyper-alkaline conditions although the oxygen concentration was reduced as much as technically achievable (deaeration of water, N_2 atmosphere in glove box).

7.5 Alkali-silica reaction in concrete

The alkali-silica reaction (ASR) is a deterioration mechanism, which can severely limit the lifetime of concrete structures such as dams and bridges. In ASR the alkaline pore solution of concrete reacts with silica present in rocks used as concrete aggregates. In concrete structures the reaction product is able to accumulate water and to swell, consequently generating stress and cracks. As the reaction proceeds very slowly, the first damages are usually observed only several decades after the concrete structures have been built. Substantial damages have been observed worldwide. In Switzerland, several hundreds of structures, including bridges and dams, are affected, causing substantial costs due to repair or replacement. Although the first cases of ASR were reported in the 1940's, to date scientific understanding of the process knowledge is still poor. It is further to be noted that ASR-type reactions also have an impact on the temporal evolution of the chemical conditions in cement-stabilized waste packages, in particular pH of the pore solution, due to the dissolution of aggregate materials (e.g. sand, quartz sand) used to make the waste-solidifying concrete.

Researchers from Empa, EPFL and PSI have teamed up in the SNSF funded Sinergia project with the aim to gain insights into the mechanisms of the reaction and gain knowledge about how damage develops with time. At LES the ASR will be investigated with state-

of-the-art synchrotron spectroscopic techniques, continuing previous work (DÄHN et al. 2016). The project started successfully in July 2017 with the hiring of Dr. Guoqing Geng, and the submission of several beamtime proposals. Additional funding could be acquired from the European Union's Horizon 2020 research and innovation programme under the Marie Skłodowska-Curie grant agreement No 701647. Thus, this project is fully financed by SNSF and EU Horizon 2020 fundings.

7.6 References

DÄHN R., ARAKCHEEVA A., SCHAUB PH., PATTISON P., CHAPUIS G., GROLIMUND D., WIELAND E., LEEMANN A. (2016)

Application of micro X-ray diffraction to investigate the reaction products formed by the alkali-silica reaction in concrete structures. *Cem. Concr. Res.* 79, 49-56.

HUANG Y., NAGEL T., SHAO H. (2017)

Comparing global and local implementations of nonlinear complementary problems for the modelling of multi-component two-phase flow with phase change phenomena. *Environ. Earth Sci.* 76, 643-661.

KOSAKOWSKI G., BERNER U., WIELAND E., GLAUS M.A., DEGUELDRE C. (2014)

Geochemical evolution of the L/ILW near field. Nagra Tech. Rep. NTB 14-11. Nagra, Wettingen, Switzerland.

KOSAKOWSKI G., HUANG Y. (2017)

Notes on benchmarking a look-up table for degradation of a concrete by carbonation and Alkali-Silica-Reaction (ASR). Internal Report AN-44-17-02, PSI, Villigen, Switzerland.

NAGRA (2002)

Project Opalinus Clay. Safety report. Demonstration of disposal feasibility for spent fuel, vitrified high-level waste and long-lived intermediate-level waste (Entsorgungsnachweis). Nagra Tech. Rep. NTB 02-05, Nagra, Wettingen, Switzerland.

NAGRA (2014)

Modellhaftes Inventar für radioaktive Materialien MIRAM 14. Nagra Tech. Rep. NTB 14-04, Nagra, Wettingen, Switzerland.

WIELAND E., KOSAKOWSKI G., LOTHENBACH B., KULIK D.A. (2017)

Preliminary assessment of the temporal evolution of waste packages in the near field of an L/ILW repository. Nagra Arbeitsbericht NAB (in review).

8 DISSOLUTION OF SPENT FUEL AND VITRIFIED WASTE

E. Curti

8.1 Overview

Dissolution of spent fuel and vitrified nuclear waste provides the source term for radionuclide release in the planned repository for high-level radioactive waste. This source-term obviously influences directly or indirectly all other safety assessment parameters and calculations relative to other repository compartments (near-field, geosphere and biosphere). This topic has been therefore intensively studied for decades within the community of radioactive waste disposal science. Although many issues have been resolved, and therefore research efforts have been reduced, some key questions remain open.

Concerning spent fuel dissolution, the response of so-called modern fuels to aqueous attack is coming into the focus of current research. Such are fuels doped with Cr or Al to increase the grain-size of the UO_2 particles in order to reduce internal pressures caused by the release of fission gas. This allows increasing the linear power rating of the fuels, thereby increasing achievable burn-ups and modifying microstructural features of spent fuel. The effects of these changes on the release of radionuclides under repository conditions need to be understood and quantified.

Recent studies on nuclear waste glass dissolution mostly deal with the effect of engineered barrier materials, particularly cement, clay and steel corrosion products. Both mechanistic and kinetic studies are carried out in dedicated scientific laboratories in France, Belgium and UK. At LES, no experimental programme is currently active.

8.2 Spent fuel dissolution

8.2.1 DisCo project

The 4 years EURATOM project DisCo, (Modern spent fuel Dissolution and chemistry in failed Container conditions) has been approved by the European commission in April 2017 and has officially started on June 1st 2017. This collaborative project is focussed on the dissolution of Cr/Al doped and MOX spent fuels under repository conditions. LES participates with the following modelling activities:

(I) The theoretical determination of oxygen potential for conventional (UO_2) and unconventional (MOX/doped UO_2) spent fuels as a function of temperature. To this aim a sublattice solid solution

model describing the effects of non-stoichiometric $(\text{U,Pu})\text{O}_2$ and Cr/Al dopants will be developed and implemented. The oxygen potential is a key parameter which determines the primary oxidation state of multivalent radionuclides in the fuel, thus potentially affecting their release under repository conditions.

(II) The calculation of chemical equilibrium inside the water-saturated canister under repository-relevant conditions, taking into account all the materials involved and formation of secondary solids.

Both objectives will be pursued via state-of-the-art thermodynamic calculations and compilation of necessary thermodynamic data.

Currently, thermodynamic high-temperature data for the anhydrous Cr-O system are being reviewed. They will be incorporated in the in-house HERACLES database, which will serve as a basis for the foreseen thermochemical calculations. Moreover, a conceptual model for a multivalent U-Cr non-stoichiometric oxide solid solution is under development. The next year will be devoted to the development and set-up of an operational model with GEMS.

8.2.2 Comparative analysis of Instant Release Fraction (IRF) data from Swiss spent fuel obtained in the framework of the GAP and FIRST-Nuclides projects

Because of the heterogeneous distribution of radionuclides in spent nuclear fuel, a source-term model describing radionuclide release from spent fuel in a geological repository must differentiate between the fast release of easily soluble water-accessible nuclides (the "instant release fraction", shortly IRF) and the long-term release due to slow dissolution of the fuel ("matrix dissolution"). A key objective of the collaborative EU-project FIRST-Nuclides was the collection of comprehensive data on promptly released nuclides (I, Cs and Se) upon aqueous leaching of high-burnup UO_2 and MOX fuels from operating European light-water nuclear reactors. PSI participated by carrying out leach experiments on spent fuels from the Gösigen and Leibstadt nuclear power plants and complementary spectroscopic investigations.

The evaluation of the data continued after the formal finalization of the project in 2017. A synthesis paper on the leach experiments was published recently

(LEMMENS et al. 2017). Here, we report on the key findings from the leach experiments and compare the results with similar data obtained in the framework of the earlier GAP-project (JOHNSON et al. 2012). The FIRST-Nuclides leach experiments were similar, but not identical, to those carried out during the GAP project. In the GAP experiments, sample preparation was optimized to detect differences in the fast radionuclide release from the central pellet region and the structurally modified microporous rim, which develops at high burn-up. In contrast, the FIRST-Nuclides experiments aimed at distinguishing release contributions from bulk fuel and fuel/cladding gap region. This was achieved by different types of sample preparation in the two projects.

Fig. 8.1a-d shows the fast release data for ^{137}Cs and ^{129}I , expressed as Fractions of Inventory in the Aqueous Phase (FIAP), obtained during both projects on similar fuels (in terms of burn-up and reactor origin) from the Leibstadt and Gösgen reactors.

The main and most relevant conclusion from this comparison in the perspective of safety assessment is that in general, FIAP% values from the FIRST-Nuclides experiments were found to roughly reflect the earlier GAP results, thus reinforcing the reliability of IRF(Cs) and IRF(I)-values used in safety assessment calculations. FIAP% maxima from the Leibstadt UO_2 samples were in the order of 2-3% for both ^{137}Cs and ^{129}I ; 4-8% for ^{137}Cs and 10-11% for ^{129}I from Gösgen UO_2 as well as MOX samples. In the GAP experiments, a gradual increase of the cumulative FIAP over 98 days was observed for ^{137}Cs , whereas "plateau" values were reached in the FIRST-Nuclides experiments already after 28 days. However, at leaching times of 98 days, both ^{137}Cs and ^{129}I FIAP% values of GAP and FIRST-Nuclides experiments are comparable (Fig. 8.1a).

One of the major aims of the FIRST-Nuclides project was to expand the IRF database, particularly by including data on high-burnup fuels, with the aim to find empirical correlations between IRF and known reactor operational parameters, such as Fission Gas Release (FGR), Burn-up (BU) and Linear Power Rating (LPR). These parameters are anticipated to be correlated with the segregation of Cs and I out of the fuel matrix taking place during in-reactor irradiation, induced by thermal diffusion. A good correlation would help in increasing the reliability of IRF

estimations for safety assessment, reducing the need for further technically complex and costly experiments on used fuels. The analysis of the FIRST-Nuclides and earlier data (LEMMENS et al. 2017) reveals a fairly promising positive correlation with LPR (Fig. 8.2) whereas correlations with BU and FGR (not shown) were less pronounced.

In contrast to ^{137}Cs and ^{129}I , in both GAP and FIRST-Nuclides experiments, aqueous concentrations of Se were below the detection limit of the analytical method (hydride generation multicollector ICP-MS). Such analyses are technically demanding due to the very low fission yield of ^{79}Se (leading to aqueous concentrations in the low ppb range) and due to mass interferences with isobaric isotopes of Ar (from air) and Br (salt impurities). The GAP analyses on solutions sampled after 98 days leach time systematically yielded concentrations below the experimental ^{79}Se detection limit of 0.5 ppb. Based on these data an upper limit of 0.22% was inferred for the FIAP of ^{79}Se (JOHNSON et al. 2012).

In the framework of the FIRST-Nuclides project Se aqueous concentrations were also measured at Studsvik (SE) on spent fuel samples irradiated in the Swedish Oskarshamn-III boiling water reactor. In this study care was taken to lower the detection limit of ICP-MS measurements by using a collision cell operated with CH_4 in order to eliminate isobaric mass interferences from Ar isotopes. This improvement was successful and allowed detection of Se isotopes in the leach solutions with a precision sufficient to reduce the detection limit below the 0.22% FIAP limit achieved by the PSI's instrument for ^{79}Se .

The data from conventional UO_2 fuel were in good agreement with the limit inferred in the PSI experiments, as a FIAP% of $0.2 \pm 0.1\%$ could be determined for ^{79}Se after 87 days of leaching. However, the experiments performed with the spent fuel samples irradiated in the Swedish Oskarshamn-III reactor indicated further release of Se at approximately constant rate up to FIAP=0.4 % after 360 days leaching time. For a Cr/Al doped samples the inferred FIAP values were even higher and reached 0.8%. A comparison with the release of other radionuclides in the same experiments (^{100}Mo and ^{238}U) suggests that this continued release is probably due to Se enriched in the UO_2 intergranular space (grain boundaries).

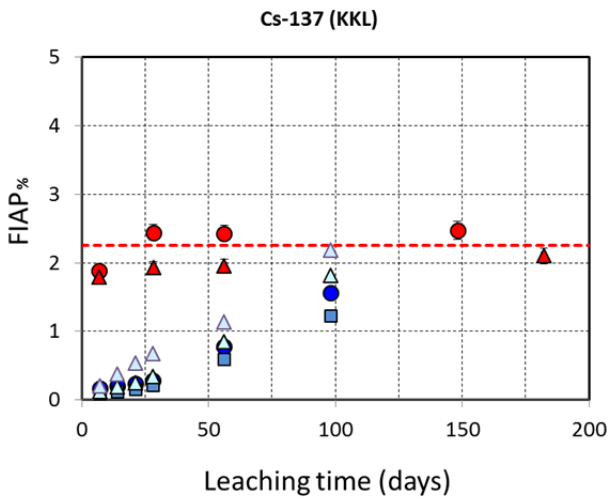


Fig. 8.1a: Cumulative FIAP% values of ¹³⁷Cs for UO₂ fuel samples (± cladding) from the Leibstadt reactor, compared with the experimental fission gas release (red broken line). Data from FIRST-Nuclides (red) are compared with those from the GAP project (blue). Each symbol represents a distinct sample.

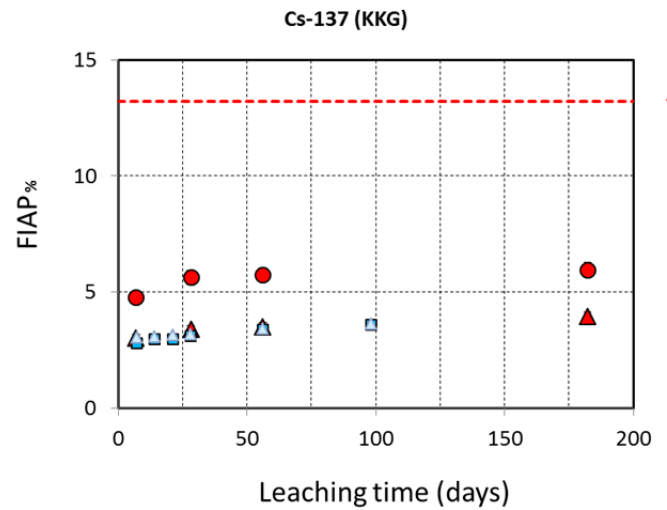


Fig. 8.1b: Cumulative FIAP% values of ¹³⁷Cs for UO₂ fuel samples (± cladding) from the Gösigen reactor, compared with the experimental fission gas release (red broken line). Data from FIRST-Nuclides (red) are compared with those from the GAP project (blue). Each symbol represents a distinct sample.

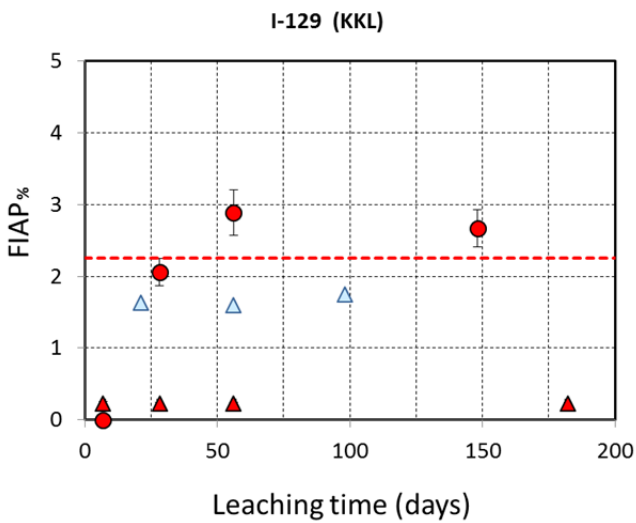


Fig. 8.1c: Cumulative FIAP% values of ¹²⁹I for UO₂ fuel samples (± cladding) from the Leibstadt reactor, compared with the experimental fission gas release (red broken line). Data from FIRST-Nuclides (red) are compared with those from the GAP project (blue). Each symbol represents a distinct sample.

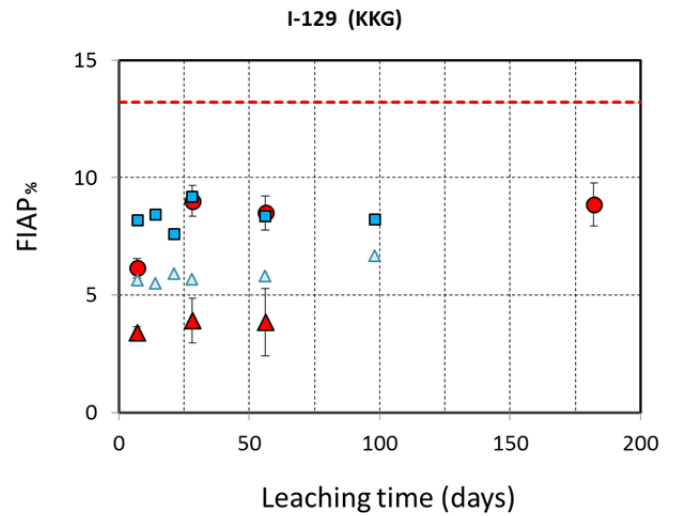


Fig. 8.1d: Cumulative FIAP% values of ¹²⁹I for UO₂ fuel samples (± cladding) from the Gösigen reactor, compared with the experimental fission gas release (red broken line). Data from FIRST-Nuclides (red) are compared with those from the GAP project (blue). Each symbol represents a distinct sample.

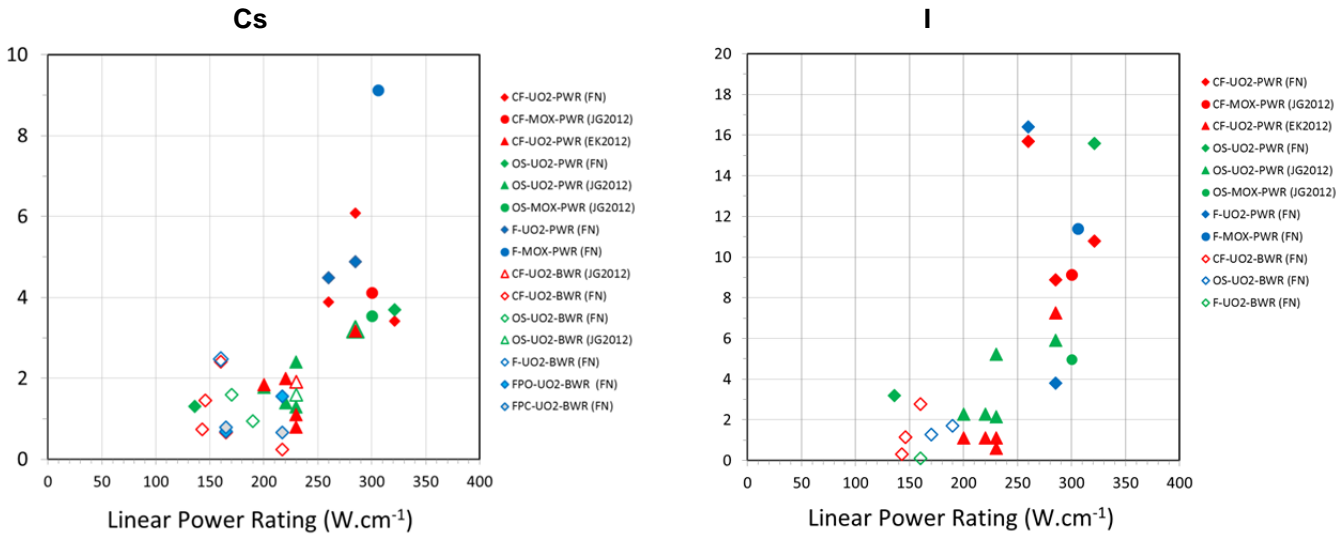


Fig. 8.2: Cs and I IRF data correlated with linear power rating (LPR). The LPR values apply either to the fuel sample itself or are average values from the corresponding fuel rod. Key for the legend: CF= intact cladded pellet segment; OS = cladded pellet segment opened in two pieces; F = fuel fragments; FPO = fuel powder (outer pellet region); FPC = fuel powder (core pellet region); label 2 gives the fuel type (UO₂ or MOX) and label 3 the reactor type (PWR=pressurized water reactor, BWR=boiling water reactors). Data origin is given in parentheses (FN= FIRST-Nuclides data, JG2012 = JOHNSON et al. (2012), EK2012 = EKEROTH et al. (2012)).

Some doubts remain, nevertheless, on how representative these data are. Because the experiments were carried out in normal air and using young spent fuel (strong radiolysis), one cannot exclude a priori that the observed Se release may have been enhanced by radiolytic oxidation of reduced Se on the surface of the grains. If the segregated, water-accessible Se was present in metallic form or as selenide, these species should be converted to easily soluble Se(VI) due to the radiolysis induced oxidizing conditions. Simple half-cell potential calculations indicate that even nanomolar hydrogen peroxide concentrations would provide an environment with Eh sufficiently high to oxidize any released selenide or metallic selenium (Fig. 8.3). Under repository conditions, one has to consider that hydrogen produced via canister corrosion would have probably the same oxidation-protective effect observed for UO₂ (CARBOL et al. 2009). Therefore, only leach experiments carried out under strictly reducing conditions in the presence of H₂ could reveal whether the observed continued Se release is representative of repository environments.

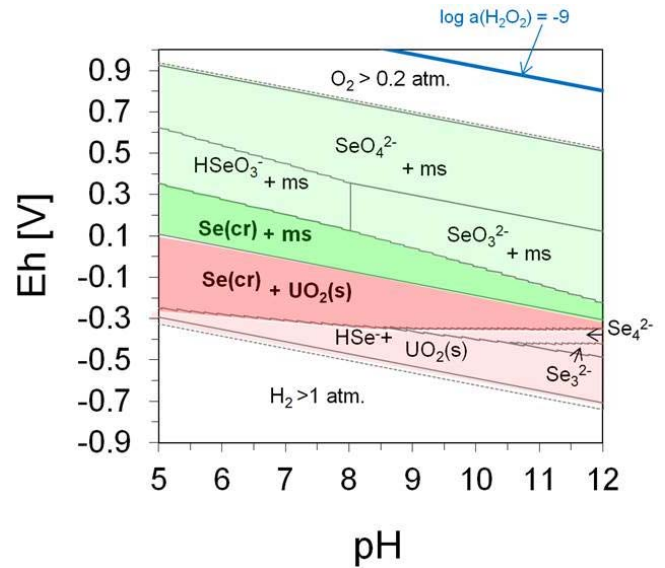


Fig 8.3: Combined Eh-pH predominance diagram at 25 °C and 1 bar for the Se-U-CO₃ system, for $[Se]_{tot} = 10^{-4} M$, $[CO_3]_{tot} = 10^{-2} M$ and $[NaCl] = 0.1 M$ and an initial UO₂(s) excess. The PSI-Nagra database v. 12/07 was used (THOENEN et al. 2014). Abbreviations: ms = metaschoepite, UO₃·2H₂O(s). The blue line indicates (metastable) conditions corresponding to 1 nM hydrogen peroxide.

8.3 References

CARBOL P., FORS P., GOULDER T., SPAHIU K. (2009)
Hydrogen suppresses UO₂ corrosion. *Geochim. Cosmochim. Acta*, 73, 4366–4375.

EKEROTH E., CUI D., LOW J., GRANFORS M., ZWICKY H.-U., SPAHIU K., ZETTERSTRÖM L., EVINS L.Z. (2012)

Instant release fractions from corrosion studies with high burnup LWR fuel. *MRS Proceedings*, 1475, imrc11-1475-nw35-o36, doi:10.1557/opl.2012.565.

JOHNSON L., , GÜNTHER-LEOPOLD I., KOBLER WALDIS J., LINDER H.P., LOW J., CUI D., EKEROTH E., SPAHIU K., EVINS L.Z. (2012).

Rapid aqueous release of fission products from high burn-up LWR fuel: Experimental results and correlations with fission gas release. *J. Nucl. Mater.* 420, 54–62.

LEMMENS K., GONZALEZ-ROBLES E., KIENZLER B., CURTI E., SERRANO-PURROY D., SUREDA R., MARTÍNEZ-TORRENTS A., ROTH O., SLONSKI E., MENNECART T. (2017)

Instant release of fission products in leaching experiments with high burnup nuclear fuels in the framework of the Euratom project FIRST-Nuclides, *J. Nucl. Mater.* 484, 307-323.

THOENEN T., HUMMEL W., BERNER U, CURTI E. (2014)

The PSI/Nagra Chemical Thermodynamic Database 12/07. Nagra Arbeitsbericht NAB 14-49, Nagra, Wettingen, Switzerland.

9 PUBLICATIONS

9.1 Peer reviewed journals

Aldaba D., Glaus M.A., Van Loon L.R., Rigol A.¹, Vidal M.¹

Diffusion of radi sulphate and radio cesium in kaolinite clay (KG): testing the applicability of the pore-water diffusion model. *Appl. Geochem.* 86, 84-91 (2017).

¹ University of Barcelona, Barcelona, Spain

Cametti G.¹, Churakov S.V., Armbruster Th.¹

Reinvestigation of the zemannite structure and its dehydration behavior: a single-crystal X-ray and atomistic simulation study. *Europ. J. Miner.* 29, 53-61 (2017).

¹ University of Bern, Bern, Switzerland

Churakov S.V., Labbez Ch.¹

Thermodynamics and molecular mechanism of Al incorporation in calcium silicate hydrates. *J. Phys. Chem. C* 121, 4412-4419 (2017).

¹ Université de Bourgogne, Dijon, France

Fukatsu Y.¹, Van Loon L.R., Shafizadeh A., Grolimund D., Ikeda Y.¹, Tsukahara T.¹

Effect of celestite precipitation in compacted illite on the diffusion of HTO, ³⁶Cl⁻ and ²²Na⁺. *Energy Procedia* 131, 133-139 (2017).

¹ Tokyo Institute of Technology, Tokyo, Japan

Jenni A., Gimmi T., Alt-Epping P.¹, Mäder U.¹, Cloet V.²

Interaction of ordinary Portland cement and Opalinus Clay: Dual porosity modelling compared to experimental data. *Phys. Chem. Earth* 99, 22 (2017).

¹ University of Bern, Bern, Switzerland

² Nagra, Wetztingen, Switzerland

Keri A., Daehn R., Krack M., Churakov S.V.

Combined XAFS spectroscopy and ab initio study on the characterization of iron incorporation by montmorillonite. *Environ. Sci Technol.* 51, 10585-10594 (2017).

Lemmens K., González-Rodríguez R.E., Kienzler B., Curti E., Serrano-Purroy D., Sureda R., Martínez-Torrents A., Roth O., Slonszki E., Mennecart T., Günther-Leopold I., Hózer Z.

Instant release of fission products in leaching experiments with high burn-up nuclear fuels in the framework of the Euratom project FIRST- Nuclides. *J. Nucl. Mater.* 484, 307 (2017).

Leupin O.X.¹, Van Loon L.R., Gimmi T., Wersin P.², Soler J.M.³

Exploring diffusion and sorption processes at the Mont Terri underground rock laboratory: lessons learned from 20 years of field research. *Swiss J. Geosci.* 110, 391-403 (2017).

¹ Nagra, Wetztingen, Switzerland

² University of Bern, Bern, Switzerland

³ UPC-CSIC, Barcelona, Spain

Miron G.D., Wagner T.¹, Kulik D., Lothenbach B.²

An internally consistent thermodynamic dataset for aqueous species in the system Ca-Mg-Na-K-Al-Si-O-H-C-Cl to 800 °C and 5 kbar. *Americ. J. Sci.* 317, 755 (2017).

¹ University of Helsinki Helsinki, Finland

² Empa, Dübendorf, Switzerland

Prasianakis N.I., Curti E., Kosakowski G., Poonosamy J., Churakov S.V.

Deciphering pore-level precipitation mechanisms. *Scientific Reports* 7, 13765 (2017).

Safi M.A.¹, Prasianakis N., Turek S.²

Benchmark computations for 3D two-phase flows: A coupled lattice Boltzmann-level set study. *Comput. Mathem. Applic.* 73, 520 (2017).

² TU Dortmund, Dortmund, Germany

Safi M.A., Prasianakis N.I., Mantzaras J., Lamibrac A., Buchi F.N.

Experimental and pore-level numerical investigation of water evaporation in gas diffusion layers of polymer electrolyte fuel cells. *Intern. J. Heat Mass Transfer* 115, 238-249 (2017).

¹ TU Dortmund, Dortmund, Germany

Sui R., Es-Sebbar E.T., Mantzaras J., Prasianakis N.I. Experimental and numerical investigation of fuel-lean H₂/CO/Air and H₂/CH₄/Air catalytic microreactors. *Comb. Sci. Technol.* 190, 336 (2017).

Vespa M.¹, Dähn R., Huthwelker T., Wieland E.

Soft X-ray absorption near-edge investigations of Mg-containing mineral phases relevant for cementitious materials. *Phys. Chem. Earth* 99, 168-174 (2017).

¹ KIT-INE, Karlsruhe, Germany

Wigger C., Van Loon L.R.

The importance of interlayer equivalent pores for anion diffusion in clay-rich sedimentary rocks. *Environ. Sci. Technol.* 51, 1998-2006 (2017).

Wu T.¹, Wang H.², Wang Z.¹, Zhang Y.¹, Van Loon L.R.

Salt effects on Re(VII) and Se(IV) diffusion in bentonite. *Appl. Clay Sci.* 141, 104-110 (2017).

¹ Huzhou University, Huzhou, China

² University of South China, Hengyang, China

Yapparova A., Gabellone T.¹, Whitaker F.¹, Kulik D.A., Matthäi St.K.²

Reactive Transport Modelling of Dolomitisation Using the New CSMP++GEM Coupled Code: Governing Equations, Solution Method and Benchmarking Results. *Transport Porous Media* 117, 385 (2017).

¹ University of Bristol, Bristol, UK

² University of Melbourne, Melbourne, Australia

Yapparova A., Gabellone T.¹, Whitaker F.¹, Kulik D., Matthäi St.K.²

Reactive transport modelling of hydrothermal dolomitisation using the CSMP++GEM coupled code: Effects of temperature and geological heterogeneity. *Chem. Geol.* 466, 562 (2017).

¹ University of Bristol, Bristol, UK

² University of Melbourne, Melbourne, Australia

9.2 PSI and Nagra reports

Bradbury M.H., Marques Fernandes M., Baeyens B. Estimates of the influence of radioisotope solubility limits and sorption competition on the sorption values in the SDBs of MX-80 bentonite and Opalinus Clay. PSI Bericht Nr. 17-04 and Nagra Tech. Rep. NTB 17-11 (2017).

Baeyens B., Bradbury M.H.

The development of a thermodynamic sorption data base for montmorillonite and the application to bentonite. PSI Bericht Nr. 17-05 and Nagra Tech. Rep. NTB 17-13 (2017).

Bradbury M.H., Baeyens B.

The development of a thermodynamic sorption data base for Illite and the application to argillaceous rocks. PSI Bericht Nr. 17-06 and Nagra Tech. Rep. NTB 17-14 (2017).

Hummel W.

Chemistry of selected dose-relevant radionuclides. Nagra Tech. Rep. NTB 17-05 (2017).

9.3 Conference Proceedings

Hummel W., Weibel G.

Heavy metal complexes in recycling and waste disposal: Application of the PSI Chemical Thermodynamic Database. Acta of the International Symposia on Metal Complexes – ISMEC 2017, ISMEC GROUP SERIES, ISSN: 2239-2459, Volume 7, 135-136 (2017).

Meng S., Pfingsten W.

Radioactive waste confinement: clays in natural and engineered barriers.

Geological Society, London, Special Publications 443 (2017)

Wersin P., Traber D., Mäder U.K., Mazurek M., Waber H.N., Rufer D., Gimmi T., Cloet V.

Porewater chemistry in claystones in the context of radioactive waste disposal. *Procedia Earth and Planetary Science* 17, 718-721 (2017).

9.4 Conferences/workshops/presentations

Aldaba D., Glaus M.A., Van Loon L.R., Rigol A., Vidal M.

Diffusion of radiosulphate and radiocaesium in kaolinite clay (KGa-2): testing the applicability of the pore-water diffusion model. Clay Conference 2017, Davos, Switzerland, 24-27 September 2017.

Baeyens B., Marques Fernandes M.

Competitive sorption on montmorillonite and illite. Clay Conference 2017, Davos, Switzerland, 24-27 September 2017.

Cloet V., De Cannière P., Elam W.T., Gimmi T., Grundl T.J., Jakob A., Leupin O.X., Schefer S., Yang T.

In-situ XRF measurements to track iodide diffusion in Opalinus Clay. Clay Conference 2017, Davos, Switzerland, 24-27 September 2017.

Curti E., Krack M., Grolimund D., Churakov S.V.

The chemical state of ⁷⁹Se in spent nuclear fuel: Implications for the performance assessment. International High-Level Radioactive Waste Management Conference (IHLRWM) 2017, Charlotte NC, USA, 9-13 April, 2017.

- Curti E, Prasianakis N.I.
Implementing baryte nucleation/precipitation kinetics and radium uptake at the pore level using the Lattice-Boltzmann method. 5th Granada-Munster Discussion Meeting: Mineral Reactivity GMDM: From biomineralization and Earth's climate evolution to CO₂ capture and built heritage conservation, Granada, Spain, 30 November – 1 December 2017.
- Dähn R., Osán J., Marques M., Grolimund D., Baeyens B.
X-ray absorption investigations of uptake processes by argillaceous rocks. From pure mineral phases to real systems. 7th Workshop on Speciation, Techniques, and Facilities for Radioactive Materials at Synchrotron Light Sources (Actinide-XAS-2017), Oxford, England, 11-13 April 2017.
- Delavernhe L., Kupcik T., Joseph C., Montoya V., Glaus M.A., Schuhmann R., Emmerich K., Schäfer T.
Multitracer (HTO, ³⁶Cl, ⁸⁵Sr²⁺) diffusion in compacted natural and reduced-charge dioctahedral smectites. Clay Conference 2017, Davos, Switzerland, 24-27 September 2017.
- Gimmi T., Jenni A., Alt-Epping P., Mäder U.
Donnan equilibrium: An alternative modelling approach. EBS-Task force meeting, Hannover, 9-10 May 2017.
- Gimmi T., Alt-Epping P.
Donnan equilibria in clays simulated by using the Nernst-Planck equation. Migration 2017, Barcelona, 10-15 September 2017.
- Gimmi T., Alt-Epping P.
Donnan equilibria in clays simulated by using the Nernst-Planck equation. Clay Conference 2017, Davos, Switzerland, 24-27 September 2017.
- Gimmi T.
Cement-clay interactions investigated by neutron imaging. Workshop Verbundprojekt Geochemische Radionuklidrückhaltung an Zementalterationsphasen, Potsdam, 14-15 November 2017.
- Glaus M.A., Frick S., Van Loon L.R..
Diffusive transport of Eu(III) in illite: a case study investigating the effects of chemistry and compaction. Clay Conference 2017, Davos, Switzerland, 24-27 September 2017.
- Hax Damiani L., Glaus M., Churakov S., Kosakowski G.
Modelling cement/clay interfaces with the Nernst-Planck approach. Clay Conference 2017, Davos, Switzerland, 24-27 September 2017.
- Hax Damiani L., Churakov S.V., Kosakowski G.
Rapid development of a reactive transport code with FeniCS and Reaktoro, CEBAMA 2nd Annual Workshop, Helsinki, Finland 17 May, 2017.
- Hax Damiani L., Churakov S.V., Kosakowski G.
Modelling cement/clay interfaces with the Nernst-Planck approach, 7th PhD Meeting on Reactive Transport, UFZ Leipzig, Germany, 23 February, 2017.
- Hax Damiani L., Kosakowski G., Churakov S.V.
Modelling cement/clay interfaces with the Nernst-Planck approach. Clay Conference 2017, Davos, Switzerland, 24-27 September 2017.
- Hummel W., Weibel G.
Heavy metal complexes in recycling and waste disposal: Application of the PSI Chemical Thermodynamic Database. International Symposia on Metal Complexes – ISMEC 2017, Dijon, France, 11-15 June, 2017.
- Kéri A., Dähn R., Krack M., Churakov S.V.
Iron uptake characterization of clay minerals combining ab initio calculations and XAFS spectroscopy studies. 16th ICC — International Clay Conference, Granada, Spain, 17–21 July 2017.
- Kéri A., Dähn R., Krack M., Churakov S.V.
Characteristics of iron uptake by montmorillonite combining ab initio calculations and XAFS spectroscopy studies. Clay Conference 2017, Davos, Switzerland, 24-27 September 2017.
- Kosakowski G.
Reactive transport modelling of concrete/Opalinus Clay interfaces. Clay Conference 2017, Davos, Switzerland, 24-27 September 2017.
- Kosakowski G., Huang Y., Shao H., Wieland E.
Water and gas transport in a generic cemented waste package considering spatio-temporal variations in chemical conditions. Migration 2017, Barcelona, 10-15 September 2017.
- Mancini A., Wieland E., Lothenbach B.
Interaction of Fe(II) with cement phases in anoxic conditions. Goldschmidt 2017, Paris, France 13-18 August, 2017.

Marques Fernandes M., Scheinost A., Baeyens B.
Sorption of NpO_2^+ on montmorillonite: influence of ferrous iron. Goldschmidt 2017, Paris, France 13-18 August, 2017.

Marques Fernandes M., Baeyens, B.,
Competitive metal sorption on illite. Migration 2017, Barcelona, 10-15 September 2017.

Marques Fernandes M., Scheinost A., Baeyens B.
Influence of Fe^{II} on the retention mechanisms of NpO_2^+ by montmorillonite. 7th Workshop on Speciation, Techniques, and Facilities for Radioactive Materials at Synchrotron Light Sources (Actinide-XAS-2017), Oxford, England, 11-13 April 2017.

Marques Fernandes M., Scheinost A., Baeyens B.,
Sorption of redox sensitive NpO_2^+ montmorillonite: influence of ferrous iron. Clay Conference 2017, Davos, Switzerland, 24-27 September 2017.

Mibus J., Diomidis N., Swanton S., Suzuki-Muresan T., Rodríguez Alcalá M., Leganés Nieto J.L., Bottomley D., Herm M., de Visser-Týnová E., Cvetković B.Z., Sakuragi T., Druyts F., Heikola T., Williams S.

Speciation of carbon-14 released from activated steels under conditions of a geological repository. Migration 2017, Barcelona, 10-15 September 2017.

Miron G.D., Kulik D.A., Thoenen T.
Predicting thermodynamic properties at elevated temperatures using isocoulombic reactions generated in the ThermoMatch code. ThermAc Workshop, München-Garching, 25 October, 2017.

Montoya V., Kupcik T., Van Laer L., Glaus M.A., Marques Fernandes M., Baeyens B., Bruggeman C., Maes N., Schäfer T.

Sorption of Sr, Co and Zn on Na-illite: batch sorption experiments and modelling including some reference measurements on compacted clay samples. Clay Conference 2017, Davos, Switzerland, 24-27 September 2017.

Nedyalkova L., Lothenbach B., Tits J., Wieland E., Mäder U.

Effect of redox conditions on sulfur and selenium binding in AFm phases. Goldschmidt 2017, Paris, France 13-18 August, 2017.

Nedyalkova L., Lothenbach B., Tits J., Wieland E., Mäder U.

Effect of redox conditions on sulfur and selenium binding in AFm phases. CEBAMA 2nd Annual Workshop, Helsinki, Finland 17 May, 2017.

Patel R.

Lattice Boltzmann methods for pore-scale physico-chemical processes and their application to cement paste. SCK•CEN Academy Topical Day: "Bridging experiments and continuum scale models: Role of modelling physical-chemical processes at the pore scale", Mol, Belgium, 14-16 November 2017.

Pfingsten W.

Eu and other tri- and bi-valent cation diffusion and sorption competition in bentonite. Clay Conference 2017, Davos, Switzerland, 24-27 September 2017.

Poonoosamy J., Kosakowski G., Curti E., Prasianakis N.I.

Dissolution-precipitation processes in tank experiments: an experimental benchmark and modelling strategies. 9th International Conference on Porous Media and Annual Meeting (InterPore), Rotterdam, The Netherlands, 8-11 May 2017.

Poonoosamy J., Kosakowski G., Deissmann G., Prasianakis N.I., Brand F., Rohmen S., Kolheyer D., Bosbach D.

Dissolution-precipitation processes in porous media: experimental benchmarks for reactive transport modelling at different scales. Migration 2017, Barcelona, 10-15 September 2017.

Poonoosamy J., Prasianakis N.I., Kohlheyer D., Bosbach D.

Dissolution-precipitation processes in tank experiments: experimental benchmarks for reactive Transport Modelling at different scales. International Workshop "Reactive Transport for the Earth and Environmental Sciences in the 21st Century", Amboise, France, 2-5 October 2017.

Prasianakis N.I., Abbasi A., Gatschet M., Kosakowski G., Curti E., Churakov S.V.

Obtaining porosity-permeability relationships in reacting environments from pore-scale simulations. Clay Conference 2017, Davos, Switzerland, 24-27 September 2017.

Prasianakis N.I., Curti E., Poonoosamy J., Kosakowski G., Churakov S.V.

Reactive transport modelling of pore-size dependent mineral dissolution and precipitation. 9th International Conference on Porous Media and Annual Meeting (InterPore), Rotterdam, The Netherlands, 8-11 May 2017.

Prasianakis N.I.

Bridging of scales in reactive transport: from interatomic interaction to macroscopic dissolution-precipitation mechanisms. International Workshop, "Reactive Transport for the Earth and Environmental Sciences in the 21st Century", Amboise, France, 2-5 October 2017.

Prasianakis, N.I.

Lattice Boltzmann method and pore scale reactive transport, Excellence in Education and Research: An Adaptive and Integrative Approach for Oil Exploration & Production EPTEK 2017, College of Petroleum Engineering & Geosciences, King Fahd University of Petroleum and Minerals, KFUPM, Dhahran, Kingdom of Saudi Arabia, 15-17 October 2017.

Prasianakis N.I.

Resolving dissolution-precipitation mechanisms at the pore-scale, comparison with experiments and upscaling procedure. SCK•CEN Academy Topical Day: "Bridging experiments and continuum scale models: Role of modelling physical-chemical processes at the pore scale", Mol, Belgium, 14-16 November 2017.

Rufer D., Waber H.N., Gimmi T.

Helium in porewater and groundwater at the interface Opalinus Clay – Passwang-Formation at the Mont Terri URL (Switzerland). Clay Conference 2017, Davos, Switzerland, 24-27 September 2017.

Safi M.A., Prasianakis N.I., Mantzaras J., Lamibrac A., Büchi F.N.

Pore-level modelling of flow and mass transfer during evaporation in porous gas diffusion layers of polymer electrolyte fuel cells (PEFC). 9th International Conference on Porous Media and Annual Meeting (InterPore), Rotterdam, The Netherlands, 8-11 May 2017.

Salazar G., Cvetković B.Z., Kunz D., Wieland E., Szidat S.

Method development for CSRA of leakage markers from nuclear waste underground repositories, AMS14 Conference, Ottawa, Canada, 14-18 August, 2017.

Shafizadeh A., Gimmi T., Van Loon L.R., Kaestner A., Mäder U., Churakov S.V.

Neutron imaging allows time-resolved measurement of porosity changes at cement-clay interfaces. Clay Conference 2017, Davos, Switzerland, 24-27 September 2017.

Tits J., Kunz D., Laube A., Wieland E.

Chemical stability of ¹⁴C-containing low molecular weight organic compounds in the cementitious near-field of a radioactive waste repository. Migration 2017, Barcelona, 10-15 September 2017.

Van Loon L.R., Glaus M.A., Baeyens B., Marques Fernandes M.

Transferability of sorption data from dispersed to compact clay systems: a case study of caesium and strontium sorption on bentonite and argillaceous rocks. Clay Conference 2017, Davos, Switzerland, 24-27 September 2017.

Voegelin A., Wick S., Marques Fernandes M., Baeyens B.

Thallium sorption onto illite. Goldschmidt 2017, Paris, France 13-18 August, 2017.

Wersin P., Gimmi T., Mazurek M., Alt-Epping P., Pekala M., Traber D.

Multicomponent diffusion in a 280 m thick argillaceous rock sequence. Clay Conference 2017, Davos, Switzerland, 24-27 September 2017.

Wieland E., Cvetković B.Z., Kunz D., Salazar G., Szidat S.

Identification and formation of carbon-14 containing organic compounds during anoxic corrosion of activated steel in alkaline conditions. International High-Level Radioactive Waste Management Conference (IHLRWM) 2017, Charlotte NC, USA, 9-13 April 2017.

Wieland E., Cvetković B. Z., Kunz D., Salazar G., Szidat S.

Carbon-14 speciation during anoxic corrosion of activated steel in a repository environment. Eurosafe, Paris, France, 6-7 November 2017.

Wigger C., Van Loon L.R.

Anion accessible porosity in low porosity dense clay systems. Migration 2017, Barcelona, 10-15 September 2017.

Yang G.

Atomistic scale modelling for hydration of interlayer cations. Clay Conference 2017, Davos, Switzerland, 24-27 September 2017.

Yang G.

Classical density functional theory and molecular dynamics modelling of mineral-fluid interfaces. Workshop Goldschmidt on "Mineral-fluid reactions: from rocks to atoms. Computer simulations and models at different scales". Goldschmidt 2017, Paris, France, 13-18 August 2017.

Yapparova A., Miron G.D., Kosakowski G., Driesner T.
Reactive transport modelling of alteration assemblages at Butte magmatic-hydrothermal system. Goldschmidt 2017, Paris, France, 13-18 August 2017.

9.5 Invited talks

Curti E., Prasianakis N.I., Xto J., Borca C.N., Huthwelker Th.
A XAS study of barite nucleation: implications on radium mobility. Goldschmidt 2017 Paris, France 13-18 August, 2017.

Kulik D.A.
Embedding "rich chemistry" into reactive transport modelling of hydrothermal systems. Goldschmidt 2017, Paris, France, 13-18 August 2017.

9.6 Teaching

Churakov S.V.
Bachelor Course: Crystallography I + II, Institute for Geological Sciences, University of Bern.

Churakov S.V.
Bachelor Course: Crystall-optics, Institute for Geological Sciences, University of Bern.

Churakov S.V., Prasianakis N.I.
Atomistic simulations of geomaterials. University of Bern.

Churakov S.V., Kurganskaya I.
Workshop Mineral fluid reactions from rocks to atoms. University of Bern.

Curti E.
Lecturer for master course "Geological Disposal of Radioactive Waste", University of Bern, April 2017

Gimmi T.
Lecture "Ausbreitung von Schadstoffen in Böden und Grundwasser: Von der Realität zu Modell – und zurück." Weiterbildungskurs Altlasten. Universität Bern, 15-16 June 2017.

Gimmi T., Alt-Epping P.
Lecture and examinations "Geochemical Modelling II: Reactive Transport", Master Course in Environmental and Resource Geochemistry, University of Bern, Spring semester 2017.

Hummel W., Plötze L.M.
Master Course: Landfilling, Contaminated Sites and Radioactive Waste Repositories, ETH Zurich.

Kulik D.
GEMS course: a) the Hebrew University of Jerusalem in Israel (23-26 February 2017), and b) at the University of Melbourne in Australia (24-28 April 2017).

Patel R.
A two-day course on "Yantra: A lattice Boltzmann method based tool for pore scale modelling" at Belgium nuclear research center (SCK•CEN). 14-15 November 2017).

Pfingsten W.
Modelling of Processes in Soils and Aquifers (701-1334-00L). Department for Environmental Sciences, ETH Zurich, Spring semester 2017.

Prasianakis N.I.
Mineral reactivity at the pore scale: Lattice Boltzmann (LB) technique and the modelling of reactive fluid flow. Workshop "Mineral-fluid reactions: from rocks to atoms. Computer simulations and models at different scales". Goldschmidt 2017, Paris, France 13-18 August, 2017.

Prasser H.-M., Günther-Leopold I., Hummel W., Zuidema P.K., Hirschberg S.
Master Course: Nuclear Energy Systems, ETH Zurich.

9.7 PhD thesis defences

Chen Y.
Transport of low molecular weight organic compounds in compacted illite, kaolinite and Opalinus Clay, PhD defence, University of Bern, June 1, 2017.

Wigger C.
Anion accessibility in low porosity argillaceous rocks, PhD defence, University of Bern, December 19, 2017.

9.8 Other

Churakov S.V., Van Loon L.R., Glaus M.A.
Examination PhD thesis of Yanhua Chen, University of Bern, June 1, 2017.

Churakov S.V., Van Loon L.R., Gimmi T.
Examination PhD thesis of Cornelia Wigger University of Bern, December 19, 2017.

Gimmi T.
Associate editor of the Applied Geochemistry journal.

Kosakowski G.
Supervision of Bachelor Thesis of Adeline Ong. Precipitation in partially saturated porous media. Bachelor of Science, Hochschule Luzern/FHZ in Energy Systems Engineering. Date of defence: January 13, 2017.

Kulik D.

Associate editor of the Applied Geochemistry journal.

Patel R.

Secretary of RILEM technical committee TC 244-
NUM.

Prasianakis N.I., Churakov S.V.

Supervision of Master Thesis of A. Abbasi: Lattice Boltzmann model for pore-scale mineral dissolution, Matr. 108014252757, University of Bern and Ruhr-Universität Bochum, Deutschland (Jan.-Oct. 2017).

Wieland E.

Executive guest editor, special issue on mechanisms and modelling of waste/cement interactions, Journal of Physics and Chemistry of the Earth.

Wieland E.

Examination PhD thesis of Bin Ma. L'Institut des Sciences de la Terre, Université Grenoble, France, December 19, 2017.

